

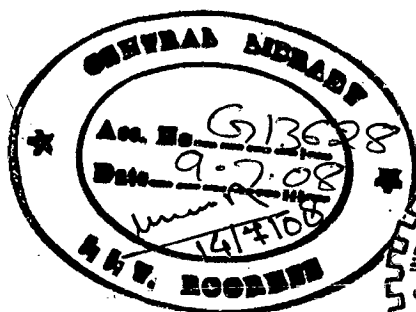
ZEOLITE-Y ENCAPSULATED COPPER COMPLEXES AND THEIR CATALYTIC ACTIVITIES

A DISSERTATION

*Submitted in partial fulfillment of the
requirements for the award of the degree*
of
MASTER OF TECHNOLOGY
in
ADVANCED CHEMICAL ANALYSIS

By

BALJIT SINGH



DEPARTMENT OF CHEMISTRY
INDIAN INSTITUTE OF TECHNOLOGY ROORKEE
ROORKEE - 247 667 (INDIA)
JUNE, 2007



**INDIAN INSTITUTE OF TECHNOLOGY ROORKEE
ROORKEE**

CANDIDATE'S DECLARATION

I hereby certified that the work which is being presented in the dissertation entitled **ZEOLITE-Y ENCAPSULATED COPPER COMPLEXES AND THEIR CATALYTIC ACTIVITIES** in partial fulfillment of the requirements for the award of the degree of **Master of Technology** with specialization in **Advance Chemical Analysis** submitted in the Department of Chemistry of Indian Institute of Technology Roorkee, Roorkee is an authentic record of my own work carried out during a period from July 2006 to June 2007 under the supervision of **Dr. M R. Maurya**, Associate Professor, Department of Chemistry, Indian Institute of Technology Roorkee, Roorkee.

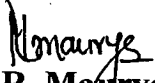
The matter embodied in this dissertation to the best of my knowledge has not been submitted by me for the award of any other degree of this or any other Institute.

Date: June 25, 2007
Place: Roorkee


(BALJIT SINGH)

CERTIFICATE

This is to certify that the above statement made by the candidate is correct to the best of my knowledge and belief.


(M. R. Maurya)
Associate Professor
Department of Chemistry
Indian Institute of Technology
Roorkee – 247667 (India)

ABSTRACT

ABSTRACT

Interaction of Copper(II) exchanged zeolite-Y with N,N'-ethylenebis(pyridoxyliminato) (H₂pydx-en, **I**) and N,N'-propylenebis(pyridoxyliminato) (H₂pydx-1,3-pn, **II**) in refluxing methanol leads to the formation of corresponding complexes, abbreviated here in as [Cu(pydx-en)]-Y (**1**) and [Cu(pydx-1,3-pn)]-Y (**2**) in the super cages of the zeolite-Y. Neat complexes, [Cu(pydx-en)] (**3**) and [Cu(pydx-1,3-pn)] (**4**) have also been prepared with these ligands. Spectroscopic studies (IR, electronic and EPR), elemental analyses, thermal study, magnetic susceptibility, scanning electron micrographs (SEM) and X-ray diffraction patterns have been used to characterise these complexes. The crystal and molecular structure of **4**.CH₃OH, has been determined, confirming the ONNO binding mode of the ligands. The encapsulated complexes catalyse the oxidation, by H₂O₂ and *tert*-butylhydroperoxide, of styrene, cyclohexene and thioanisole efficiently. Under the optimised reaction conditions, the oxidation of styrene catalysed by **1** and **2** gave 23.6 % and 28.0 % conversion, respectively using H₂O₂ as oxidant where styreneoxide, benzaldehyde, benzoic acid, and phenylacetaldehyde being the major products. Oxidation of cyclohexene catalysed by these complexes gave cyclohexenepoxide, 2-cyclohexene-1-ol, cyclohexane-1,2-diol and 2-cyclohexene-1-one as major products. A maximum of 90.1% conversion of cyclohexene with **1** and 79.3% with **2** was obtained under optimized conditions. Similarly, a maximum of 68.4% conversion of methyl phenyl sulfide with **1** and 81.0 % with **2** was observed where the selectivity of major product methyl phenyl sulfoxide was found to be ca. 60 %. Tests for recycle ability and heterogeneity of the reactions have also been carried out and results suggest their recyclability. A possible reaction mechanism has been proposed by titrating methanolic solution of **3** and **4** with H₂O₂ and identifying the possible intermediate.

ACKNOWLEDGMENTS

I reach on the culminating point of my thesis, a sense of achievement with gigantic satisfaction has transcended in me and it is pleasant and exhilarating moment of my life when I want to reminisce and acknowledge all those who were associated with me during this period

First and foremost I thank *Lord Almighty* for blessing me with the strength, Dedication and wisdom at each and every step.

Right at the outset, I owe this opportunity as my distinct privilege to express my profound sense of gratitude and reverence to my mentor **Dr. M. R. Maurya**, for introducing me to the present field of study with his meticulous guidance, brilliant creativity, prudent support, cooperation and enthusiastic interest through out my M.Tech. and selfless support for bringing the present work in the final shape. His pertinent suggestions and constructive criticism not only strengthen my skill in research methodology but also helped me to develop a never ending quest of knowledge and creates interest in this field to touch the zenith.

I am highly grateful to Prof. Ravi Bhushan, the Head of the Department of Chemistry, Indian Institute of Technology Roorkee, Roorkee for providing me necessary facilities and support to carry out this work. I am thankful to Dr. Shri Chand, Professor & Head, Department of Chemical Engineering, for giving permission to carry out catalytic activity in his department.

Special thanks to Mr. Maneesh for his affection, friendship selfless support and help rendered at different stages of my work. I must accolade the versatile, convivial and vibrant company of my lab mates Dr. Shewta Sirkawar, Dr. Anil Chandraker, Dr. Umesh Kumar, Aftab, Aarti and Manisha for their company, selfless support and motivation to complete my work.

I wish to acknowledge Mr. Abdul Hauque, Mr. V.P. Saxena, Mr. Wazid Ali for the technical assistance. I am also grateful to all members of Chemistry Department for their cooperation and timely help for my research work.

I also acknowledge Mr. Ayodhya Prasad Singh, Mr. Tara Chand, Mr. Satpal for their instant help in all kind of work.

I express my sincere thank to Head , Institute Instrumentation Center of our institute for providing necessary instrumentation facility. My special thanks to Mr. Anil Saini for recording TGA , Mrs. Rekha Sharma and Mr. Shiv Kumar for SEM and XRD analysis of my samples.

My heartfelt regard and gratitude to my beloved parents for all their sacrifices, encouragement, blessing and consistent support throughout my study. Their presence always kept me energetic and full of spirits. I humbly acclaim my indebtedness to them for prudently shaping my life. I thank my brother Avtar Singh for his love and admiration, which continues to support me through my difficult times.

I am in dearth of proper words to express my abounding feeling for my dearest wife Sanu and her parents for their deepest love, support, and encouragement, positive spirit and strength have inspired me to be the best I can be. I thank to my daughter Sargun for her cute and charming conversations, from which I forget about my all tensions and stress. I thank my elder sisters Jaswinder and Kuldeep for their love and appreciation.

Last, but not least, I wish to thank all those, whose names have not figured alone, but have helped me directly or indirectly during this period.

List of Figures

- Figure 1.1. Model showing the complete catalytic reaction.
- Figure 1.2. Representative zeolite structures: (a) Zeolite-A and (b) Zeolite-Y (adopted from Reference [13]).
- Figure 1.3. 3D model structure of $[\text{Fe}(\text{hybe})(\text{H}_2\text{O})_2]^+$.
- Figure 3.1 Crystal structure of $\{[\text{Cu}(\text{pydx-1,3-pn})] \cdot \text{CH}_3\text{OH}\}_2$. Both molecules of asymmetric unit are shown together.
- Figure 3.2 Scanning electron micrograph of Cu-Y (A), $[\text{Cu}(\text{pydx-en})]\text{-Y}$ (B) and $[\text{Cu}(\text{pydx-1,3-pn})]\text{-Y}$ (C).
- Figure 3.3. XRD patterns of Na-Y, Cu-Y and $[\text{Cu}(\text{pydx-en})]\text{-Y}$ (3).
- Figure 3.4 TGA, DTA and DTG profiles of $[\text{Cu}(\text{pydx-en})]\text{-Y}$.
- Figure 3.4.1 TGA and DTG profiles of $[\text{Cu}(\text{pydx-1,3pn})]\text{-Y}$.
- Figure 3.5 Figure 3.5. Electronic spectra of neat complexes $[\text{Cu}(\text{pydx-en})]$ shows d-d transition and other bands
- Figure 3.5.1 Electronic spectra of neat complexes.
- Figure 3.6 Electronic spectra of $[\text{Cu}(\text{pydx-en})]\text{-Y}$ and $[\text{Cu}(\text{pydx-1,3-pn})]\text{-Y}$.
- Figure 3.7 EPR spectra of $[\text{Cu}(\text{pydx-en})]$ (above) and $[\text{Cu}(\text{pydx-1,3-pn})]$ (below) in DMF at 77K . $\nu=9.453$ GHz.
- Figure 3.8 Correlation between A_{\parallel} and g_{\parallel} for Cu(II) complexes with several types of coordinating atoms with tetragonal or tetrahedral distortion: $\text{S}_4(\blacklozenge)$, $\text{N}_4(\bullet)$, $\text{O}_4(\blacktriangle)$, $\text{N}_2\text{O}_2(0)$ and $\text{N}_2\text{S}_2(\square)$.
- Figure 3.9 EPR spectra of the complexes encapsulated in zeolite-Y.

- Figure 3.10 Effect of H₂O₂ on the oxidation of styrene. Reaction conditions: styrene (1.04 g, 10 mmol), [Cu(pydx-en)]-Y (3) (0.025 g), CH₃CN (20 mL) and temp. (80° C).
- Figure 3.11 Effect of amount of catalyst on the oxidation of styrene. Reaction conditions: styrene (1.04 g, 10 mmol), 30 % H₂O₂ (), CH₃CN (20 mL) and temp. (80° C).
- Figure 3.12 Effect of temperature on the oxidation of styrene. Reaction conditions: styrene (1.04 g, 10 mmol), [Cu(pydx-en)]-Y (0.025 g), 30 % H₂O₂ (2.27 g, 20 mmol) and CH₃CN (20 mL).
- Figure 3.13 Catalytic comparison of zeolite-encapsulated and neat complexes for the oxidation of styrene in presence of H₂O₂ as oxidant. Reaction conditions: styrene (1.04 g, 10 mmol), catalyst (0.025 g for encapsulated and 0.00133 g in case of neat complexes), H₂O₂ (2.27 g, 20 mmol), CH₃CN (20 ml) and temperature (80 °C).
- Figure 3.14 Catalytic comparison of zeolite-encapsulated metal complexes and neat complexes for the oxidation of styrene in presence of TBHP as oxidant. Reaction conditions: styrene (1.04 g, 10 mmol), catalyst (0.025 g for encapsulated and 0.00133 g in case of neat complexes), TBHP (2.57 g, 20 mmol), CH₃CN (20 ml) and temperature (80 °C).
- Figure 3.15 Effect of H₂O₂ on the oxidation of cyclohexene. Reaction conditions: cyclohexene (0.82 g, 10 mmol), [Cu(pydx-en)]-Y (0.025 g), CH₃CN (20 mL) and temp. (75° C).
- Figure 3.16 Effect of amount catalyst on the oxidation of cyclohexene. Reaction conditions: cyclohexene (0.82 g, 10 mmol), 30 % H₂O₂ (3.40 g, 30 mmol), CH₃CN (20 mL) and temp. (75° C).
- Figure 3.17 Effect of temperature on the oxidation of cyclohexene. Reaction conditions: cyclohexene (0.82 g, 10 mmol), [Cu(pydx-en)]-Y (0.025 g), 30 % H₂O₂ (3.40 g, 30 mmol) and CH₃CN (20 mL).
- Figure 3.18 Effect of amount of H₂O₂ on the oxidation of methyl phenyl sulfide.
Reaction conditions: methyl phenyl sulfide (1.242 g, 10 mmol), [Cu(pydx-1,3-pn)]-Y (0.025 g) and acetonitrile (10 mL).

- Figure3.18.1 Effect of volume of solvent on the oxidation of methyl phenyl sulfide. Reaction conditions: methyl phenyl sulfide (1.242 g, 10 mmol), [Cu(pydx-1,3-pn)]-Y (0.025 g) and acetonitrile (10 ml and 20 mL).
- Figure 3.19 Effect of amount of catalyst on the oxidation of methyl phenyl sulfide. Reaction conditions: methyl phenyl sulfide (1.242 g, 10 mmol), H₂O₂ (2.27 g, 20 mmol) and acetonitrile (10 mL).
- Figure 3.20 Oxidation of methyl phenyl sulfide by various catalysts using H₂O₂ as an oxidant.
- Figure 3.21 Oxidation of methyl phenyl sulfide by various catalysts using *tert*-butylhydroperoxide as an oxidant.
- Figure 3.22 Titration of methanolic solution of [Cu(pydx-en)] with aqueous 30 % H₂O₂ dissolved in methanol.
- Figure 3.23 Figure 3.23. Titration of methanolic solution of [Cu(pydx-1,3-pn)] with aqueous 30 % H₂O₂ dissolved in methanol.

List of Tables

- Table 3.1. Crystal Data and Structure Refinement Parameters for [Cu(pydx-1,3-pn)].CH₃OH.
- Table 3.2. Various bond lengths in [Cu(pydx-1,3-pn)].CH₃OH
- Table 3.3. Various bond angles in [Cu(pydx-1,3-pn)].CH₃OH
- Table 3.4. IR and electronic spectral data of ligand, pure and encapsulated complexes.
- Table 3.5. EPR parameters obtained for neat complexes in DMF at 77K.
- Table 3.6. Products selectivity and percent conversion of styrene after 6 h of reaction time with H₂O₂ as oxidant
- Table 3.7. Products selectivity and percent conversion of styrene with TBHP after 6 h of reaction time
- Table 3.8. Oxidation of cyclohexene and product selectivity using various catalysts
- Table 3.9. Selectivity of different products with time using [Cu(pydx-1,3-pn)]-Y as catalyst and H₂O₂ as oxidant.
- Table 3.10. Conversion percentage of methyl phenyl sulfide using H₂O₂ as an oxidant and selectivity of sulfoxide and sulfone
- Table 3.11. Conversion percentage of methyl phenyl sulfide using TBHP as an oxidant and selectivity of sulfoxide and sulfone
- Table 3.12. Selectivity of different products with time using [Cu(pydx-1,3-pn)]-Y as catalyst and H₂O₂ as oxidant

PUBLICATIONS

- 1. M. R. Maurya*, Singh Baljit**
Zeolite encapsulated copper (II) complexes of pyridoxal based tetradentate ligands for the oxidation of styrene, cyclohexene and methyl phenyl sulfide, Communicated

CONTENTS

CANDIDATE'S DECLARATION	Page No.
ABSTRACT	(i)
ACKNOWLEDGEMENTS	(ii)
LIST OF FIGURES	(iii)
LIST OF TABLES	(v)
	(viii)

CHAPTER 1

Introduction

1.1	Introductory	1
1.2	Supports used for catalysts	2
1.3	Zeolites and their use as solid support to homogeneous catalysts	5
	1.3.1 Methods for the synthesis of zeolite encapsulated metal complexes	7
	1.3.2 Zeolite encapsulated metal complexes and their catalytic activities	8
1.4	Objective of the present investigation	19

CHAPTER 2

Experimental

2.1	Materials	21
2.2	Preparations	21
2.3	Physical methods and analysis	23
2.4	Catalytic activity	24

CHAPTER 3

Results and discussions

3.1.	Synthesis and characterization of catalysts	26
	3.1.1. Structure description of [Cu(pydx-1,3-pn)]-Y	27
	3.1.2. Scanning electron micrograph studies	35
	3.1.3. Powder X-ray diffraction studies	36
	3.1.4. Thermogravimetric analysis studies	37
	3.1.5. IR spectral studies	39
	3.1.6. Electronic spectral studies	40
	3.1.7. EPR studies	43

3.2.	Catalytic activity studies	
3.2.1.	Oxidation of styrene	46
3.2.2.	Oxidation of cyclohexene	53
3.2.3.	Oxidation of methyl phenyl sulfide	58
3.3.	Test for recycle ability and heterogeneity of the reactions	66
3.4.	Possible reaction pathway of the catalysts	66

CHAPTER 4

<i>Conclusions</i>	69
--------------------	----

CHAPTER 5

<i>References</i>	71
-------------------	----

<i>Appendix</i>	77
-----------------	----

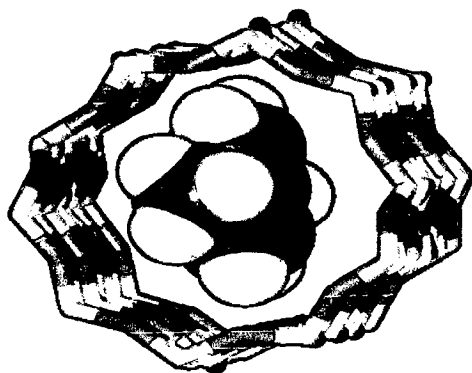
Abbreviations & Symbols used

Schematic diagram of encapsulated catalyst

UV & IR –Spectra Of ligand H₂pydx-En

Basic theory of some techniques used

INTRODUCTION



CHAPTER-1

INTRODUCTION

1.1. INTRODUCTION

The material that helps in the attainment of chemical equilibrium by reducing the potential energy barriers in the reaction path is called catalyst. Brezeliuss introduced the term “catalyst” in 1835. Catalysis has been an important area of research since then and continuous efforts have been made to understand and utilize the phenomenon for practical purposes. Catalysts activate the reactant molecules to bind with it at milder conditions where they react and finally products separate out leaving the catalyst for the next cycle; Figure 1.1

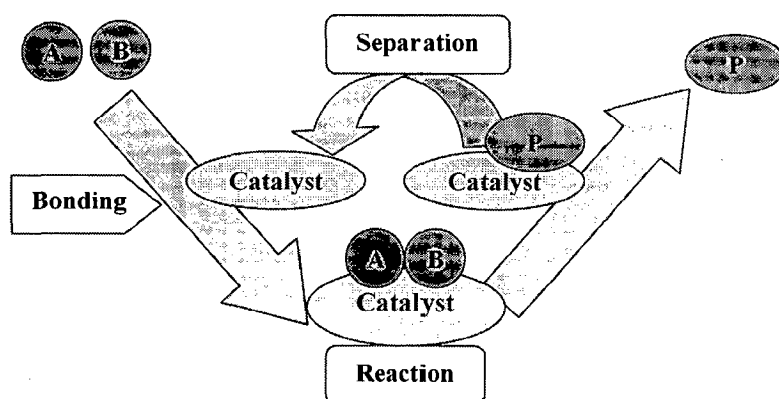


Figure 1.1. Model showing the complete catalytic reaction.

The catalytic reaction occurs at the specific site called “active site” and rate of the reaction can be significantly improved by enhancing the surface area of the catalyst which in turn enhances the availability of the active sites. Normally, the speed of the catalytic reaction is presented in terms of a “Turn-over Rate” (TOF), which is defined as number of moles of substrate converted on an ‘active site’ or on a unit catalytic surface area per second at a given condition. In 20th century

catalysts have played a vital role as 95 % processes used in the chemical industries today are catalysts based technologies. Directly or indirectly catalysts have contributed more than 20% GDP of developed nations. Major catalyst based technologies for the past 50 years are given in Table 1.1 chronologically.

Table 1.1. Major catalytic technology developments during the past 50 years [1].

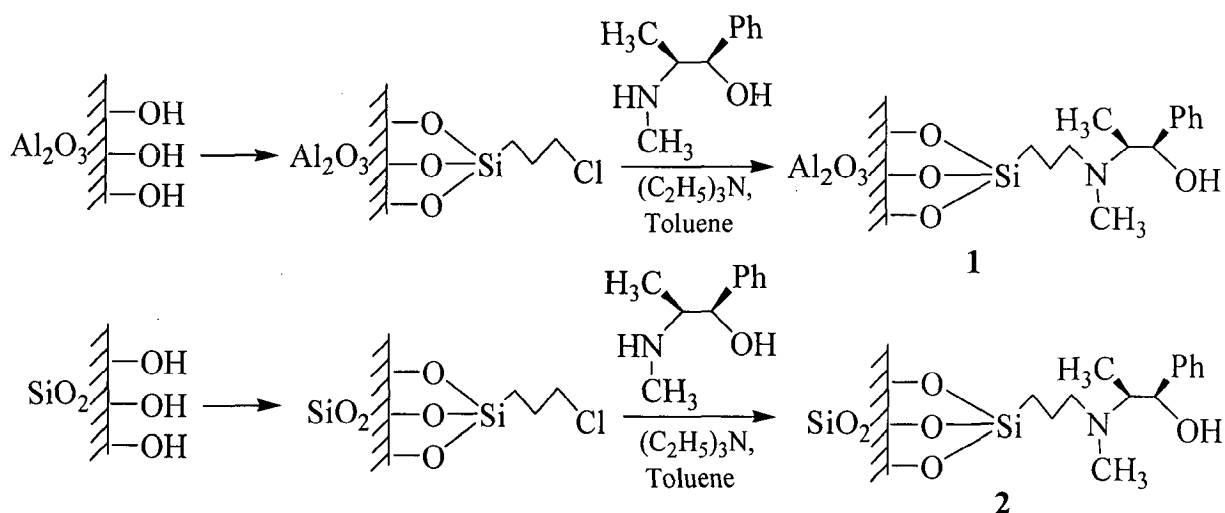
Year	Process	Catalyst
1949	Monometallic reforming	Pt-Al ₂ O ₃
1957	Polymerization	Zeigler-Natta
1962	Steam reforming	Ni-K- Al ₂ O ₃
1964	Zeolite catcracking	X,Y-zeolites
1967	Bimetallic reforming	Pt-Re / Pt-Ir
1968	Selectoreforming	Erionite
1972	Low pressure CH ₃ OH	Cu-Zn- Al ₂ O ₃
1974	Acetic acid (carbonylation)	Rh-I
1976	Auto emission control	Pt- Al ₂ O ₃
1980	Gasoline from methane	ZSM-5
1982	Auto emission; stack gas	Pt-Rh; V ₂ O ₅ -TiO ₂
1988	Selective oxidation	Ti-silicates
1988	Chiral catalysts	Cinchonidine-Pt; BINAP
1991	Polymerization	Metallocenes

1.2. SUPPORTS USED FOR CATALYSTS

All kinds of materials that are thermally stable and chemically inert can be used as support for catalyst. Amongst various supports, alumina, silica and carbon are the most common. One of the oldest methods to prepare supported catalysts is the co-precipitation of the catalytically active component and the support to give a mixture which is subsequently dried, calcined and reduced to give a porous

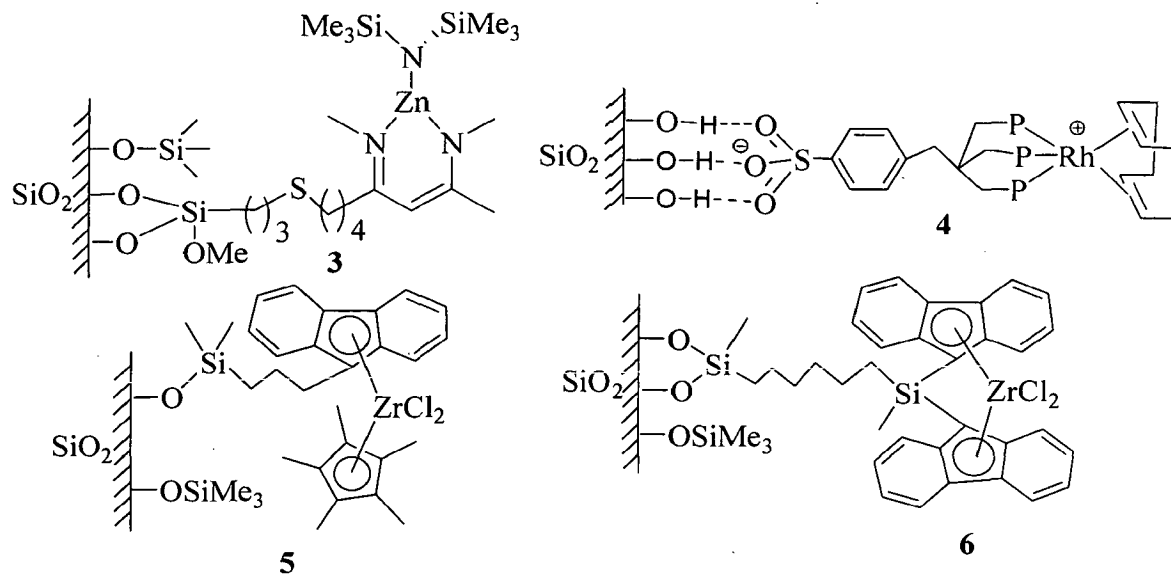
material with a high surface area. Another but most preferred method is loading pre-existing support materials in the form of shaped bodies with the catalytic active phase by means of impregnation or precipitation from solution [2].

Immobilization of homogeneous catalysts facilitates easy product separation, catalysts recovery and recycles ability. Alumina and silica gels are readily available inorganic compounds and have been modified to immobilize various catalysts by direct reaction of surface hydroxyl groups with reactive species; Scheme 1.1 [3].



Scheme 1.1. Immobilization of catalysts on silica and alumina.

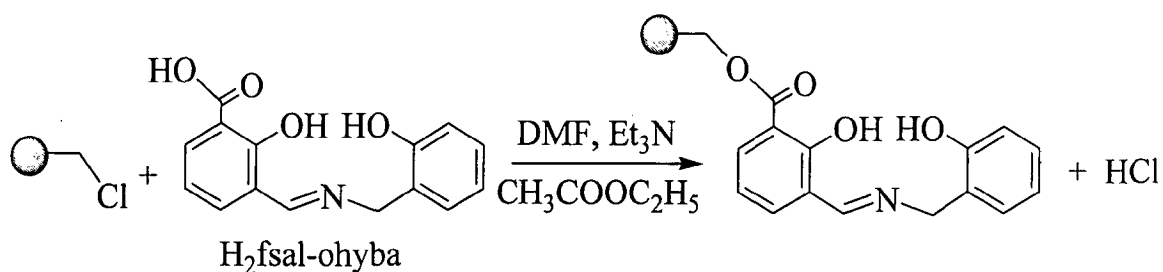
Other examples of immobilized catalysts are given in Scheme 1.2 [4, 5].



Scheme 1.2

Recent review article by Jacob *et al.* [6] provides detail accounts of such immobilized complexes. These immobilized catalysts have been suggested to be better over the polymer-anchored catalysts, which is discussed in the following paragraph. This is because polymer-anchored catalysts require their swelling in suitable solvent before their use for catalytic reactions.

Metal complexes as such may form covalent bond if suitable coordinating site is present on the functional group. Functionalized group of polymer may also react with organic molecules having suitable coordinating site(s) followed by its coordination with metal ions to give polymer-supported metal complexes. Complete recoveries of the catalytic reaction products are thus possible. Besides, regeneration and recyclability make them commercially beneficial. One of the most straight forward methods is the reaction of $-\text{CH}_2\text{Cl}$ group of chloromethylated polystyrene with organic molecules bearing functional groups such as carboxylic, sulfonic and hydroxyl groups [7-10]. Scheme 1.3 represents the synthetic approach [10].



Scheme 1.3

1.3. ZEOLITES AND THEIR USE AS SOLID SUPPORT TO HOMOGENEOUS CATALYSTS

Zeolites are crystalline hydrated aluminosilicates with open framework structures constructed from AlO_4 and SiO_4 tetrahedra linked to each other by sharing all of the oxygens. Each oxygen atom is shared by two silicon or aluminum atoms. Nature has provided many zeolites as minerals and plenty of other zeolites have also been synthesized. These large varieties of zeolites are due to the flexibility of Al-O-Si linkage, which depends on the conditions used during their hydrothermal synthesis. The natural faujasite and synthetic X and Y zeolites contain the super cage of ca. 13 Å internal diameter which is connected via 12 rings of 8 Å to four other cages in a tetrahedral arrangement. Thus, zeolite-Y has a three-dimensional pore structure with the pores running perpendicular to each other in three dimensional planes; Figure 1.2. Hydrated zeolite-Y is represented by the formula $\text{Na}_{56}\text{Al}_{56}\text{Si}_{136}\text{O}_{384} \cdot 250\text{H}_2\text{O}$ where Na^+ balances the formal negative (-1) charge generated by each $[\text{AlO}_4]^-$ units. The number of water molecules gives an idea of the volume of the channels in relation to the total volume, while Na^+ can be exchanged with other metal ions as well as H^+ reversibly [11, 12].

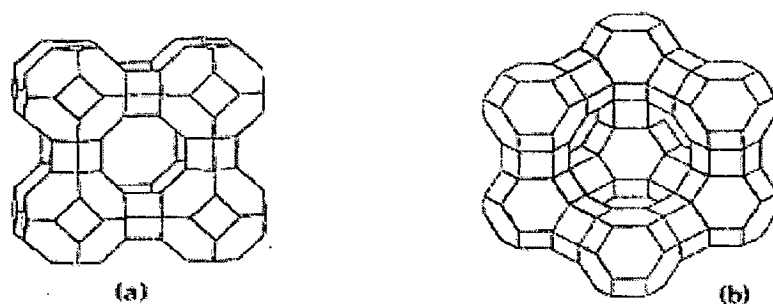


Figure 1.2. Representative zeolite structures: (a) Zeolite-A and (b) Zeolite-Y (adopted from Reference [13]).

Zeolites find applications in many scientific disciplines, catalysts and all types of chemical engineering process technologies. They are often called molecular sieves because the large number of small but identical pores can be used to separate small molecules from large molecules, which can pass through the pores. The exchangeable property of extra-frame work with cations and suitable cavity size of the zeolites allow their modification by inclusion of chemically interesting molecules. Homogeneous catalyst e.g. metal complex may be considered one of such interesting molecules and hence the term zeolite encapsulated metal complexes. A large size of the encapsulated homogeneous catalysts and their rigidity make them difficult to escape out of the zeolite cages. Zeolite encapsulated metal complexes having good catalytic activities possess all the advantages of solid heterogeneous catalysts as well as share many advantageous features of homogeneous catalysts.

Zeolites as catalysts for chemical reactions has marked ability which take place within the internal cavities. An important class of reactions is that catalysed by hydrogen-exchanged zeolites, whose framework-bound protons give rise to very high acidity. This is exploited in many organic reactions, including crude oil cracking, isomerisation and fuel synthesis. Zeolites can also serve as oxidation or reduction catalysts, often after metals have been introduced into the framework. Examples are the use of titanium ZSM-5 in the production of caprolactam, and

copper zeolites in NO_x decomposition. Underpinning all these types of reaction is the unique microporous nature of zeolites, where the shape and size of a particular pore system exerts a steric influence on the reaction, controlling the access of reactants and products. Thus zeolites are often said to act as shape-selective catalysts. Increasingly, attention has focused on fine-tuning the properties of zeolite catalysts in order to carry out very specific syntheses of high-value chemicals e.g. pharmaceuticals and cosmetics.

1.3.1. Methods for the synthesis of zeolite encapsulated metal complexes

Three general approaches have been suggested for the preparation of zeolite encapsulated metal complexes. These are: flexible ligand method, template synthesis method and zeolite synthesis method. In addition to these, other two approaches, such as, ion exchange method and adsorption method may also be considered. These methods are briefly discussed below [13, 14].

Encapsulation of $[\text{Cu}(\text{en})_2]^{2+}$ in faujasites by exchanging small cation e.g. Na^+ present in the cavity of the zeolite with $[\text{Cu}(\text{en})_2]^{2+}$ has been referred to as ion exchange method. The complex, $[\text{Cu}(\text{en})_2]^{2+}$ can pass through the pore opening of the zeolites [15]. Several such complexes have been prepared in the cavity of zeolites and characterized [16 – 19].

If the ligand is flexible enough to diffuse freely through the zeolite pores, this may react easily with the previously exchanged metal ions in the cavity to give stable metal complexes. The size of the resulting metal complexes will be too large to escape out. Such method is referred to as flexible ligand method. Lunsford *et al.* first applied this method for encapsulation of a series of metal-2,2'-dipyridyl complexes [20-22]. Metal-salen complexes are the best examples prepared by this method [14, 23, 24]. Here, the diffusion of ligands has been facilitated mostly in the molten state. Later, suitable solvent has also been used to facilitate the diffusion [25].

Encapsulation of metal carbonyls by the reaction of metal (e.g. Ru, Rh etc.) exchanged zeolite-Y with CO/H₂ or CO/H₂O to give metal carbonyls is the example of adsorption method. Slow diffusion of small metal carbonyls in to the cavity of zeolite has also been tried. Several metal carbonyls, such as, Ni(CO)₄, Ir₄(CO)₁₂, Rh₄(CO)₁₂, Rh₆(CO)₁₆ have been encapsulated in zeolite-Y by these methods [26-30].

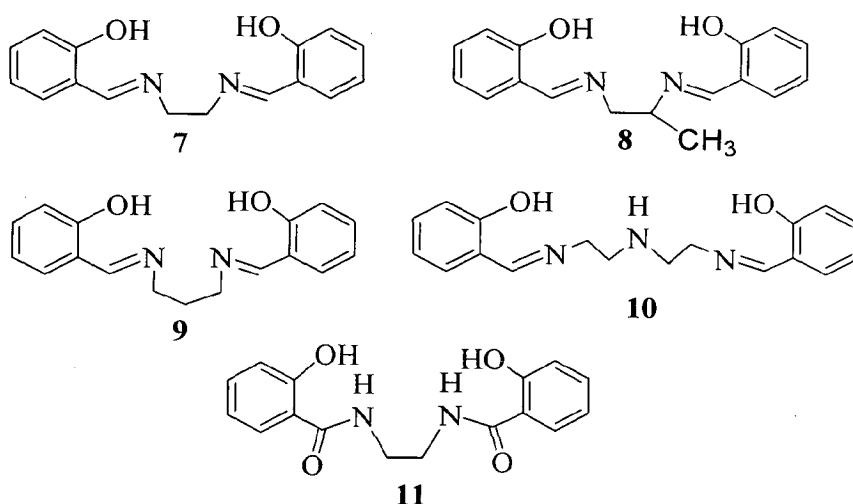
In template synthesis method, ligand is synthesized in-situ in the cavity of the zeolite from its constituents in the presence of previously exchanged metal ions. This method has largely been applied to prepare metallophthalocyanines where dicyanobenzene was allowed to diffuse into zeolite cavity through the pores followed by cyclization in presence of previously exchanged metal ions to give complexes [13, 31-37]. Zeolite synthesis method involves the addition of preformed metal complex in a template role to a reaction mixture of starting materials followed by crystallization of zeolite host. This method is advantageous as well defined encapsulated metal complexes under milder conditions can be prepared. This method has been applied to synthesize neutral metallophthalocyanines and metalloprophyrins in the cavity of zeolite-Y [38, 39].

1.3.2. Zeolite encapsulated metal complexes and their catalytic activities

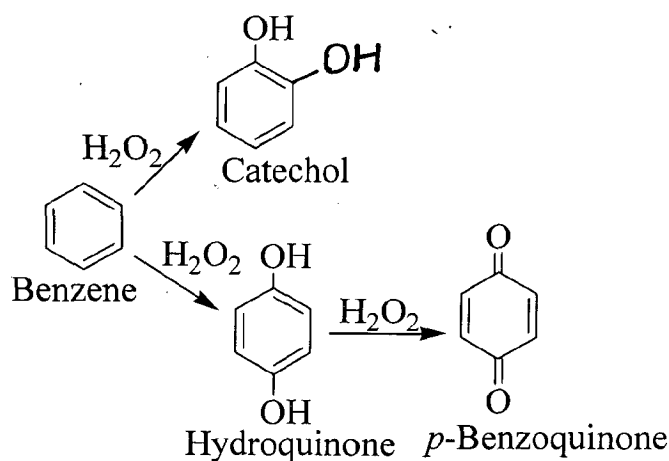
As zeolite encapsulated metal complexes enjoy the advantageous features of homo- as well as heterogeneous catalysts, these materials have provided opportunities to develop catalytic processes for various reactions such as hydrogenation, oxidation, alkylation, cyclization, acylation and isomerisation etc. A brief literature survey dealing with selected complexes encapsulated in the cavity of zeolite and their catalytic activity has been presented here.

Maurya *et al.* have reported oxovanadium(IV) complexes of ligands H₂salen (**7**), H₂sal-1,2-pn (**8**), H₂sal-1,3-pn (**9**), H₂saldien (**10**) and Hehybe (**11**) of Scheme 1.4 encapsulated in the cavity of zeolite-Y [40]. These complexes catalyse the oxidation of phenol. As the hydroxyl group on phenol is *ortho* and *para*

directing, the catalytic oxidation of phenol usually gives two products catechol and hydroquinone. In some cases a further oxidation also occurs to give *p*-benzoquinone as shown in Scheme 1.5. Under the optimized conditions [VO(sal-1,3-pn)]-Y has shown ca. 34 % conversion while other two complexes, [VO(salen)]-Y and [VO(saldien)] register only 33 % conversion. As high as 90 % selectivity of catechol has been observed by later two complexes [40]. The [VO(salen)]-Y has also been used as active catalyst in the oxidation of toluene by H₂O₂ to produce benzaldehyde, benzylalcohol, *o*-cresol and *p*-cresol [41]. Oxidation of cyclohexane has also been carried out by similar complexes [42, 43].



Scheme 1.4



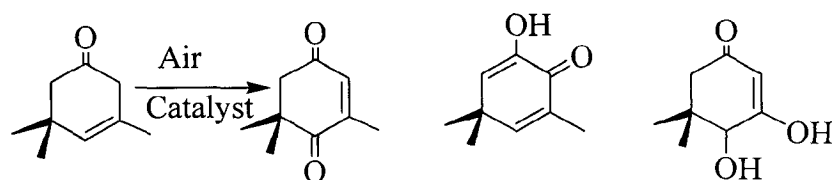
Scheme 1.5. Various products of phenol oxidation.

as catalysts. The oxidation products are mainly catechol and hydroquinone. In no cases the formation of 1,4-benzoquinone was detected.

Copper(II) and manganese(III) complexes of salen derivatives encapsulated in the cavity of zeolite-X and zeolite-Y by zeolite synthesis method have been reported by Ratnasamy *et al.* [49, 48]. The structures of the complexes have been established by FTIR, UV-visible and EPR spectroscopic techniques, XRD, SEM, thermal and elemental analysis, as well as nitrogen absorption and cyclic voltametric studies. The oxidation of styrene under aerobic conditions using *tert*-butylhydroperoxide gave benzaldehyde, styrene and phenylacetaldehyde. The catalytic efficiency of these encapsulated complexes was much higher than that of the neat complexes. Electron withdrawing substituents such as -Cl, -Br, -NO₂ on the aromatic ring enhances the rate of oxidation. These complexes also catalyze the oxidation of phenol and *p*-xylene. The aerobic oxidation of *p*-xylene in the absence of added hydrogen promoters and using *tert*-butyl hydroperoxide as the initiator and Mn(X-sal-1,3-pn)Cl]-X and [Mn(sal-dach)Cl]-X (H₂sal-dach = Schiff derived from salicylaldehyde and 1,2-diaminocyclohexane) at low temperature showed as high as 60 % conversion [51, 52].

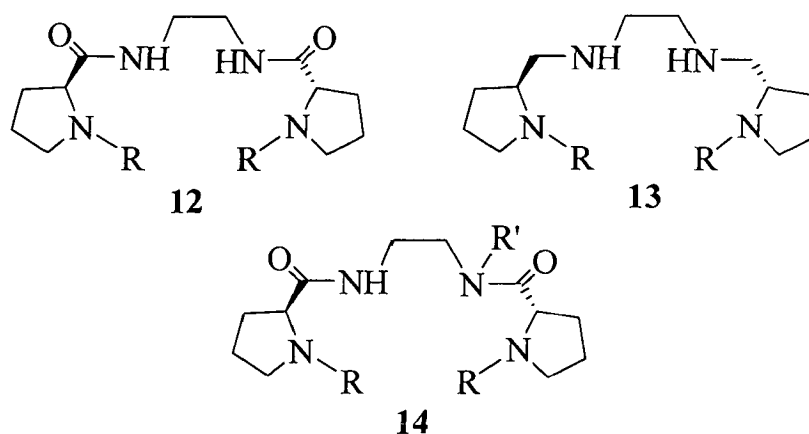
Complex, [Mn(salen)]⁺ encapsulated in zeolite-Y has been used for the asymmetric epoxidation of *cis*-β-methylstyrene with sodium hypochlorite [53]. Other similar complexes have also been used for the epoxidation of various types of alkenes, arenes and cycloalkenes [54, 55]. The [Mn(salen)]⁺-Y has been reported to be stereospecific in the epoxidation of *trans* stilbene as well as active for the epoxidation of *cis*-substituted aryl alkenes [56, 57]. Manganese(III) and nickel(II) complexes of H₂salen have also been used as catalyst for the epoxidation of cyclohexene, cyclooctene and 1-hexene using NaOCl and KHSO₅ as terminal oxidants. Selectivity in the epoxidation of linear olefins is possibly the result of small pore size of the zeolite host which governs the molecular sieving and orientation properties [58].

Halligudi *et al.* have reported complexes, [Co(salophen)]-Y and related derivatives and used as catalyst for the oxidation of β -isophorone (β IP) to keto isophorone (KIP) along with other minor products using air as an oxidant at ambient conditions of temperature and pressure; Scheme 1.6. The activities of these encapsulated catalysts follow the order: [Co(Cl-salophen)]-Y > [Co(Br-salophen)]-Y > [Co(NO₂-salophen)]-Y > [Co(salophen)]-Y. The selectivity for KIP was >95 % at β IP conversion of ~30 % in the beginning which slowly decreased with time to ~60 % selectivity at higher conversion (>95 %) of β IP [59]. Ruthenium(III) and Cobalt(II) complexes of H₂X-salophen (X = Cl, Br and NO₂) encapsulated in zeolite-Y has been found to be efficient for the allylic oxidation of α -pinene [60].



Scheme 1.6. Reaction scheme of oxidation of β -isophorone.

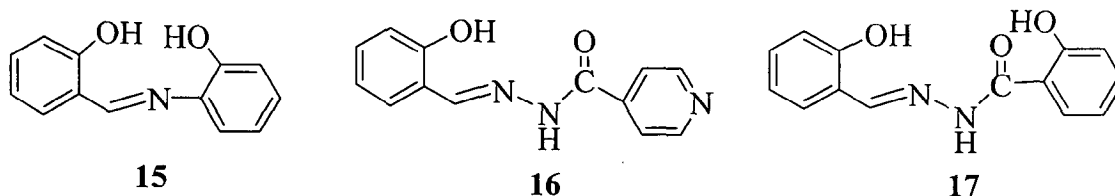
Alcón *et al.* have reported encapsulation of manganese(II) and Cu(II) complexes of chiral ligands **12**, **13** and **14** (Scheme 1.7) in zeolite-Y. Encapsulation was affected by flexible ligand method. These encapsulated complexes catalyse the oxidation of methyl phenyl sulfide and (2-ethylbutyl)phenyl sulfide. Conversions of these substrates vary in the range 73 – 100 %. The greater stability of these encapsulated complexes over homogeneous analogues has been attributed to the suppression of dimeric or polymeric species formation [61, 62].



Scheme 1.7

Copper(II)-salicylaldehyde-*p*-aminobenzoic complex, $[\text{Cu}_2(\text{sal-amba})(\text{H}_2\text{O})_5]\text{-Y}$ has been encapsulated in zeolite-Y. The EPR spectrum of the encapsulated complex suggests the existence of binuclear complex with coordination of nitrogen and oxygen atoms (from carboxylic, phenolic and water). Its encapsulation has also been confirmed by X-ray diffraction study. This complex adsorbs CO and form Cu(I)-CO species which is stable to thermal evacuation [63].

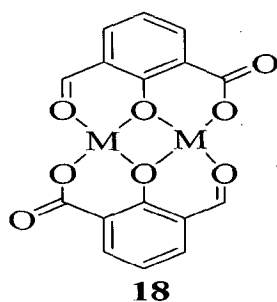
Maurya *et al.* have reported $\text{NH}_4[\text{VO}_2(\text{sal-oap})(\text{H}_2\text{O})]\text{-Y}$ ($\text{H}_2\text{sal-inh}$ = Schiff base derived from salicylaldehyde and *o*-aminophenol, **15**) and $\text{NH}_4[\text{VO}_2(\text{sal-inh})(\text{H}_2\text{O})]\text{-Y}$ ($\text{H}_2\text{sal-inh}$ = Schiff base derived from salicylaldehyde and iso nicotinic acid hydrazide, **16**)(Scheme 1.8) encapsulated in zeolite-Y. These complexes have been encapsulated by reacting pre-exchanged ammonium vanadate with zeolite-Y with sodium salt of ligand in aqueous solution followed by adjusting pH to ca. 7.5 [64]. Complexes $\text{NH}_4[\text{VO}_2(\text{sal-inh})(\text{H}_2\text{O})]\text{-Y}$ and $\text{NH}_4[\text{VO}_2(\text{sal-oap})(\text{H}_2\text{O})]\text{-Y}$ catalyze the oxidative bromination of salicylaldehyde to give 5-bromosalicylaldehyde with 90 % selectivity. They also catalyze the oxidation of phenol to give catechol and hydroquinone with good selectivity towards catechol [65]. Dioxomolybdenum(VI) complex of similar ligand $\text{H}_2\text{sal-shz}$ (**17**) catalyze aerial oxidation of cyclooctene [66].



Scheme 1.8

Iron(II) and manganese(II) complexes of 2,2'-dipyridyl have been isolated by Niassary *et al.* for the oxidation of cyclic ethers, such as, tetrahydrofuran, tetrahydropyron, 2,3-dihydropyron and 1,4-dioxane using H_2O_2 and TBHP as oxidant. Mainly cyclic ether-2-ols and cyclic ether-2-ones have been obtained. Minor product, 2,3-dihydro cyclic ether has also been detected in some cases [67].

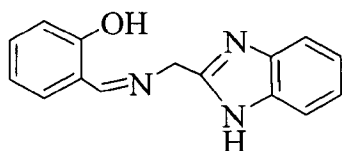
Binuclear copper(II), nickel(II) and cobalt(II) complexes of 3-formylsalicylic (H₂fsal) (**18**) have been encapsulated in zeolite-Y for the oxidation of benzyl alcohol and ethylbenzene; Scheme 1.9. Their catalytic potential vary in the order: $[\{\text{Cu}(\text{fsal})\}_2]\text{-Y} > [\{\text{Co}(\text{fsal})\}_2]\text{-Y} > [\{\text{Ni}(\text{fsal})\}_2]\text{-Y}$ [68]. Partial oxidation of these substrates has also been catalyzed by zeolite-Y encapsulated copper(II), nickel(II) and cobalt(II) complexes of dimethylglyoxime [69]. The same group has also reported the catalytic oxidation of ascorbic acid by atmospheric oxygen using $[\text{Cu}(\text{dmpz})_2]\text{-Y}$ (Hdmpz = 3,5-dimethyl-1H-pyrazole) as catalyst. The oxidation of ascorbic acid to dehydroascorbic acid was monitored spectroscopically at 245 nm after exposing deoxygenated methanolic solution of ascorbic acid in air in the presence of catalyst. It has been proposed that oxidation proceeds through Cu(I)-ascorbate intermediate [70].



Scheme 1.9. Dinuclear structure of $[\{\text{M}(\text{fsal})\}_2]$ complexes; M = Cu(II), Ni(II), Co(II).

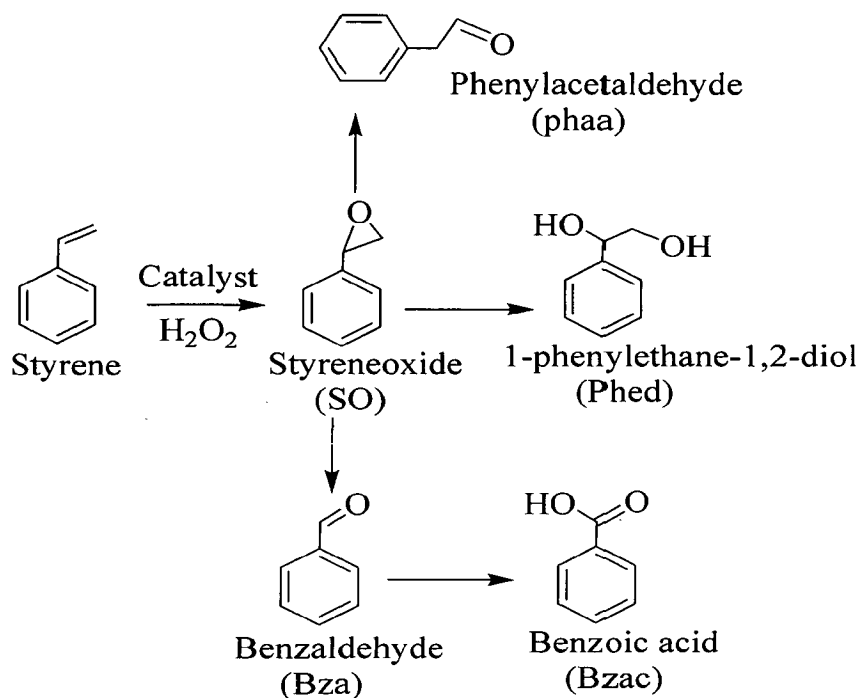
Complexes $[\text{VO}_2(\text{sal-ambmz})]$ and $[\text{Cu}(\text{sal-ambmz})\text{Cl}]$ of Hsal-ambmz (**19**, Scheme 1.10) have been encapsulated in the super cages of zeolite-Y. The integrity of encapsulation was confirmed by spectroscopic studies as well as chemical and thermal analysis. These encapsulated complexes are found active for the oxidation of phenol and styrene with good conversion. A maximum of 43.9 % of phenol oxidation was observed with vanadium-based catalyst, which is followed by copper-based catalyst. However, the copper based catalyst is more selective (73.9 %) towards the formation of catechol than the vanadium based catalyst (65.2 %). The oxidation of styrene gives at least four different products (Scheme 1.11), where expected product styrene oxide was found only in small yield (4.2-6.8 %), and the percentage of benzaldehyde was relatively high.

Oxidation of methyl phenyl sulfide gave as high as 96 % conversion with 97 % selectivity towards methyl phenyl sulfoxide and only 3 % towards methyl phenyl sulfone. It is concluded from the catalytic data and turn over frequency that encapsulated complexes are better catalysts than the neat ones. These catalysts are recyclable without loss of the catalytic potential. They do not leach in any of the catalytic reactions and are heterogeneous in nature [71].



19: Hsal-ambmz

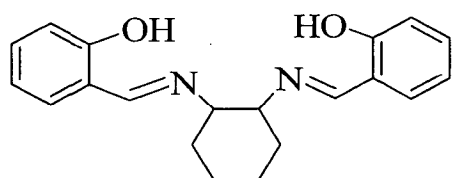
Scheme 1.10



Scheme 1.11

Maurya *et al.* have reported complexes $[\text{VO}(\text{sal-dach})]$ and $[\text{Cu}(\text{sal-dach})]$ ($\text{H}_2\text{sal-dach}$ (**20**) = Schiff base derived from salicylaldehyde and 1,2-diaminocyclohexane, Scheme 1.12) encapsulated in the super cages of zeolite-Y [72]. These complexes have potential catalytic activities for the oxidation of styrene, cyclohexene and cyclohexane. A maximum of 94.6 % conversion with five different oxidation products of styrene has been obtained with $[\text{VO}(\text{sal-dach})]$ -Y. The selectivity of these products follows the order: benzaldehyde (54.5 %) > 1-phenylethane-1,2-diol (22.5 %) > benzoic acid (8.9 %) > styrene oxide (7.6 %) > phenyl acetaldehyde (4.9 %). With four products having selectivity order: benzaldehyde (69.0 %) > styreneoxide (12.9 %) > phenyl acetaldehyde (12.0 %) > benzoic acid (7.1 %), $[\text{Cu}(\text{sal-dach})]$ -Y gave only 12.7 % conversion. With 86.6 % conversion of cyclohexene for $[\text{VO}(\text{sal-dach})]$ -Y, the selectivity of four different products follow the order: 2-cyclohexene-1-one (53.1 %) > 2-cyclohexene-1-ol (27.9 %) > cyclohexane-1,2-diol (10.4) > cyclohexeneoxide (5.0 %). $[\text{Cu}(\text{sal-dach})]$ -Y gave only 18.1 % conversion and only three products have been obtained

with the following order of selectivity: 2-cyclohexene-1-ol (49.2 % %) > 2-cyclohexene-1-one (32.0 %) > cyclohexeneoxide (18.8 %). This order of catalytic activity is reverse during the oxidation of cyclohexane. A maximum of 78.1 % of cyclohexane with [Cu(sal-dach)]-Y and only 21.0 % with [VO(sal-dach)]-Y has been obtained where selectivity of three major products follows the order: cyclohexanol > cyclohexane-1,2-diol > cyclohexanone. These complexes are stable and do not leach during the catalytic reaction as have been confirmed by testing the filtrate for the corresponding metal ion and thus suggest their heterogeneous nature.

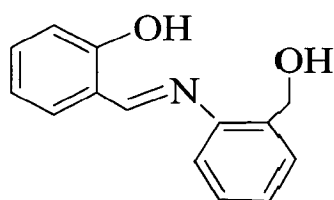


H₂sal-dach (20)

Scheme 1.12

The zeolite encapsulated metal complexes, [VO(sal-oaba)(H₂O)]-Y, [Cu(sal-oaba)(H₂O)]-Y and [Ni(sal-oaba)(H₂O)₃]-Y with H₂sal-oaba (21, Scheme 1.13) have been reported by Maurya *et al.* [73]. Catalytic activities of these complexes have been tested for the oxidation of styrene, cyclohexane and methyl phenyl sulfide using H₂O₂ as oxidant. Styrene catalysed by [VO(sal-oaba)(H₂O)]-Y gives five reaction products, styrene oxide, benzaldehyde, 1-phenylethane-1,2-diol, benzoic acid and phenylacetaldehyde. Except, 1-phenylethane-1,2-diol, all four products have also been obtained with [Cu(sal-oaba)(H₂O)]-Y. Styrene oxide, an important product has been obtained only in poor yield, while the yield of benzaldehyde is highest. Complex, [Ni(sal-oaba)(H₂O)₃]-Y gave benzaldehyde selectively, though conversion is only 6.6 %. With 45.8 % conversion of cyclohexane by [Cu(sal-oaba)(H₂O)]-Y, the selectivity of two products follow the order: cyclohexanone (50.7 %) > cyclohexanol (44.8 %). [VO(sal-oaba)(H₂O)]-Y

has shown only 14.8 % conversion. No oxidation of substrates has been observed in absence of catalysts. A maximum of 93.2 % conversion of methyl phenyl sulfide has been achieved with $[\text{VO}(\text{sal-oaba})(\text{H}_2\text{O})]\text{-Y}$ using H_2O_2 as oxidant, where selectivity of sulfoxide and sulfone are 96.9 % and 3.1 %, respectively. Other catalysts are found inactive towards the oxidation of methyl phenyl sulfide. Neat complex, $[\text{VO}(\text{sal-oaba})]$ has shown equally good catalytic activity. All heterogeneous catalysts are stable and free from leaching as have been confirmed by testing the filtrate for the corresponding metal ion. They are recyclable at least up to two cycles.



21: $\text{H}_2\text{sal-oaba}$

Scheme 1.13

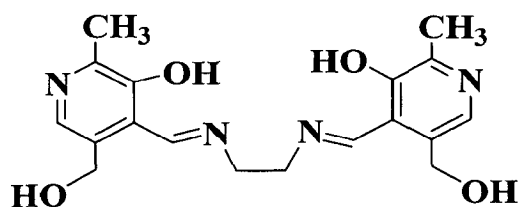
OBJECTIVE

OBJECTIVE

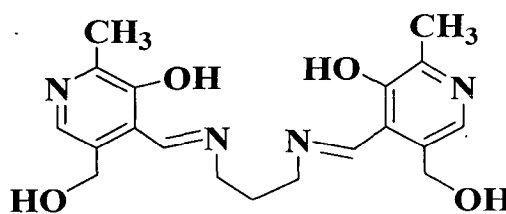
1.4. OBJECTIVE OF THE PRESENT INVESTIGATION

It is clear from the review of the literature that zeolite encapsulated metal complexes are potential catalysts, particularly for the oxidation reactions. It was, therefore, reasonable to undertake systematic study on the synthesis and characterization of new zeolite-Y encapsulated metal complexes and to explore their catalytic potential for the oxidation of organic substrates under optimized reaction conditions.

The present study is aimed to describe the syntheses and characterization of zeolite-Y encapsulated metal complexes of copper(II) with ligands H₂pydx-en (I) and H₂pydx-1,3-pn (II).



H₂pydx-en (I)



H₂pydx-1,3-pn (II)

Synthesized complexes have been well characterized and Catalytic potentials of these complexes have been tested considering the oxidation of the following reactions.

- (i) Oxidation of styrene
- (ii) Oxidation of cyclohexene
- (iii) Oxidation of methyl phenyl sulfide

Various parameters as mentioned below have been optimized to effect maximum oxidation of substrates.

- Concentration of Oxidant
- Amount of Catalyst
- Volume of Solvent
- Type of Oxidant
- Type of Catalyst
- Reaction Time

CHAPTER – 2

EXPERIMENTAL

2.1. MATERIALS

Analytical reagents grade pyridoxal hydrochloride (Hpydx.HCl, Himedia, Mumbai, India) acetylacetone (Hacac, Aldrich, Milwaukee, U.S.A.), methyl phenyl sulfide (Alfa Aeser, U.S.A.), styrene, cyclohexene (Acros Organics, New Jersey, U.S.A.), cupric nitrate (E. Merck, Mumbai, India) and 30 % aqueous H₂O₂ (Qualigens, Mumbai, India) were used as obtained. Y-zeolite (Si/Al = 10) was obtained from Indian Oil Corporation (R&D), Faridabad, India. All other chemicals and solvents used were of AR grade. Ligands H₂pydx-en and H₂pydx-pn were prepared as described in the literature [74, 75].

2.2. PREPARATIONS

2.2.1. Preparation of [Cu(pydx-en)].CH₃OH, 1

A stirred solution of H₂pydx-en (0.05 g, 2 mmol) dissolved in methanol (20 mL) was added to cupric acetate (0.20 g, 2mmol) dissolved in methanol (30 mL) with stirring and the reaction mixture was refluxed on a water bath for 5 h. On reducing the solvent volume to ca. 20 mL and keeping to ambient temperature a brown solid of [Cu(pydx-en).CH₃OH] slowly separated out within few hours. This was filtered off, washed with methanol and dried in vacuum over silica gel. Yield: 78 %. C₁₉H₂₄N₄O₅Cu (435.97) [Cu(pydx-en)].CH₃OH: Calcd. C, 52.35; H, 5.55; N, 12.85; Cu, 14.58 %. Observed: C, 52.21; H, 5.59; N, 12.78; Cu, 14.07 %.

2.2.2. Preparation of [Cu(pydx-1,3-pn)].CH₃OH, 2

[Cu(pydx-1,3-pn)] was prepared following essentially the same procedure as for 1. The light brown solid was obtained. Yield: 65 %. Brown crystals suitable for X-ray diffraction study were obtained from filtrate on keeping it for slow evaporation at ambient temperature (30°C) yield: 70 %. C₁₉H₂₄N₄O₅Cu (450.0) [Cu(pydx-1,3-pn)].CH₃OH: Calcd. C, 53.38; H, 5.82; N, 12.45; Cu, 14.12 %. Observed: C, 52.85; H, 5.75; N, 12.55; Cu, 13.85 %.

2.2.3. Preparation of Cu-Y

An amount of 5.0 g of Na-Y zeolite was suspended in 300 ml of distilled water and after addition of cupric nitrate (xx g, 12 mmol), the reaction mixture was heated at 90 °C for 24 h with stirring. The pale-bluish solid was filtered, washed with hot distilled water until filtrate was free from any copper(II) ion content, and dried at 150 °C for 24 h in an air oven. Observed: Cu, 7.60 %.

2.2.4. Preparation of [Cu(pydx-en)]-Y, 3

Cu-Y (3.0 g) and H₂pydx-en (3.0 g) were mixed in methanol (50 mL) and the reaction mixture was heated at reflux for 14 h in an oil bath with stirring. The resulting material was suction filtered and then Soxhlet extracted with methanol to remove unreacted ligand. It was finally treated with hot DMF while stirring for 1 h, filtered, washed with DMF followed by hot methanol. The uncomplexed metal ions present in the zeolite were removed by stirring with doubly distilled aqueous 0.01 M NaCl (150 ml) for 10 h. The resulting pale-yellow solid was filtered, washed with hot distilled water until no precipitate of AgCl is observed in filtrate on treating with AgNO₃. Finally it is dried at 120 °C for several hours. Observed: Cu, 0.79 %.

2.2.5. Preparation of [Cu(pydx-1,3-pn)]-Y, 4

The pale-yellow [Cu(pydx-1,3-pn)]-Y was prepared following essentially the same procedure as outlined for 3. Observed: Cu, 0.74 %.

2.3. PHYSICAL METHODS AND ANALYSIS

The copper content was measured using inductively coupled plasma (ICP^{spect}-_{me}) Labtam 8440 Plasmalab) after leaching the metal ions with conc. nitric acid and diluting with double distilled water to specific volumes. IR spectra were recorded as KBr pellet on a Nicolet NEXUS Aligent 1100 series FT-IR spectrophotometer after grinding the sample with KBr. Electronic spectra of zeolite encapsulated metal complexes were recorded in Nujol using a Shimadzu 1601 UV-vis spectrophotometer by layering a mull sample to inside of one of the cuvettes and keeping other one layered with Nujol as reference. Electronic spectra of other ligands neat complexes were recorded in methanol. X-ray powder diffractograms of solid catalysts were recorded using a Bruker AXS D8 advance X-ray powder diffractometer with a Cu-K α target. Thermogravimetric analyses of pure as well as encapsulated complexes were carried out using TG Stanton Redcroft STA 780. Scanning electron micrographs (SEM) of zeolite containing samples were recorded on a Leo instrument model 435VP. The sample were dusted on alumina and coated with a thin film of gold to prevent surface changing and to protect the surface material from thermal damage by electron beam. In all analysis, a uniform thickness of about 0.1 mm was maintained. The EPR spectra were recorded with a Bruker ESP 300E X-band spectrometer. For the polymer-anchored complex samples the spectra were measured at room temperature and for the neat complex samples in DMSO the EPR spectra were measured at 77 K (with glasses made by freezing the solutions in liquid nitrogen). The spin Hamiltonian parameters were obtained by simulation of the spectra with the computer program of Rockenbauer and Korecz.

Crystal data were collected on a Bruker SMART Apex CCD diffractometer at 153(2) K, using a graphite monochromator and Mo- K_{α} radiation ($\lambda = 0.71073$ Å). Hydrogen atoms were found, or placed into calculated positions and included in the last cycles of refinement. Absorption corrections were carried out with SADABS. The program systems SHELXS 86 and SHELXL 93 were used throughout for the treatment and refinement of the data.

All catalysed reaction products were analysed using Thermoelectron Gas Chromatograph fitted with HP-1 capillary column (30 m \times 0.25 mm \times 0.25 μ m) and FID detector.

2.4. CATALYTIC ACTIVITY

2.4.1. Oxidation of Styrene

The catalytic oxidation of styrene was carried out in a 50 ml flask fitted with a water-circulated condenser. In a typical reaction, an aqueous solution of 30% H₂O₂ or 70% *tert*-butylhydroperoxide (TBHP) (20 mmol) and styrene (1.04 g, 10 mmol) were mixed in acetonitrile (20 mL). After acquiring the temperature of the oil bath to 80 °C, the zeolite-Y encapsulated catalyst (0.025 g) was added to the reaction mixture and continuously stirred. During the reaction, the products were analysed by withdrawing small aliquots after specific interval of time using a gas chromatograph, and their identities were confirmed by GC-MS. Various parameters, such as amounts of oxidant and catalyst as well as the temperature of the reaction mixture were studied in order to see their effect on the conversion and patterns of the reaction products.

2.4.2. Oxidation of Cyclohexene

The catalytic oxidation of cyclohexene was also carried out using [Cu(pydx-en)]-Y and [Cu(pydx-1,3-pn)]-Y. An aqueous 30 % H₂O₂ (2.28 g, 20 mmol), cyclohexene (0.82 g, 10 mmol) and catalyst (0.025 g) were mixed in acetonitrile (20 mL) and the reaction mixture was heated at 75 °C with continuous

stirring in an oil bath. The progress of the reaction was monitored as mentioned above and identity of various products confirmed by GC-MS.

2.4.3. Oxidation of Methyl Phenyl Sulfide

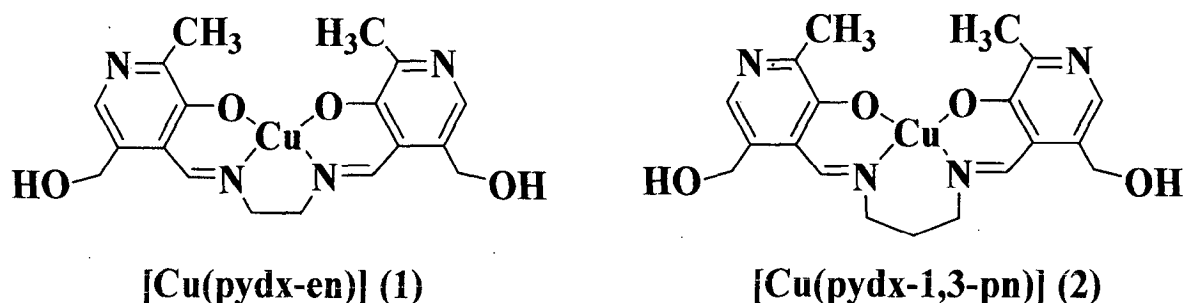
Aqueous 30 % H_2O_2 (2.28 g, 20 mmol) and catalyst (0.025 g) were added to a solution of methyl phenyl sulfide (1.24 g, 10 mmol) dissolved in acetonitrile (20 mL) and the reaction mixture was stirred at ambient temperature for 3 h. As mentioned above, GC monitored the formations of reaction products.

CHAPTER – 3

RESULTS AND DISCUSSIONS

3.1. SYNTHESIS AND CHARACTERIZATION OF CATALYSTS

Scheme 3.1 presents the structure of the neat complexes prepared in this study. Their structures are based on elemental and various spectroscopic studies and single crystal structure of 2.



Scheme 3.1

Reaction of cupric acetate with ligands $\text{H}_2\text{pydx-en}$ (**I**) and $\text{H}_2\text{pydx-1,3-pn}$ (**II**) in refluxing methanol yields $[\text{Cu}(\text{pydx-en})]$ (**1**) and $[\text{Cu}(\text{pydx-1,3-pn})]$ (**2**), respectively. Complex **1** has previously been isolated by reacting **I** with cupric acetate in aqueous solution. Encapsulation of these complexes in the nano-cavities of zeolite-Y involved the exchange of copper(II) ion with Na-Y in water followed by reaction of the metal exchanged zeolite-Y with **I** or **II** in methanol. This method is referred to as flexible ligand method. Here, these ligands enter into the cavity of zeolite-Y due to their flexible nature and interact with the metal ion to give $[\text{Cu}(\text{pydx-en})]\text{-Y}$ (**3**) and $[\text{Cu}(\text{pydx-1,3-pn})]\text{-Y}$ (**4**). Finally extraction of

impure samples with methanol using Soxhlet extractor removed excess free ligand and stirring in DMF removed neat metal complex formed on the surface of the zeolite, if any. The molecular formulae of the encapsulated complexes are based on the respective neat complex. As crude mass was extracted well, the metal content found after encapsulation is only due to the presence of copper(II) complexes in the super cages of the zeolite-Y.

3.1.1. Structure description of [Cu(pydx-1,3-pn)]-Y

The structure of complex [Cu(pydx-1,3-pn)].CH₃OH is shown in Figure 3.1. Crystal data of the complex is presented in Table 3.1 while bond lengths and bond angles are given in Table 3.2 and Table 3.3, respectively. There are two molecules in asymmetric unit, each having one methanol solvent. It is clear from the table that bond lengths of two Cu-Os are 1.887(4) and 1.948(4) Å and two Cu-Ns are 1.984(5) and 1.998(5) Å. The bond angle of O2-Cu1-O1 with the value of 82.10(18)° is less than 90° while of O2-Cu1-N2 with value of 92.32(19)° is more than 90°. Similarly, bond angles of O1-Cu1-N2 and O2-Cu1-N3 are 166.5(2) and 9.70(19)°, respectively indicating that these atoms are not linear. Thus, the complex has distorted square planer geometry with slight distortion towards tetrahedral. These bond lengths and bond angles are very similar to the one reported for similar complex [Ni(pydx-en)]. Structure of the complex is also very similar to [Ni(pydx-en)]. Pyridinic ring and alcoholic group of pyridoxal moiety do not participate in coordination. Each molecule is also associated with a solvent methanol in which crystals were grown. But the bond length of ca. 2.4 Å suggests no interaction of methanol with copper centre.

Table 3.1. Crystal Data and Structure Refinement Parameters for [Cu(pydx-1,3-pn)].CH₃OH.

	2
Empirical formula ^a	C ₄₀ H ₅₂ Cu ₂ N ₈ O ₈
Crystal system	Triclinic
Space group	P1
Unit cell dimensions:	
<i>a</i> , Å	8.0870(2)
<i>α</i> , deg	105.864(1)
<i>b</i> , Å	9.0492(2)
<i>β</i> , deg	90.903(1)
<i>c</i> , Å	14.2599(3)
<i>γ</i> , deg	95.512(1)
Cell volume, Å ³	998.20(3)
<i>Z</i>	13
Calculated density, g cm ⁻³	2.30
Absorption coefficient, mm ⁻¹	6.830
<i>F</i> (000)	662.7
Crystal size, mm	0.60 x 0.22 x 0.11
<i>θ</i> range for data collection, deg	2.4 to 30.0
Index ranges	-13 ≤ <i>h</i> ≤ 13, -15 ≤ <i>k</i> ≤ 15, -24 ≤ <i>l</i> ≤ 24
Reflections collected	17749
Independent reflections	13262
Completeness to <i>θ</i> (max), %	37.960
Data / restraints / parameters	13262/3/749
Goodness-of-fit on <i>F</i> ²	1.012
Final <i>R</i> indices [<i>I</i> > 2σ(<i>I</i> ₀)]	<i>R</i> 1 = 0.068, <i>wR</i> 2 = 0.108
<i>R</i> indices (all data)	<i>R</i> 1 = 0.043, <i>wR</i> 2 = 0.097
Largest diff. Peak / hole, eÅ ⁻³	0.0959 and -0.623

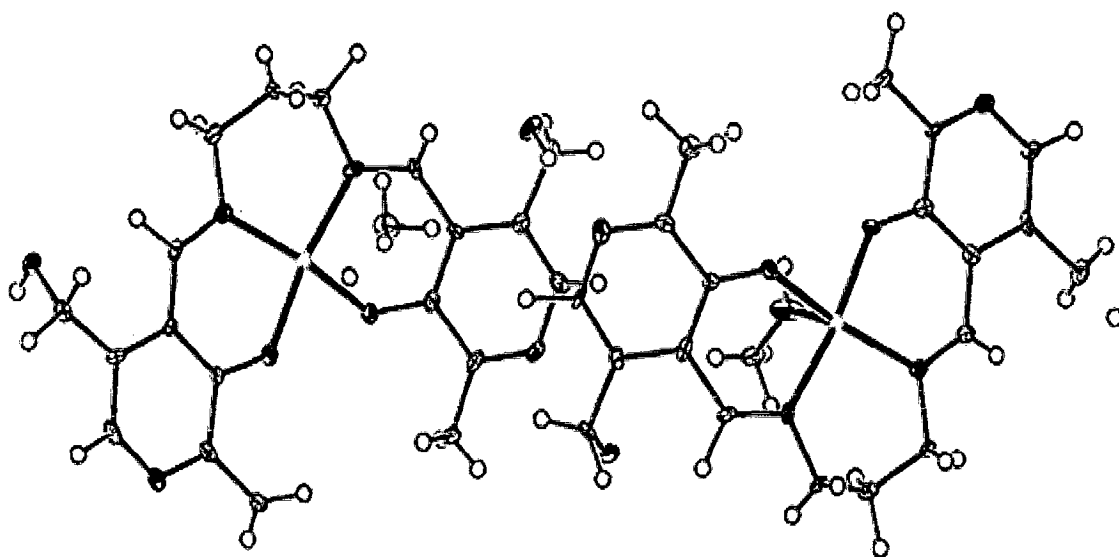


Figure 3.1. Crystal structure of $\{[\text{Cu}(\text{pydx-1,3-pn})] \cdot \text{CH}_3\text{OH}\}_2$. Both molecules of asymmetric unit are shown together.

N5-C27	1.353(7)	O5-H26	0.11(8)
C35-C34	1.446(7)	C21-H27	1.19(3)
C35-C36	1.507(8)	C21-H28	0.79(4)
C33-C34	1.404(8)	O10-C40	1.410(7)
C33-C38	1.448(8)	O10-H52	0.84(3)
C33-C32	1.458(8)	C31-H38	1.18(4)
C6-C5	1.413(7)	C31-H39	0.98(4)
C6-C7	1.436(7)	C16-H17	0.80(5)
C25-C30	1.434(7)	C16-H16	0.85(4)
C25-C24	1.485(7)	C16-H18	0.88(4)
C5-C10	1.400(8)	C28-H35	1.15(4)
C5-C4	1.431(8)	C28-H34	1.04(4)
C12-H15	0.73(4)	C28-H36	1.08(4)
C7-C8	1.484(8)	C40-H50	1.03(5)
C15-C14	1.437(7)	C40-H49	0.80(9)
C15-C16	1.488(8)	C40-H51	0.99(3)
C10-C9	1.397(8)	C20-H24	0.91(4)
C10-C11	1.505(8)	C20-H25	0.93(5)
C38-C37	1.339(8)	C20-H23	0.99(4)

Table 3.3. Various bond angles in [Cu(pydx-1,3-pn)].CH₃OH

Bond Angle	(°)
O2-Cu1-O1	82.10(18)
O2-Cu1-N2	92.32(19)
O1-Cu1-N2	166.5(2)
O2-Cu1-N3	169.70(19)
O1-Cu1-N3	87.74(19)
N2-Cu1-N3	97.96(19)
O2-Cu1-O5	90.14(18)
O1-Cu1-O5	94.5(2)
N2-Cu1-O5	97.8(2)
N3-Cu1-O5	88.99(18)
O7-Cu2-O6	82.10(17)
O7-Cu2-N6	170.13(18)
O6-Cu2-N6	88.09(18)
O7-Cu2-N7	92.22(18)
O6-Cu2-N7	166.80(19)
N6-Cu2-N7	97.60(18)
O7-Cu2-O10	90.11(18)
O6-Cu2-O10	94.14(19)
N6-Cu2-O10	89.52(18)
N7-Cu2-O10	97.8(2)
C26-O6-Cu2	122.5(3)
C14-O1-Cu1	124.0(4)
C34-O7-Cu2	128.2(4)
C24-N6-C23	115.7(5)
C24-N6-Cu2	122.5(4)
C23-N6-Cu2	121.3(3)
C6-O2-Cu1	129.3(4)
C4-N2-C3	113.6(5)
C4-N2-Cu1	124.0(4)
C3-N2-Cu1	122.4(4)
C32-N7-C21	114.8(5)
C32-N7-Cu2	124.3(4)
C21-N7-Cu2	121.0(4)
C12-N3-C1	116.7(5)
C12-N3-Cu1	123.3(4)
C1-N3-Cu1	119.9(4)
C11-O4-H14	105.5(19)
C19-O3-H22	105(2)
C31-O8-H40	111(10)
C39-O9-H48	131(10)
C35-N8-C37	119.1(5)
C18-C19-H21	116(2)
H20-C19-H21	90(3)
C29-C30-C25	116.8(5)
C29-C30-C31	120.9(5)
C25-C30-C31	122.1(5)
C7-C8-H9	110.4(17)
C7-C8-H8	106(2)
H9-C8-H8	122(3)
C7-C8-H10	110(4)
H9-C8-H10	110(5)
H8-C8-H10	98(5)
N6-C23-C22	111.8(5)
N6-C23-H32	105(2)
C22-C23-H32	105(3)
N6-C23-H31	108(2)
C22-C23-H31	122(2)
H32-C23-H31	102(3)
C1-C2-C3	112.5(5)
C1-C2-H4	108(4)
C3-C2-H4	106(4)
C1-C2-H3	110(3)
C3-C2-H3	117(3)
H4-C2-H3	103(5)
N2-C3-C2	113.2(5)
N2-C3-H6	109(2)
C2-C3-H6	110(2)
N2-C3-H5	109.3(19)
C2-C3-H5	107.8(19)
H6-C3-H5	107(3)
C18-C17-N4	123.0(5)
C18-C17-H19	123(3)
N4-C17-H19	113(3)
N1-C9-C10	124.8(5)
N1-C9-H11	114.8(18)
C10-C9-H11	119.4(18)
O4-C11-C10	115.1(5)
O4-C11-H13	102(2)
C10-C11-H13	108(2)
O4-C11-H12	104(2)
C10-C11-H12	112(2)
H13-C11-H12	115(3)

C15-N4-C17	120.4(5)	C35-C36-H42	112(2)
C18-C13-C12	119.5(5)	C35-C36-H44	106(3)
C18-C13-C14	118.3(5)	H42-C36-H44	92(3)
C12-C13-C14	121.9(5)	C35-C36-H43	110.7(19)
C7-N1-C9	118.4(5)	H42-C36-H43	117(3)
O6-C26-C25	124.9(5)	H44-C36-H43	118(4)
O6-C26-C27	119.7(4)	C38-C37-N8	123.0(5)
C25-C26-C27	115.4(5)	C38-C37-H45	116(2)
C29-N5-C27	118.0(5)	N8-C37-H45	120(2)
N8-C35-C34	123.4(5)	N5-C29-C30	125.1(5)
N8-C35-C36	119.2(5)	N5-C29-H37	115(2)
C34-C35-C36	117.3(5)	C30-C29-H37	120(2)
C34-C33-C38	118.5(5)	N2-C4-C5	126.7(5)
C34-C33-C32	121.6(5)	N2-C4-H7	117(2)
C38-C33-C32	119.9(5)	C5-C4-H7	116(2)
O2-C6-C5	124.4(5)	C17-C18-C13	118.7(5)
O2-C6-C7	116.6(5)	C17-C18-C19	117.9(5)
C5-C6-C7	119.0(5)	C13-C18-C19	123.3(5)
C26-C25-C30	120.8(5)	O9-C39-C38	114.5(5)
C26-C25-C24	119.9(5)	O9-C39-H47	121(3)
C30-C25-C24	119.2(5)	C38-C39-H47	111(3)
C10-C5-C6	118.8(5)	O9-C39-H46	113(3)
C10-C5-C4	119.1(5)	C38-C39-H46	113(3)
C6-C5-C4	122.1(5)	H47-C39-H46	81(4)
N3-C12-C13	125.9(5)	O9-C39-H48	4(4)
N3-C12-H15	115(3)	C38-C39-H48	114(3)
C13-C12-H15	119(3)	H47-C39-H48	118(4)
N1-C7-C6	121.3(5)	H46-C39-H48	115(5)
N1-C7-C8	119.8(5)	C20-O5-Cu1	134.6(4)
C6-C7-C8	118.9(5)	C20-O5-H26	111(10)
N4-C15-C14	120.2(5)	Cu1-O5-H26	112(10)
N4-C15-C16	119.8(5)	N7-C21-C22	113.6(4)
C14-C15-C16	120.0(5)	N7-C21-H27	106.7(15)
O7-C34-C33	126.1(5)	C22-C21-H27	108.4(15)
O7-C34-C35	117.2(5)	N7-C21-H28	108(3)
C33-C34-C35	116.7(5)	C22-C21-H28	114(3)
O1-C14-C13	122.0(5)	H27-C21-H28	106(3)
O1-C14-C15	118.5(5)	C40-O10-Cu2	135.3(4)
C13-C14-C15	119.5(5)	C40-O10-H52	111(2)
C5-C10-C9	117.7(5)	Cu2-O10-H52	113(2)
C5-C10-C11	123.7(5)	O8-C31-C30	112.9(5)
C9-C10-C11	118.5(5)	O8-C31-H38	104.8(17)
C37-C38-C33	119.3(5)	C30-C31-H38	111.0(18)
C37-C38-C39	119.7(5)	O8-C31-H39	102(2)
C33-C38-C39	121.0(5)	C30-C31-H39	105(2)
N6-C24-C25	125.9(5)	H38-C31-H39	122(3)

N6-C24-H33	118.5(17)	C15-C16-H17	107(3)
C25-C24-H33	115.2(17)	C15-C16-H16	103(2)
N7-C32-C33	126.6(5)	H17-C16-H16	124(4)
N7-C32-H41	119(3)	C15-C16-H18	110(3)
C33-C32-H41	114(3)	H17-C16-H18	114(4)
N3-C1-C2	112.0(4)	H16-C16-H18	97(3)
N3-C1-H1	110.1(16)	C27-C28-H35	115(2)
C2-C1-H1	110.2(17)	C27-C28-H34	113(2)
N3-C1-H2	109.0(17)	H35-C28-H34	88(3)
C2-C1-H2	102.8(16)	C27-C28-H36	109(2)
H1-C1-H2	113(2)	H35-C28-H36	123(3)
N5-C27-C26	123.9(5)	H34-C28-H36	107(3)
N5-C27-C28	117.8(5)	O10-C40-H50	116(3)
C26-C27-C28	118.3(5)	O10-C40-H49	122(6)
C21-C22-C23	113.2(4)	H50-C40-H49	103(7)
C21-C22-H29	106(3)	O10-C40-H51	110(2)
C23-C22-H29	114(3)	H50-C40-H51	90(3)
C21-C22-H30	109(2)	H49-C40-H51	110(7)
C23-C22-H30	102(2)	O5-C20-H24	110(3)
H29-C22-H30	114(3)	O5-C20-H25	105(3)
O3-C19-C18	113.2(5)	H24-C20-H25	133(4)
O3-C19-H20	107(3)	O5-C20-H23	109(2)
C18-C19-H20	112(3)	H24-C20-H23	108(4)
O3-C19-H21	115(2)	H25-C20-H23	89(4)

3.1.2. Scanning electron micrograph studies

Figure 3.2 presents the scanning electron micrographs of Cu-Y (A), [Cu(pydx-en)]-Y (B) [Cu(pydx-1,3-pn)]-Y (C) . It is clear from the micrographs that copper-exchanged zeolites as well as copper complexes entrapped zeolites have well defined crystals and there is no indication of the presence of any metal ions or complexes on the surface. It has not been possible to see any morphological changes on the surface on encapsulation of the complexes in the cavity possibly due to their poor loading.

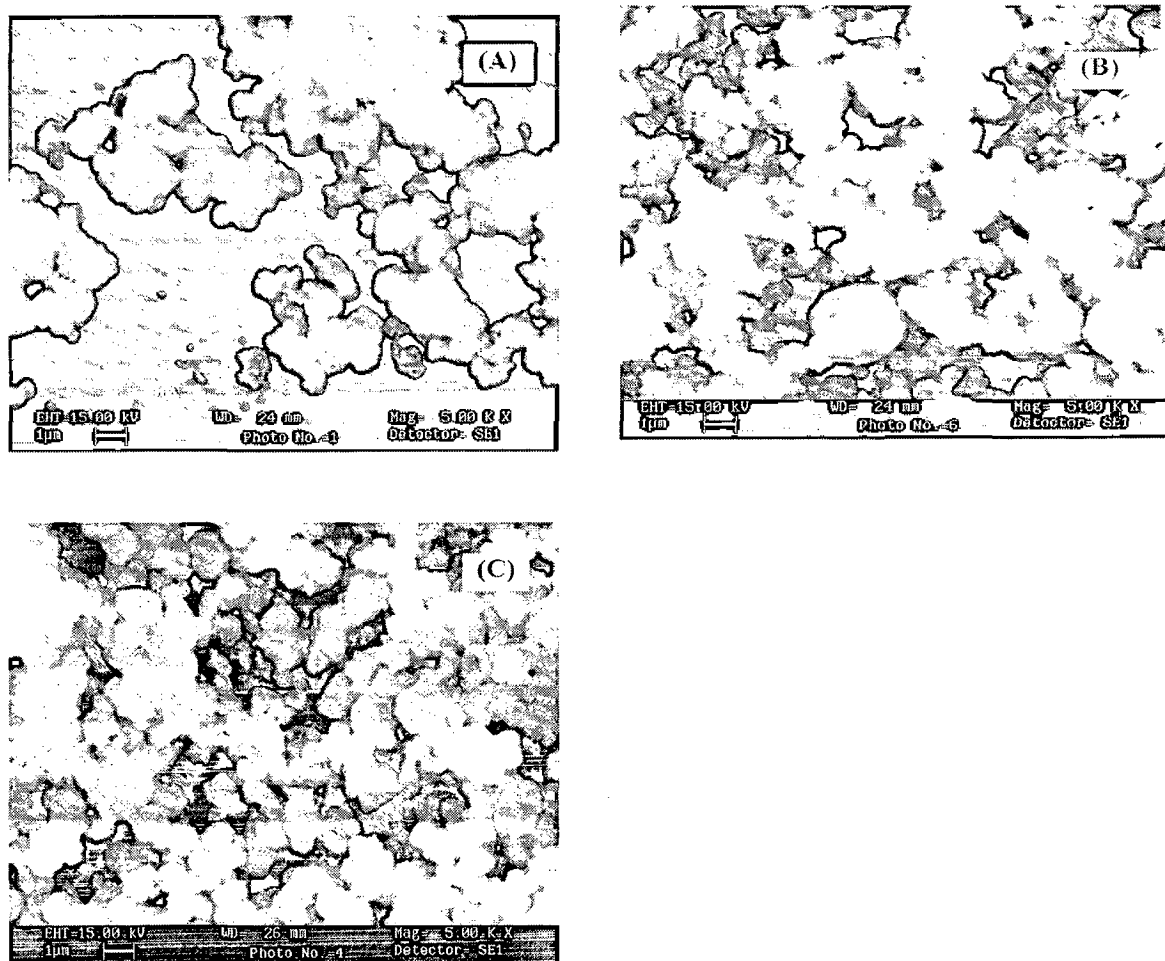


Figure 3.2. Scanning electron micrograph of Cu-Y (A), [Cu(pydx-en)]-Y (B) and [Cu(pydx-1,3-pn)]-Y (C).

3.1.3. Powder X-ray diffraction studies

The powder X-ray diffraction patterns of Na-Y, Cu-Y and encapsulated copper(II) complexes were recorded at 2θ values between 5 and 70° and some representative patterns are presented in Figure 3.3. Essentially similar diffraction patterns in encapsulated complexes, Cu-Y and Na-Y has been noticed except a slight weak intensity of the zeolite having metal complexes encapsulated. These observations indicate that the framework of the zeolite has not undergone any significant structural changes during encapsulation i.e. crystallinity of the zeolite-Y is preserved.

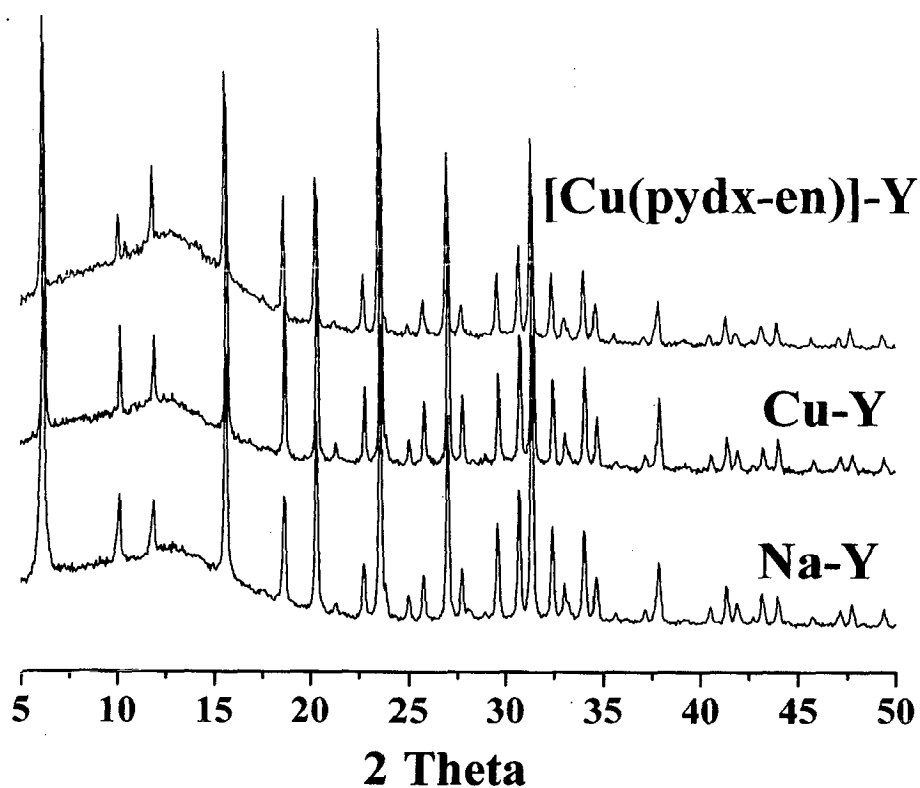


Figure 4. XRD patterns of Na-Y, Cu-Y and [Cu(pydx-en)-Y (3).

3.1.4. Thermogravimetric analysis studies

The TG, DTA and DTG profiles of the representative complex, [Cu(pydx-en)]-Y is presented in Figure 3.4. The decomposition of complexes 3 and 4 occurs in three overlapping steps. An endothermic loss of trapped water occurs between 80 – 200 °C while exothermic removal of extra-zeolite water occurs between 300 – 350 °C. This is followed by endothermic loss of ligand's residue, which continues till the removal of all organic mass at ca. 700 °C. A very low percentage weight loss (ca. 10 %) for ligands indicates the presence of only small amount of metal complexes in the cavities of zeolite. This is in agreement with the low copper content estimated for these complexes.

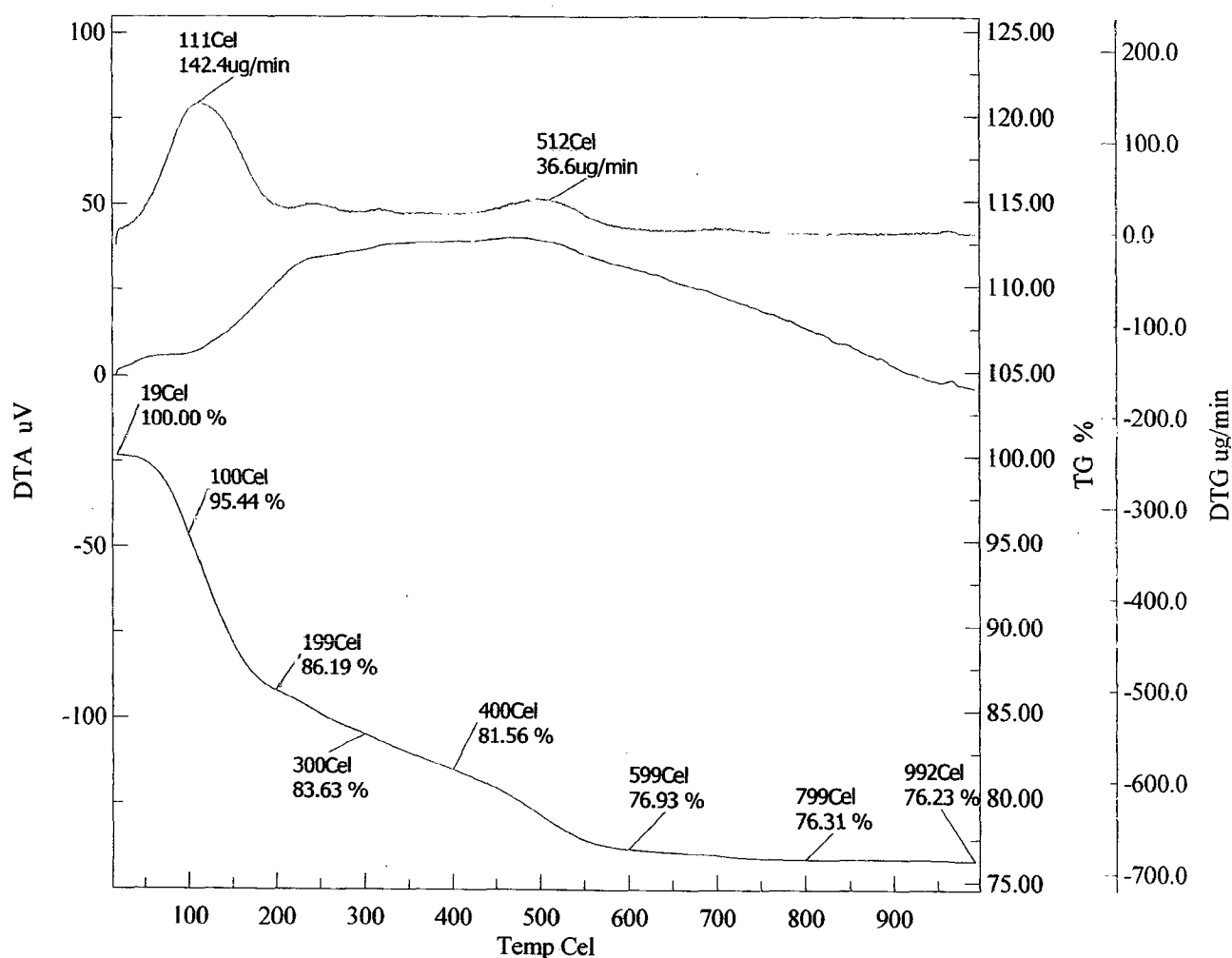


Figure 3.4. TGA, DTA and DTG profiles of [Cu(pydx-en)]-Y.

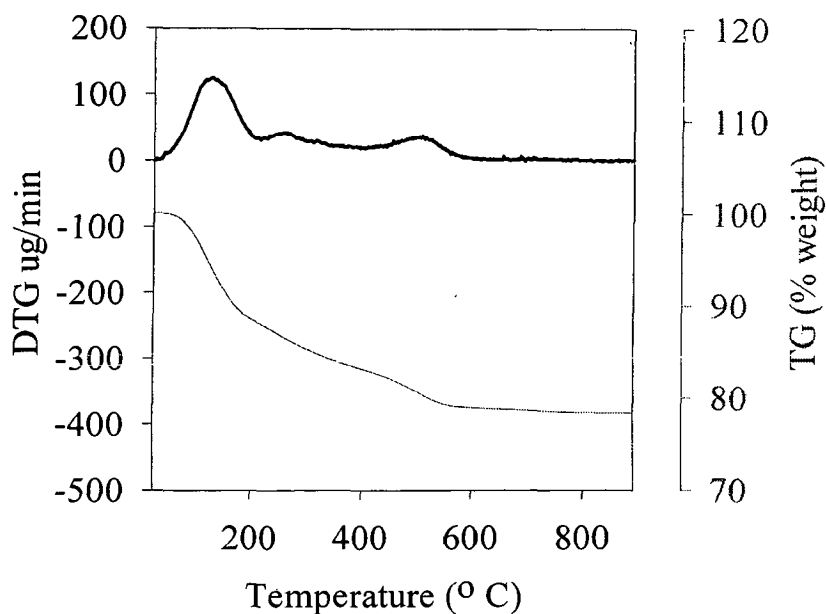


Figure 3.4.1. TGA (lower solid line) and DTG (upper dark solid line) profiles of [Cu(pydx-1,3pn)]-Y.

Complex 1 decomposes in two major steps. A weight loss of 7.8%, equivalent of methanol, occurs up to ca. 130 °C. The anhydrous complex is stable up to 290 °C and there after decomposes in a single major step that completes at 360 °C. The stabilization and formation of a final residue of 18.1 % (cal. 18.4 % for CuO) occurs at ca. 800 °C. A slightly different decomposition pattern has been observed for **2**, where decomposition of anhydrous complex occurs in two overlapping steps. The decomposition of **2** completes at ca. 375 °C. The residue of 18.1 % further loses weight up to ca 800 °C and stabilizes at 17.46 %. The calculated residue for CuO of 17.6% matches with the observed value.

3.1.5. IR Spectral studies

A partial list of IR spectral data is presented in Table 3.4. The intensity of the peaks in encapsulated complexes is, though, weak due to their low concentration in zeolite matrix, the spectra of the encapsulated as well as their neat complexes showed essentially similar bands. Comparison of the spectra of these complexes with the respective ligand provides evidence for the coordinating mode of ligands in complexes. The ligand H₂pydx-en exhibits a medium intensity band around 2700 cm⁻¹ due to intra-molecular hydrogen bonding. Absence of this band in the spectra of neat as well encapsulated complexes indicates the destruction of the hydrogen bond followed by the coordination of phenolic oxygen after deprotonation. A sharp band appearing at 1626 cm⁻¹ (in **I**) or at 1632 cm⁻¹ (in **II**) due to the $\nu(\text{C}=\text{N})$ (azomethine), shifts to higher wave number in complexes thereby suggesting the coordination of azomethine nitrogen. Several multiple bands of medium intensity covering the region 2850 – 3000 cm⁻¹ have been observed due to the presence of methylene group. The spectral patterns of these complexes are similar to [Cu(pydx-en)] reported in the literature [75].

Table 3.4. IR and electronic spectral data of ligand, pure and encapsulated complexes.

Compound	IR /cm ⁻¹		Electronic	
	$\nu(\text{OH})$	$\nu(\text{C}=\text{N})$	Solvent	$\lambda_{\text{Max}}/ \text{nm}$
H ₂ pydx-en (I)	3280 – 3450	1626	CH ₃ OH	216, 252, 335
H ₂ pydx-1,3-pn (II)	2846 – 3480	1632	CH ₃ OH	215, 252, 334
[Cu(pydx-en)] (1)	ca. 3400	1634	CH ₃ OH	207, 283, 374
[Cu(pydx-1,3-pn)] (2)	ca. 3450	1635	CH ₃ OH	217, 246, 402
[Cu(pydx-en)]-Y (3)	ca. 3400	1633	Nujol	235, 277, 378
[Cu(pydx-1,3 pn)]-Y (4)	ca. 3450	1638	Nujol	233, 273, 377

3.1.6. Electronic spectral studies

Electronic spectral studies of **1** and its copper(II) complex **1** have been discussed earlier in detail in the literature [75]. Other complexes reported here exhibit very similar spectral patterns. The well-defined band at 590 nm in **1** and a broad band at 570 – 650 nm in **2** have been assigned due to d – d transition. Such d – d band in zeolite-encapsulated complexes could not be obtained due to their poor loading while ligand bands appearing in the UV region are similar to the ones observed for neat complexes. All these data are grouped together in Table 3.4 and spectra of neat and encapsulated complexes are presented in Figure 3.5, 3.5.1 and Figure 3.6.

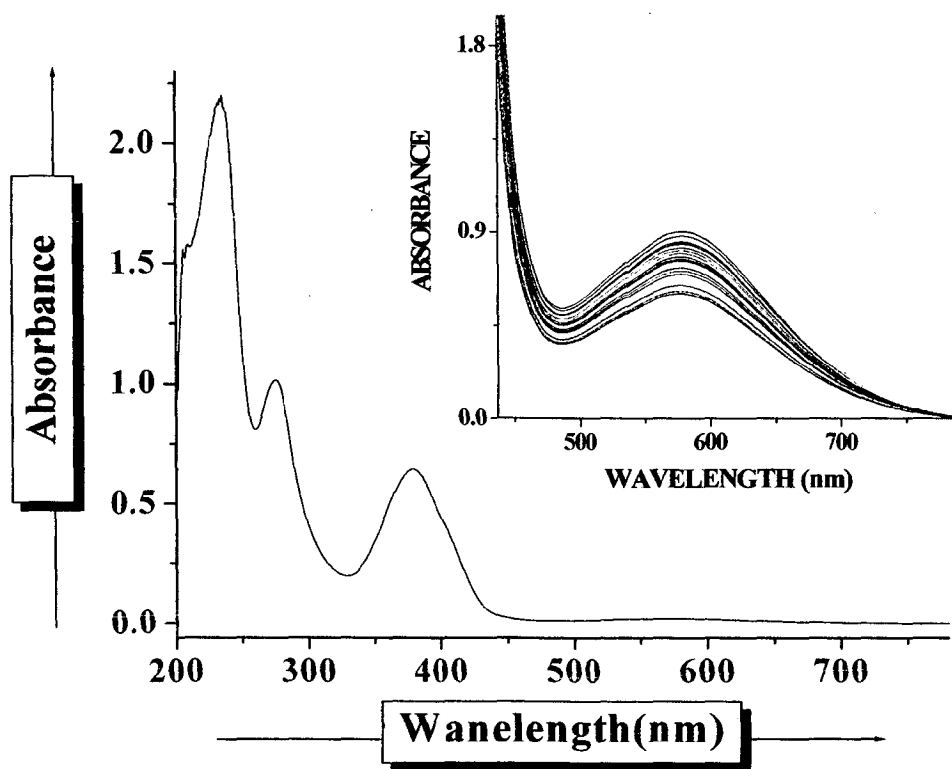


Figure 3.5. Electronic spectrum^{of} neat complex [Cu(pydx-en)]

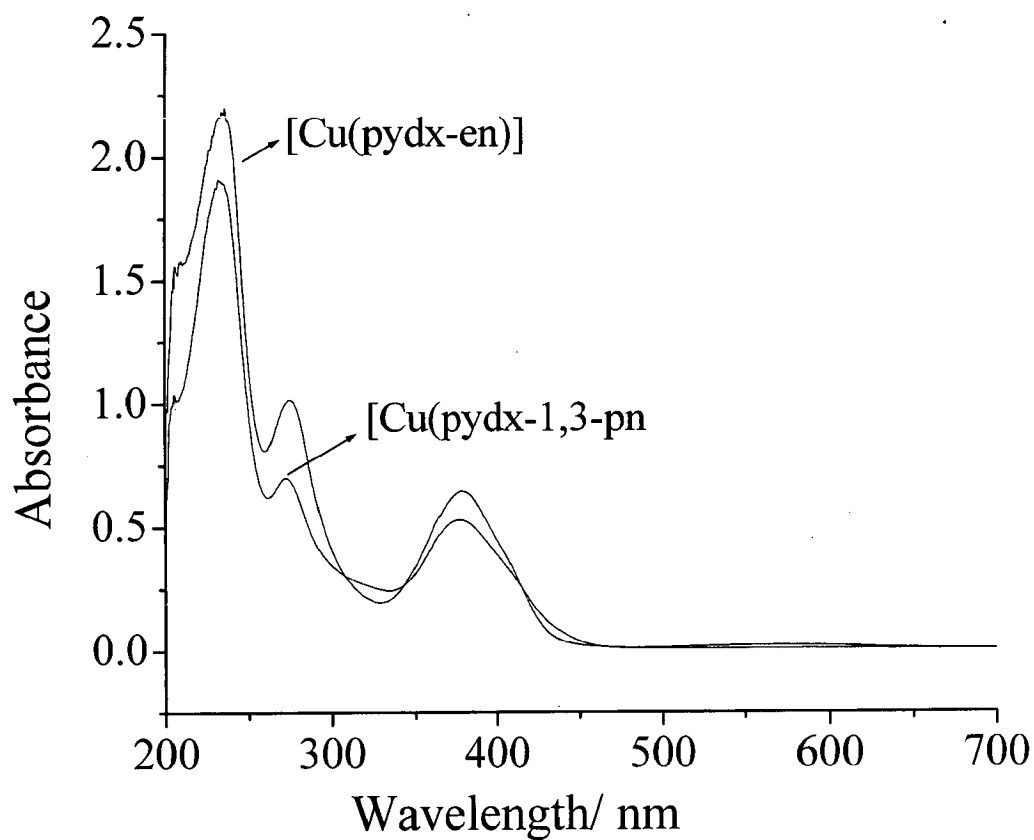


Figure 3.5.1. Electronic spectra of neat complexes [Cu(pydx-en)]and [Cu(pydx-1,3-pn)]

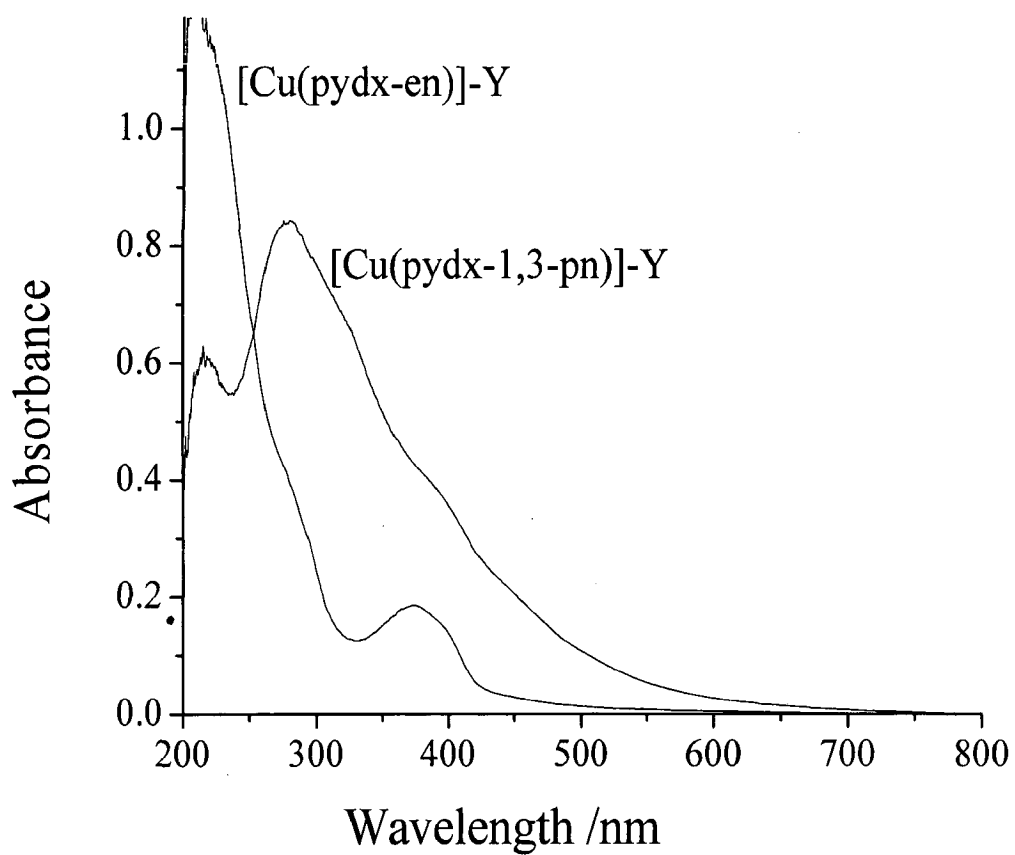
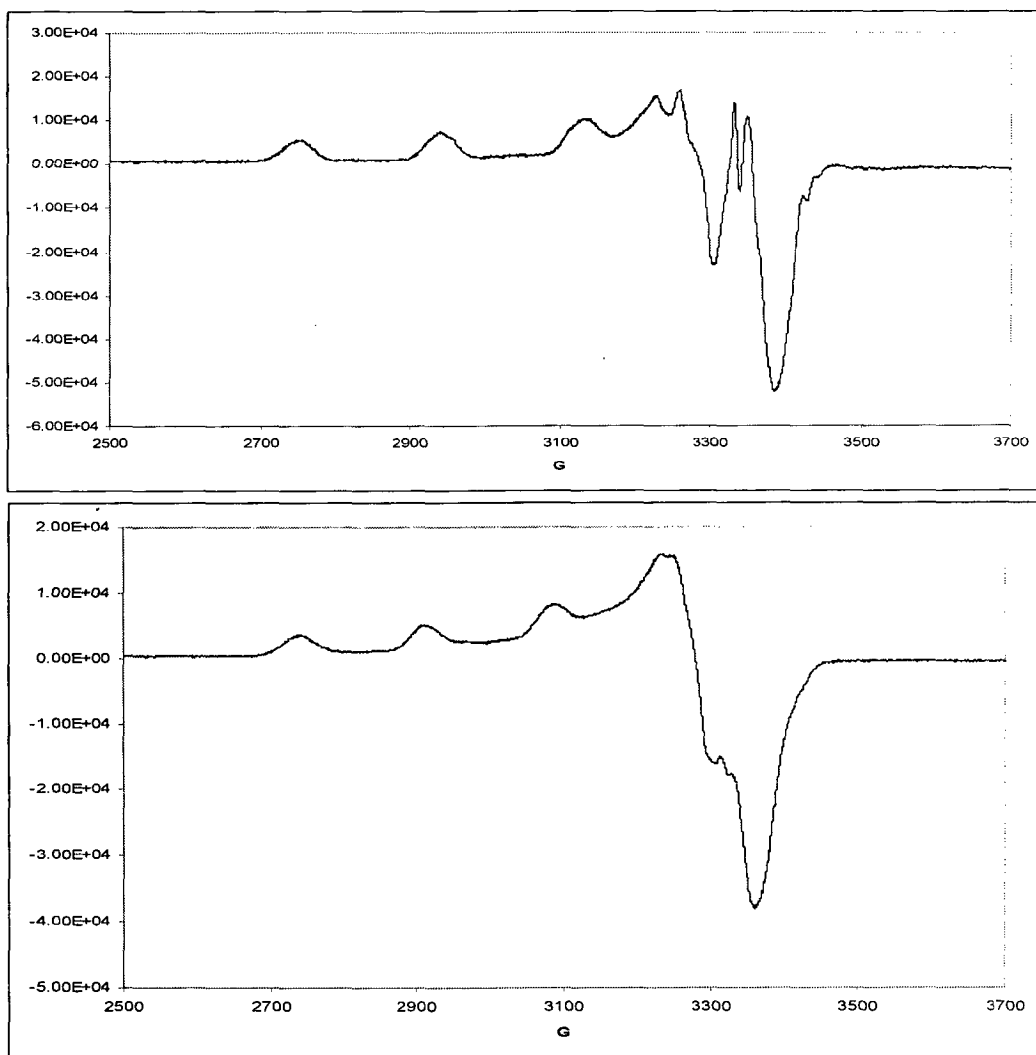


Figure 3.6. Electronic spectra of [Cu(pydx-en)]-Y and [Cu(pydx-1,3-pn)]-Y.

3.1.7. EPR studies

The EPR spectra of complexes [Cu(pydx-en)] and [Cu(pydx-1,3-pn)] were recorded in DMF at 77 K and Figure 3.8 presents the EPR spectra. In both cases, the Cu hyperfine structure is well defined. However, no superhyperfine “structure” resulting from the interaction of the unpaired d electron of Cu and the ^{14}N atoms ($I=1$) is observed. The calculated parameters are given Table 3.5.



presents a lower A_{\parallel} and a higher g_{\parallel} when compared with $[\text{Cu}(\text{pydx-en})]$. This could be compatible with a greater tetrahedral distortion of $[\text{Cu}(\text{pydx-1,3-pn})]$, in agreement with the higher flexibility of the ligand. The A_{\parallel} and g_{\parallel} obtained are in good agreement with those obtained for the corresponding $[\text{Cu}(\text{salen})]$ complexes [78 - 80].

The EPR spectra of the complexes encapsulated in zeolite-Y (Figure 3.9) are compatible with their presence as $\text{Cu}(\text{II})$ complexes with structures not much different from the “neat” analogues. In this case it is clear that either the dipolar interaction or the motional effects (or both) are operating in a stronger fashion. The superhyperfine structure is almost not seen.

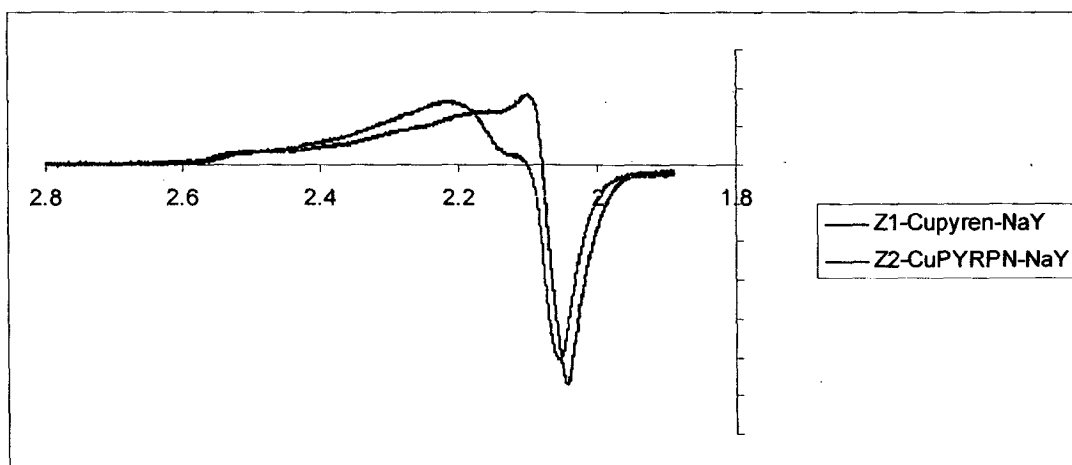


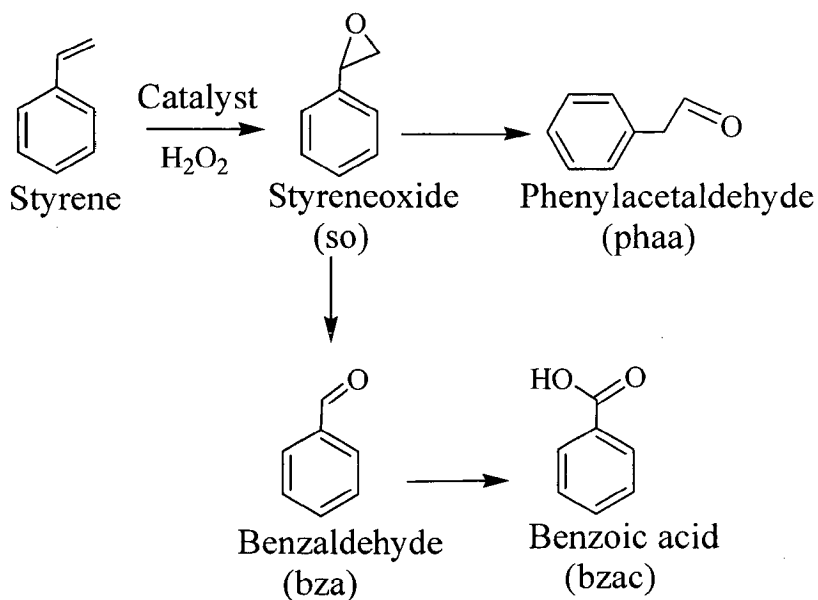
Figure 3.9. EPR spectra of the complexes encapsulated in zeolite-Y.

3.2. CATALYTIC ACTIVITY STUDIES

The catalytic activities of the zeolite encapsulated complexes as well the neat complexes have been demonstrated by studying the oxidation of styrene, cyclohexene and methylphenylsulfide.

3.2.1. Oxidation of styrene

The oxidation of styrene, catalysed by [Cu(pydx-en)]-Y and [Cu(pydx-1,3-pn)]-Y, was carried out using H₂O₂ and *tert*-butylhydroperoxide as oxidants to give styreneoxide and benzaldehyde, benzoic acid and phenylacetaldehyde (Scheme 3.3) along with minor amounts of unidentified products. Hulea *et al.* [81] have reported some of these products while using catalysts TS-1 and MCM-41. All oxidation products observed here were identified recently using polymer-anchored catalyst, PS-[VO(sal-ohyba).DMF] (H₂sal-ohyba = Schiff base derived from salicylaldehyde and *o*-hydroxybenzylamine)[10] and zeolite-Y encapsulated complex, [VO(sal-dach)]-Y (H₂sal-dach = Schiff base derived from salicylaldehyde and 1,2-diaminocyclohexane) [72].



Scheme 3.3

In search of suitable reaction conditions to achieve the maximum oxidation of styrene, catalyst **3** was taken as a representative and the effect of three different reaction parameters viz. amount of H_2O_2 (mole of H_2O_2 per mole of styrene), amount of catalyst and temperature of the reaction were studied.

Three different aqueous 30 % H_2O_2 to styrene molar ratio of 1:1, 2:1 and 3:1 were considered while keeping the fixed amount of styrene (1.04 g, 10 mmol) and catalyst (0.025 g) in CH_3CN (20 mL) at 80°C . The periodic analyses of results up to 6 h are illustrated in Figure 3.10. Increasing the H_2O_2 / styrene ratio from 1:1 to 2:1 improved the conversion from 9.1 % to 14.8 % while 3:1 ratio showed further increment of conversion to hardly 1 %. Therefore, it is clear that the 2:1 molar ratio is the best one to obtain the optimum styrene conversion of 14.8 % in 6 h reaction time.

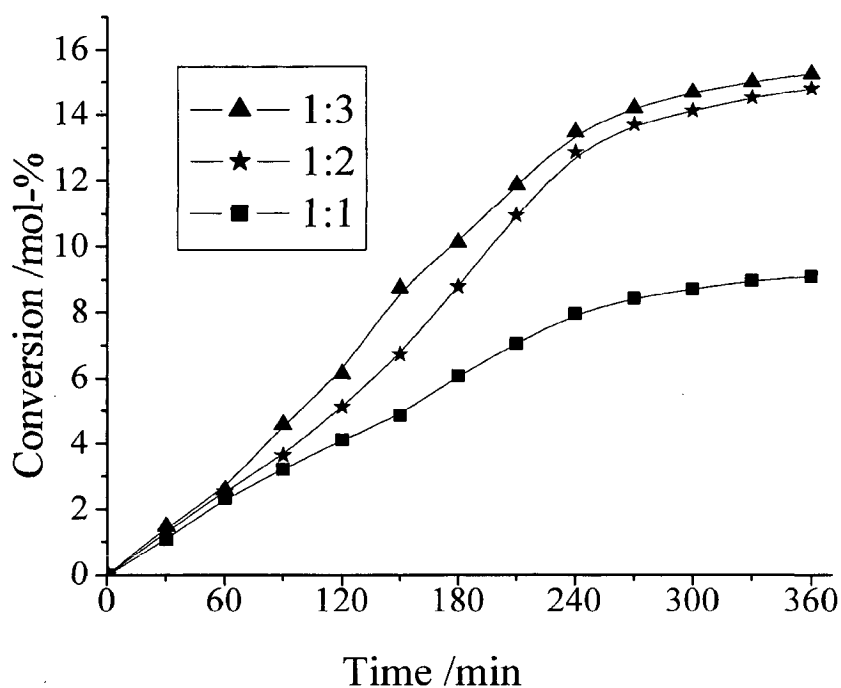


Figure 3.10. Effect of H_2O_2 on the oxidation of styrene. Reaction conditions: styrene (1.04 g, 10 mmol), $[\text{Cu}(\text{pydx-en})]\text{-Y}$ (**3**) (0.025 g), CH_3CN (20 mL) and temp. (80°C).

Similarly for three different amounts viz. 0.015, 0.025 and 0.035 g of [Cu(pydx-en)]-Y at styrene to aqueous 30 % H₂O₂ of 1:2 under above reaction conditions, 0.015 g of catalyst effected only 7.8 % conversion whereas 0.025 g catalyst gave a maximum conversion of 14.8 % in 6 h of reaction time. Further increment of catalyst (0.035 g) has shown no encouraging result; Figure 3.11. The reason for reduced activity at higher catalyst dose may possibly be attributed to adsorption/chemisorption of two reactants on separate catalyst particles, there by reducing the chance to interact.

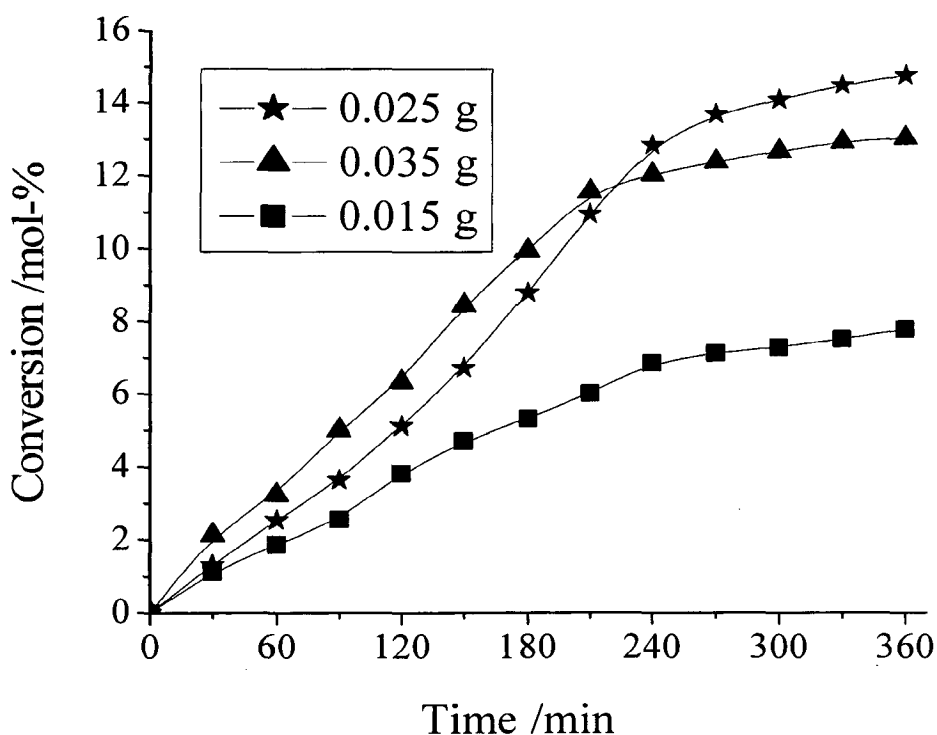


Figure 3.11. Effect of amount of catalyst on the oxidation of styrene. Reaction conditions: styrene (1.04 g, 10 mmol), 30 % H₂O₂ (), CH₃CN (20 mL) and temp. (80° C).

Figure 3.12 illustrates the oxidation of styrene at three different temperatures, viz. 60, 70 and 80 °C, while keeping the optimized conditions of 10 mmol styrene, 20 mmol H₂O₂ and 0.025 g catalyst in 20 ml of acetonitrile. It is

evident from the figure that the performance of the catalyst is poor at 60 °C wherein only 3.9 % conversion was observed. Increasing the reaction temperatures to 70 and 80° C increases the conversion to 7.0 % and 14.8%, respectively. Thus, conducting catalytic reaction at 80 °C is the most suitable one to maximize the oxidation of styrene.

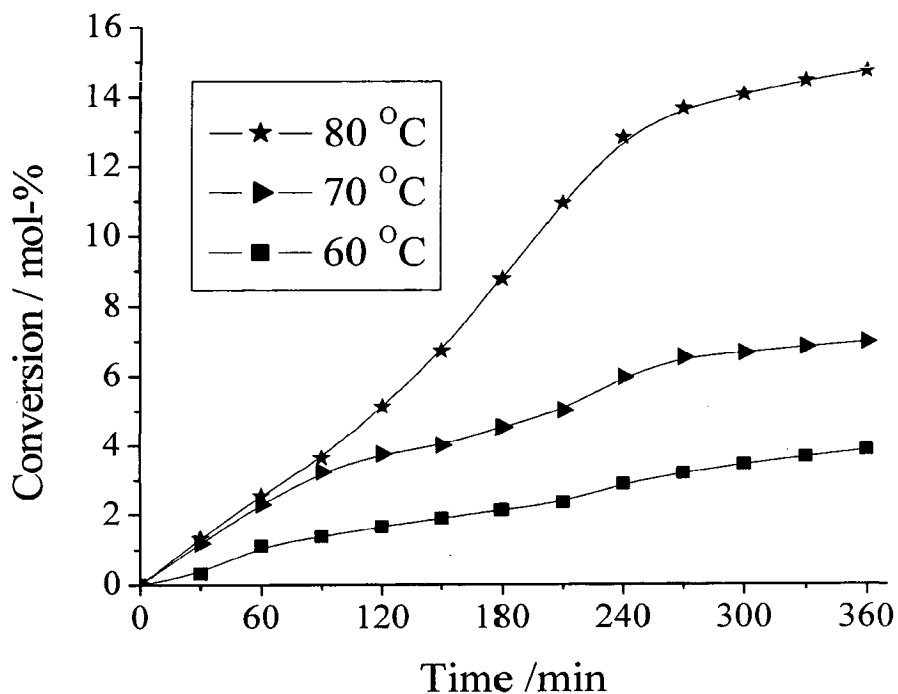


Figure 3.12. Effect of temperature on the oxidation of styrene. Reaction conditions: styrene (1.04 g, 10 mmol), [Cu(pydx-en)]-Y (0.025 g), 30 % H₂O₂ (2.27 g, 20 mmol) and CH₃CN (20 mL).

Thus, for the maximum oxidation of 10 mmol of styrene other required reagents as concluded were: [Cu(pydx-en)]-Y (0.025 g), H₂O₂ (2.27 g, 20 mmol), CH₃CN (20 ml) and temperature (80 °C). Under above optimized reaction conditions, the catalytic activity of [Cu(pydx-1,3-pn)]-Y was also tested and obtained results are compared in Figure 3.13. Table 3.6 compares the selectivity of various products obtained after 6 h of reaction time along with the percent

conversion of styrene and turn over frequency. It is clear from the table and figure that [Cu(pydx-1,3-pn)]-Y exhibits 18.5 % conversion and is better than that exhibited by [Cu(pydx-en)]-Y. Both the catalysts gave mainly two products, styrene oxide and benzaldehyde but the selectivity of benzaldehyde is very high than styrene oxide. A small amount of other products has also been obtained but their identifications have not been possible.

We have also tested the catalytic activity of the neat complexes **1** and **2**, using equimolar concentration of metal ion as in their respective zeolite encapsulated metal complex, for the oxidation of styrene. Figure 3.13 also provides the conversion as a function of time while Table 3.6 lists all other details. Thus, under the above reaction conditions, the obtained conversion of neat complexes (8.9 % for **1** and 11.6 % for **2**) is less than that shown by respective encapsulated complexes. Again, only two products with the selectivity order: benzaldehyde > styrene oxide have been obtained. Except a maximum of 9.9 % selectivity of styrene oxide in case of [Cu(pydx-en)], selectivity percentage of products calculated for other catalysts are almost same.

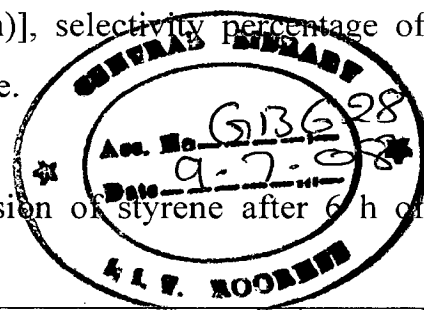
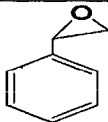
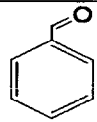


Table 3.6. Products selectivity and percent conversion of styrene after 6 h of reaction time with H₂O₂ as oxidant

Catalyst (H ₂ O ₂)	Conv. %	Product selectivity(%)			TOF h ^{-1b}
				Others	
[Cu(pydx-en)]-Y	14.8	4.7	88.6	6.7	79
[Cu(pydx-1,3-pn)]-Y	18.5	2.8	93.5	3.7	106
[Cu(pydx-en)]	8.9	9.9	84.6	5.5	852
[Cu(pydx-1,3-pn)]	11.6	3.1	95.4	1.5	1243

^b TOF h⁻¹ (Turn over frequency)-moles of substrate converted per mole of metal (in the solid catalyst) per hour.

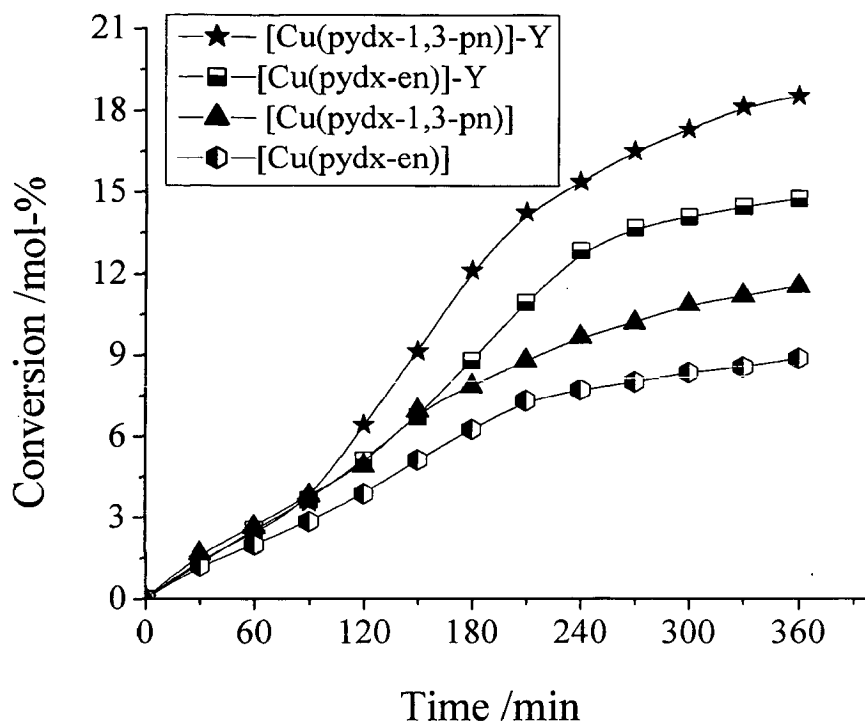


Figure 3.13. Catalytic comparison of zeolite-encapsulated and neat complexes for the oxidation of styrene in presence of H_2O_2 as oxidant. Reaction conditions: styrene (1.04 g, 10 mmol), catalyst (0.025 g for encapsulated and 0.00133 g in case of neat complexes), H_2O_2 (2.27 g, 20 mmol), CH_3CN (20 ml) and temperature (80°C).

Under the above optimized reaction conditions, the catalytic action of neat as well encapsulated complexes has also been tested using *tert*-butylhydroperoxide (TBHP) as an oxidant i.e. 70 % TBHP (2.57 g, 20 mol), catalyst (0.025 g for encapsulated and 0.00133 g, for neat complexes) and styrene (1.04 g, 10 mmol) were taken in CH_3CN (20 mL) and reaction was carried out at 80°C . Figure 3.14 provides the percentage conversion as a function of time and Table 3.7 compares the selectivity data along with the conversion percentage and turn over frequency after 6 h of reaction time. It is clear that the obtained percentage conversion varies in the range 13.6 to 28.0% with the order: $[\text{Cu}(\text{pydx-1,3-pn})\text{-Y}$ (28.0 %) >

[Cu(pydx-en)]-Y (23.6 %) > [Cu(pydx-1,3-pn)] (16.2 %) > [Cu(pydx-en)] (13.6 %). Thus the overall conversion of styrene with TBHP is better with neat as well as encapsulated complexes. The selectivity of the formation of an important component styreneoxide is also much better (43.4 – 74.5 %) but two more products namely, benzoic acid and phenyl acetaldehyde have also been obtained. A highest yield of benzaldehyde using H₂O₂ as oxidant is possibly due to further oxidation of styreneoxide formed in the first step by a nucleophilic attack of H₂O₂ on styreneoxide followed by cleavage of the intermediate hydroperoxystyrene. The formation of benzaldehyde may also be facilitated by direct oxidative cleavage of the styrene side chain double bond via a radical mechanism.

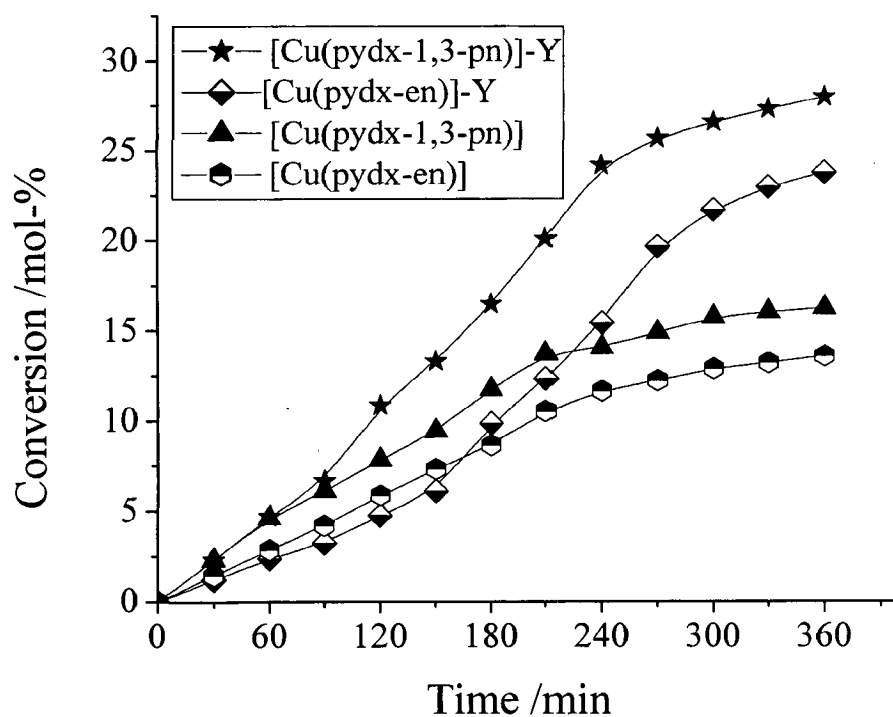
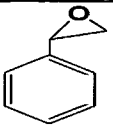
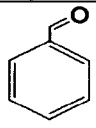
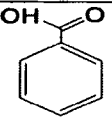
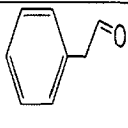


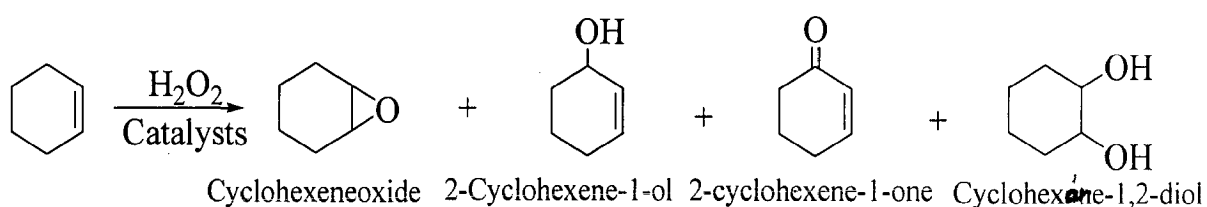
Figure 3.14. Catalytic comparison of zeolite-encapsulated metal complexes and neat complexes for the oxidation of styrene in presence of TBHP as oxidant. Reaction conditions: styrene (1.04 g, 10 mmol), catalyst (0.025 g for encapsulated and 0.00133 g in case of neat complexes), TBHP (2.57 g, 20 mmol), CH₃CN (20 ml) and temperature (80 °C).

Table 3.7. Products selectivity and percent conversion of styrene with TBHP after 6 h of reaction time

Catalyst (TBHP)	Conv. %	Product selectivity(%)					TOF h ⁻¹
						Others	
[Cu(pydx-en)]-Y	23.6	60.7	30.8	0.8	1.3	6.4	127
[Cu(pydx-1,3-pn)]-Y	28.0	43.4	33.1	0.8	2.4	20.3	160
[Cu(pydx-en)]	13.6	70.5	21.0	0.6	1.8	6.1	1298
[Cu(Pydx-1,3-pn)]	16.2	45.4	16.1	0.7	16.8	21.0	1746

3.2.2. Oxidation of Cyclohexene

Oxidation of cyclohexene catalysed by encapsulated complexes gave cyclohexeneoxide, 2-cyclohexene-1-ol, cyclohexane-1,2-diol and 2-cyclohexene-1-one as shown in Scheme 3.4.



Scheme 3.4

Reaction conditions have been optimized considering **3** as a representative catalyst and varying the amount of catalyst, oxidant, solvent and temperature of the reaction mixture. The effect of H₂O₂ concentration on the oxidation of cyclohexene is shown in Figure 3.15. Three different H₂O₂ to cyclohexene molar

ration of 1:1, 2:1 and 3:1 were taken at a fixed amount of cyclohexene (0.82 g, 10 mmol), catalyst (0.025 g) acetonitrile (20 mL) and temperature (75 °C). A maximum of 8.9 % conversion was achieved at a 30 % H₂O₂ to cyclohexene ratio of 1:1. Increasing this ratio to 2:1 increases the conversion to 14.8 % while 3:1 ratio gave 38.8 % conversion. Therefore, it is clear that 3:1 molar ratio is the best H₂O₂ to cyclohexene ratio to obtain the optimum cyclohexene conversion of 38.8 % in 6 h.

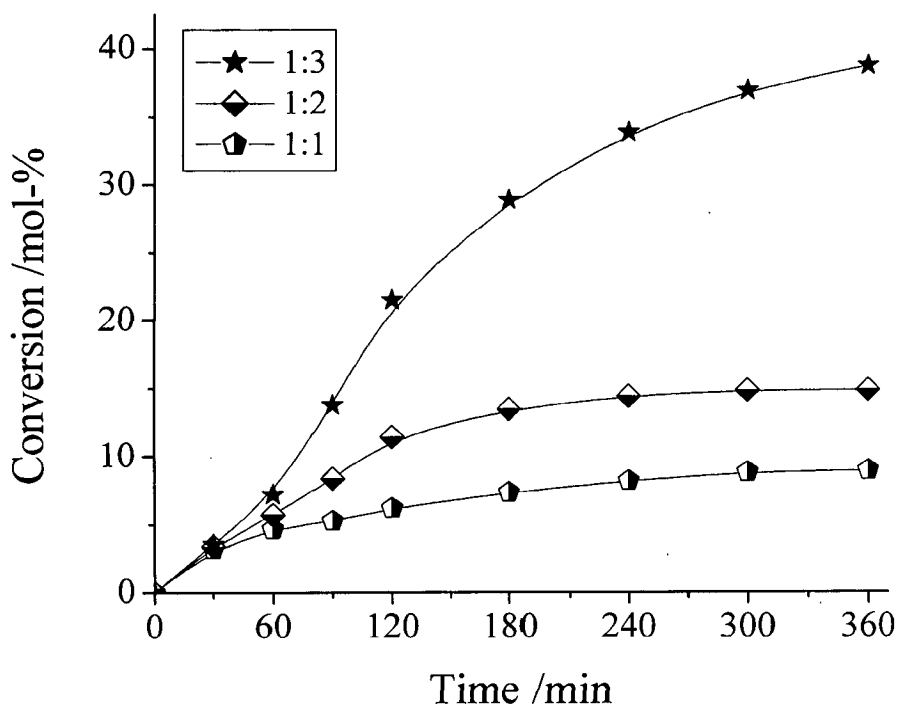


Figure 3.15. Effect of H₂O₂ on the oxidation of cyclohexene. Reaction conditions: cyclohexene (0.82 g, 10 mmol), [Cu(pydx-en)]-Y (0.025 g), CH₃CN (20 mL) and temp. (75° C).

Amount of catalyst has shown considerable affect on the oxidation of cyclohexene. For a cyclohexene to H₂O₂ ratio of 1:3, five different amount of catalyst viz. 0.015, 0.025, 0.035, 0.050 and 0.065 g were taken under above reaction conditions and the obtained results are summarized in Figure 3.16. The conversion increases with increment of catalyst amount from 0.015 g to 0.050 g

(from 28 % to 56.2 %) and then takes a lower trend with 0.065 g catalyst (52.4 %). Thus, an amount of 0.050 g of catalyst is considered sufficient to carry out the oxidation of cyclohexene. It was also noted that reducing the volume of acetonitrile to 10 mL, this conversion reached to 90.1 % with 0.050 g of catalyst under above reaction conditions.

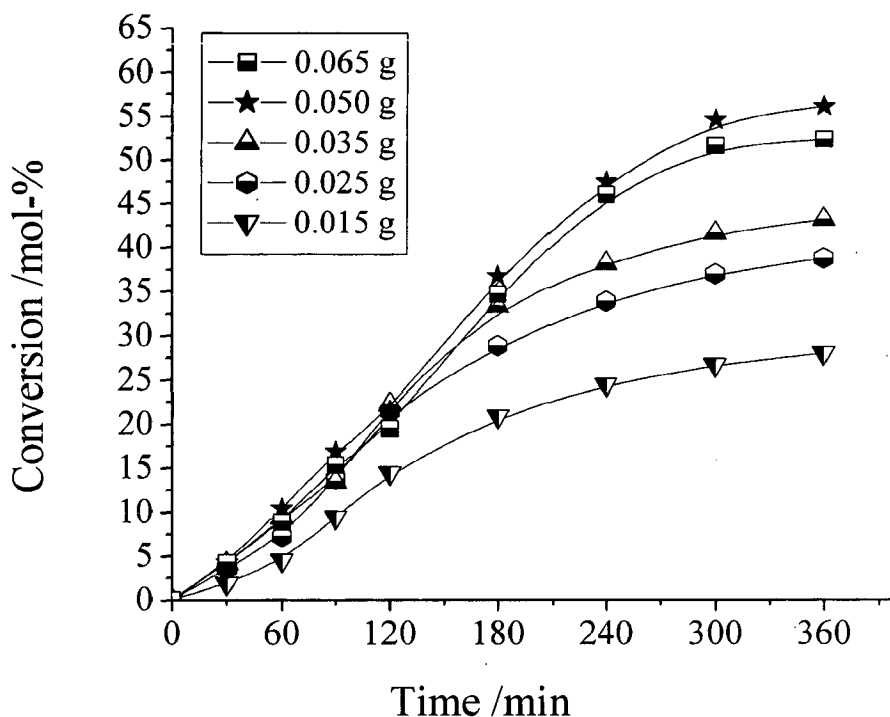


Figure 3.16. Effect of amount ^{of} catalyst on the oxidation of cyclohexene. Reaction conditions: cyclohexene (0.82 g, 10 mmol), 30 % H₂O₂ (3.40 g, 30 mmol), CH₃CN (20 mL) and temp. (75° C).

Figure 3.17 illustrates the effect of temperature of the reaction medium on the conversion of cyclohexene as a function of time. Amongst three different temperature of 55, 65 and 75 °C for the fixed amount of cyclohexene 0.82 g, 10 mmol), aqueous 30 % H₂O₂ (3.40 g, 30 mmol) and catalyst (0.025 g) in

acetonitrile (10 mL), running the reaction at 75 °C has shown best result where 90.1 % conversion has been obtained.

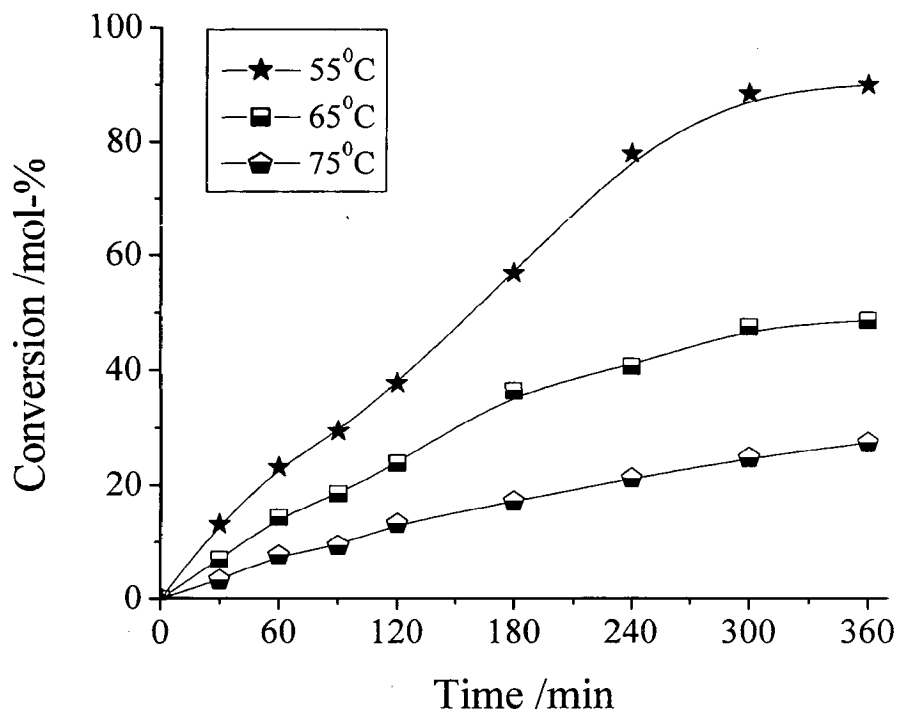


Figure 3.17. Effect of temperature on the oxidation of cyclohexene. Reaction conditions: cyclohexene (0.82 g, 10 mmol), [Cu(pydx-en)]-Y (0.025 g), 30 % H₂O₂ (3.40 g, 30 mmol) and CH₃CN (20 mL).

Thus, suitable reaction conditions for the maximum oxidation of cyclohexene were optimized as follow: cyclohexene (0.82 g, 10 mmol), H₂O₂ (3.40 g, 30 mmol) catalyst (0.025 g), acetonitrile (10 mL) and a temperature of 75 °C. Catalyst 4 was also tested under above reaction conditions and results along with the selectivity of various reaction products are summarized in Table 3.8. A maximum of 83.0 % conversion has been achieved with 4 which is less than that obtained by 3 (90.1 %) in 6 h of contact time. However, both the catalysts show highest selectivity towards the formation of 2-cyclohexene-1-ol, which is followed

by cyclohexeneoxide. The selectivity of other two products i.e. 2-cyclohexene-1-one and cyclohexane-1,2-diol has no definite trend.

We have also tested the catalytic activities of encapsulated complexes using *tert*-butylhydroperoxide as an oxidant. Thus, catalyst (0.050 g), *tert*-butylhydroperoxide (3.855 g, 30 mmol), cyclohexene (0.82 g, 10 mmol) were taken in acetonitrile (10 mL) and reaction was carried out at 75 °C. The data also presented in Table 3.8 show a poor conversion of cyclohexene (19.5 % for **3** and 17.8 % for **4**) with *tert*-butylhydroperoxide in 6 h of contact time. Here, the major product obtained is cyclohexane-1,2-diol while the selectivity of other three products are very poor.

Relatively good conversion of 45.5 % (with **1**) or 50.7 % (with **2**) using H₂O₂ as an oxidant has been achieved, Table 3.8. Here, the selectivity of cyclohexeneoxide is better (33 to 38.7 %) in comparison to the encapsulated complexes, though, overall selectivity orders of all products are same. However, the turn over rates for encapsulated complexes, their stability towards decomposition and easy recovery from the reaction mixture make encapsulated complexes better catalyst over neat ones.

Table 3.8. Oxidation of cyclohexene and product selectivity using various catalysts

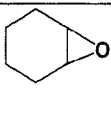
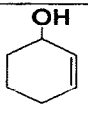
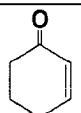
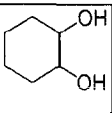
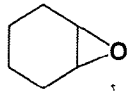
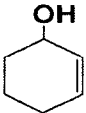
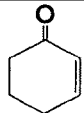
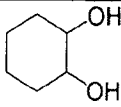
Catalyst	Oxidant	Conv. (%)	Product selectivity (%)					TOF (h ⁻¹)
							Other	
[Cu(pydx-en)]-Y	H ₂ O ₂	90.1	26.9	37.8	22.2	9.5	3.7	241
	TBHP	19.5	1.4	2.4	2.5	92.9	0.8	2417
[Cu(pydx-1,3-pn)]-Y	H ₂ O ₂	83.0	37.1	51.1	3.5	8.3	0.0	237
	TBHP	17.8	1.5	2.0	3.1	92.5	0.9	2438
[Cu(pydx-en)]	H ₂ O ₂	50.7	38.7	44.5	4.9	5.4	6.5	136
[Cu(pydx-1,3-pn)]	H ₂ O ₂	45.5	33.0	51.5	5.0	4.9	5.6	122

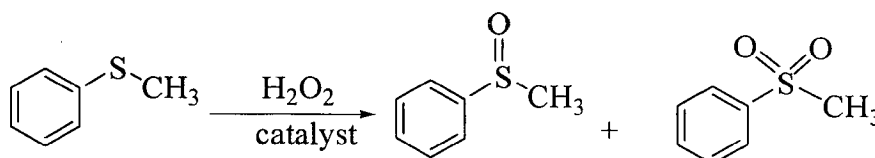
Table 3.9 presents the selectivity of different products obtained with time using catalyst [Cu(pydx-1,3-pn)]-Y and H₂O₂ as an oxidant. It is clear from the table that the selectivity of cyclohexeneoxide and 2-cyclohexene-1-ol increases with time while selectivity of other two products decreases with time.

Table 3.9. Selectivity of different products with time using [Cu(pydx-1,3-pn)]-Y as catalyst and H₂O₂ as oxidant.

Time (min.)	Conversión (%)	Product selectivity (%)				
						Other
60	20.2	20.4	35.5	26.8	14.7	2.6
120	40.7	25.5	39.7	16.9	12.5	5.4
180	58.1	30.1	42.9	12.6	11.8	2.6
240	74.4	32.4	43.6	9.9	10.2	3.9
300	81.2	34.7	45.8	6.4	9.9	3.2
360	83.0	37.1	51.1	3.5	8.3	0.0

3.2.3. Oxidation of Methyl Phenyl Sulfide (Thioanisole)

The sulfur atom of the methyl phenyl sulfide is electron rich and facilitates its electrophilic oxidation to sulfoxide and further to sulfone. Such oxidation of methyl phenyl sulfide was tested using copper complexes encapsulated in zeolite-Y. Oxidation of methyl phenyl sulfide in presence of H₂O₂ gave two products namely, methyl phenyl sulfoxide and methyl phenyl sulfone as shown in Scheme 3.5.



Scheme 3.5

The catalytic potential of these catalysts has also been optimized considering the amount of oxidant, solvent and catalyst. Thus, catalyst **4** was taken as a representative and amount of oxidant was varied at a fixed amount of methyl phenyl sulfide (1.242 g, 10 mmol), catalyst (0.025 g) in acetonitrile (20 mL) and reaction was carried out at ambient temperature. At an aqueous 30 % H₂O₂ to substrate ratio of 2:1, a maximum of 64.3 % conversion was achieved in 3 h of reaction. Decreasing this ratio to 1:1 decreases the conversion of methyl phenyl sulfide considerably while increasing this ratio to 3:1 affects only marginally on the conversion (Figure 3.18). The only influence taking 3:1 ratio is the completion of the reaction in less time. Decreasing the volume of solvent to 10 mL under above reaction conditions (Figure 3.18.1) increases the conversion considerably to 69.3 %.

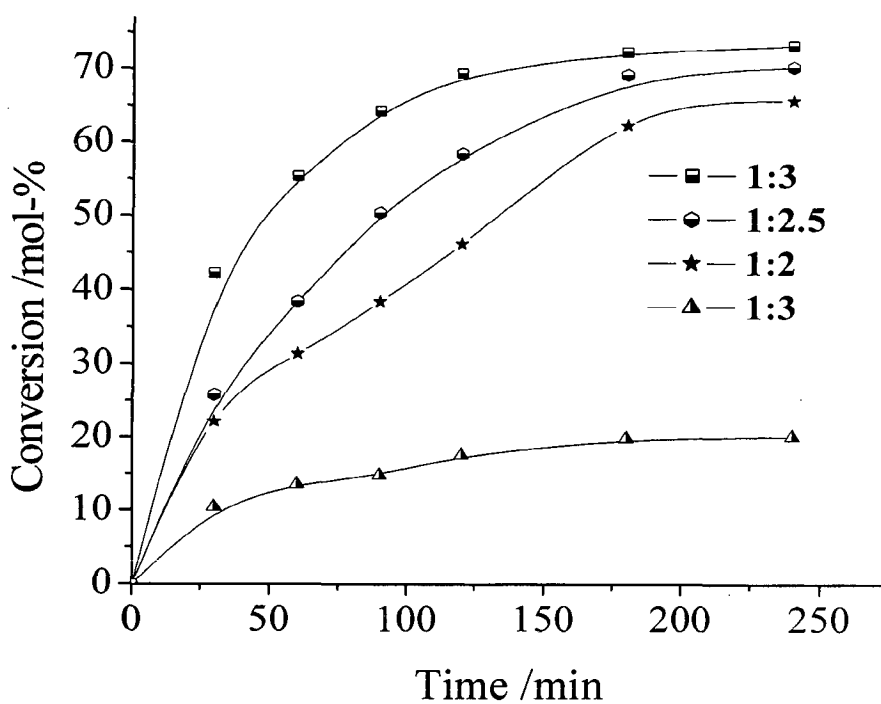


Figure 3.18. Effect of amount of H₂O₂ on the oxidation of methyl phenyl sulfide. Reaction conditions: methyl phenyl sulfide (1.242 g, 10 mmol), [Cu(pydx-1,3-pn)]-Y (0.025 g) and acetonitrile (20 mL).

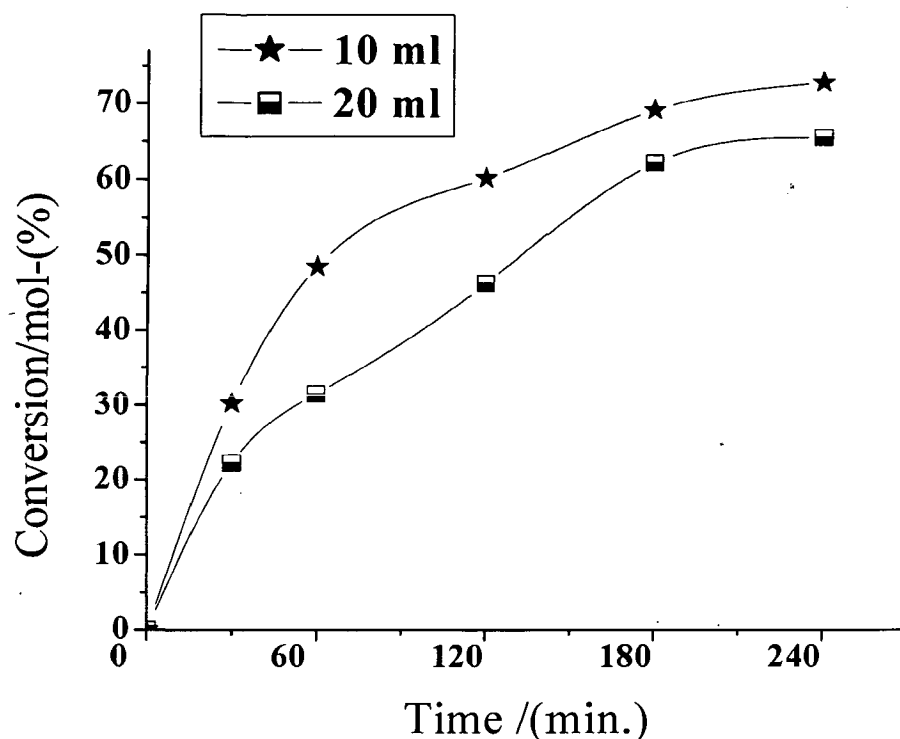


Figure 3.18.1. Effect of volume of solvent on the oxidation of methyl phenyl sulfide. Reaction conditions: methyl phenyl sulfide (1.242 g, 10 mmol), [Cu(pydx-1,3-pn)]-Y (0.025 g) and acetonitrile (10 ml and 20 mL).

Decreasing the volume of solvent to 10 mL under above reaction conditions (Figure 3.18.1) increases the conversion considerably to 69.3 %.

Similarly, four different amount of catalyst viz. 0.015, 0.025, 0.035, and 0.050 g were considered while keeping methyl phenyl sulfide (1.242 g, 10 mmol), 30 % H₂O₂ (2.27 g, 20 mmol) in acetonitrile (10 mL). As mentioned in Figure 3.19, increasing the catalyst amount from 0.015 to 0.025 g increases the conversion from 46.8 to 69.3 %. Increasing this ratio to 0.035 g improves the conversion to 81.0 % while 0.050 g just reduces the completion of the reaction along with marginal effect on the conversion. Therefore, it is clear that the 0.035 g

catalyst amount is sufficient enough to obtain the optimum methyl phenyl sulfide conversion of 81.0 % in 3 h of contact time.

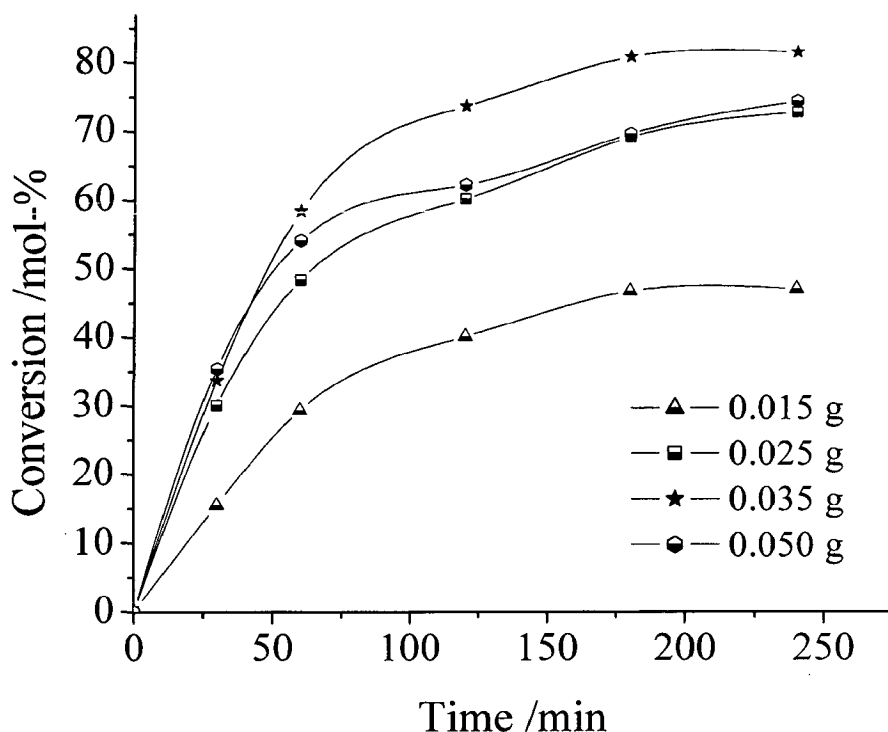
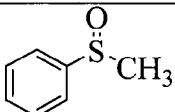
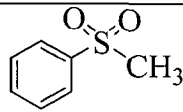


Figure 3.19. Effect of amount of catalyst on the oxidation of methyl phenyl sulfide. Reaction conditions: methyl phenyl sulfide (1.242 g, 10 mmol), H_2O_2 (2.27 g, 20 mmol) and acetonitrile (10 mL).

Thus, under the optimized reaction conditions i.e. catalyst (0.035 g), methylphenylsulfide (1.242 g, 10 mmol), 30 % H_2O_2 (2.27, 20 mmol) and acetonitrile (10 mL) catalyst **3** was also tested and results of both catalysts are compared in Figure 3.20 and Table 3.10 provides selectivity details. Under the optimized reaction conditions **3** and **4** gave 81.0 % and 68.4 % conversion, respectively. In terms of the product selectivity, the selectivities of the methyl phenyl sulfoxide and methyl phenyl sulfone are 63.3 and 36.7 %, respectively for

3 while 53.5 and 43.6 %, respectively for **4**. A blank reaction under the similar conditions i.e. methyl phenyl sulfide (1.242 g, 10 mmol), aqueous 30 % H₂O₂ (2.27 g, 20 mmol) and acetonitrile (10 mL) resulted in 35.2 % conversion with 68.3 % selectivity towards sulfoxide and 31.7 % towards sulfone. Thus, catalysts **3** and **4** only enhanced the percent conversion of methyl phenyl sulfide and have played no positive role in enhancing the selectivity of sulfoxide. A positive role in enhancing the selectivity towards the formation of sulfoxide as well as conversion of methyl phenyl sulfide has been observed by oxovanadium(IV) and copper(II) complexes encapsulated in the cavities of the zeolite-Y [72].

Table 3.10. Conversion percentage of methyl phenyl sulfide using H₂O₂ as an oxidant and selectivity of sulfoxide and sulfone

Catalyst	Conversion (%) (3h)	Product selectivity (%)		TOF h ⁻¹
				
[Cu(pydx-en)]-Y	68.42	63.34	36.66	524
[Cu(pydx-1,3-pn)]-Y	80.99	53.59	46.41	662
[Cu(pydx-en)]	80.26	39.87	60.13	741
[Cu(pydx-1,3-pn)]	73.35	44.94	55.06	632

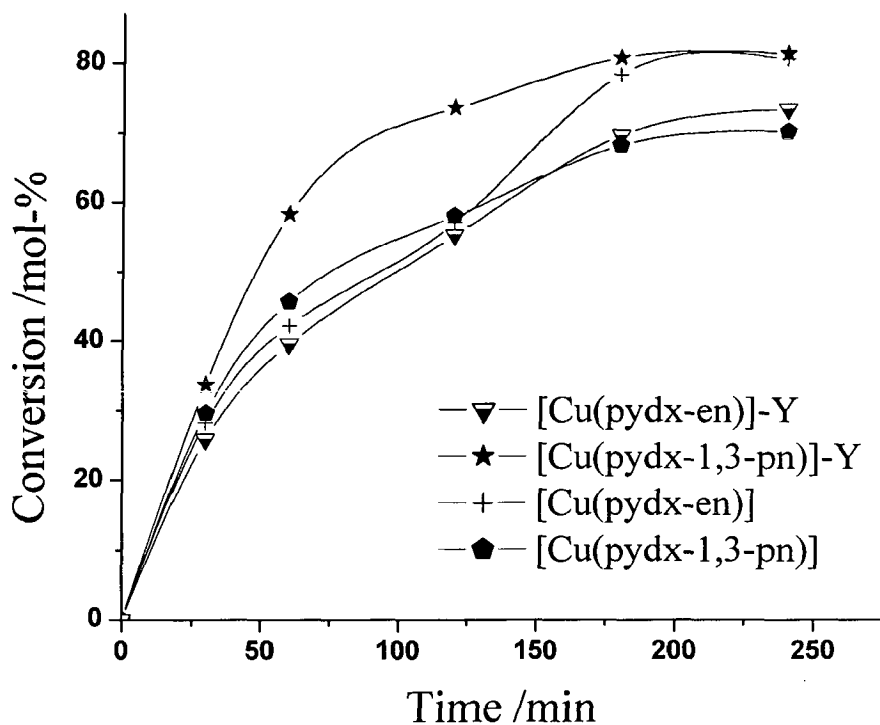
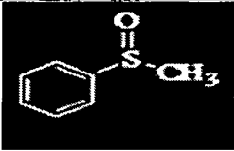
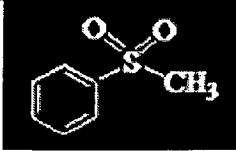


Figure 3.20. Oxidation of methyl phenyl sulfide by various catalysts using H_2O_2 as an oxidant.

Catalytic activities of these complexes have also been tested using TBHP as an oxidant under similar conditions. Again 0.035 g of catalyst has shown best results at a fixed amount of methyl phenyl sulfide (10 mmol) and TBHP (20 mmol) in acetonitrile (10 mL). A maximum of 47.1 % conversion has been recorded with **3** while **4** gave only 18.1 % conversion in 3 h of reaction time; Figure 3.21. Neat complexes **1** and **2** exhibited very poor conversion of 4.7 and 4.2 %, respectively. Independent of the catalytic systems and conversions, sulfoxide has been obtained selectively with TBHP.

Table 3.11. Conversion percentage of methyl phenyl sulfide using TBHP as an oxidant and selectivity of sulfoxide and sulfone

Catalyst	Conversion (%) (3h)	Product selectivity (%)	
			
[Cu(pydx-en)]-Y	47.1	100	0
[Cu(pydx-1,3-pn)]-Y	18.1	100	0
[Cu(pydx-en)]	4.7	100	0
[Cu(pydx-1,3-pn)]	4.2	100	0

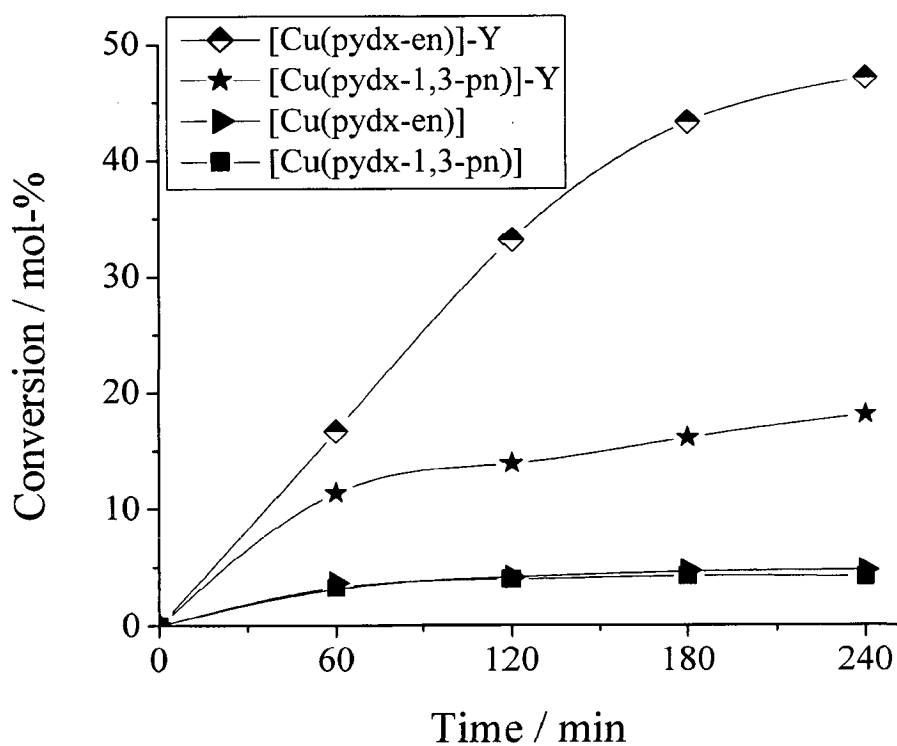


Figure 3.21. Oxidation of methyl phenyl sulfide by various catalysts using *tert*-butylhydroperoxide as an oxidant.

Table 3.12. Selectivity of different products with time using [Cu(pydx-1,3-pn)]-Y as catalyst and H₂O₂ as oxidant.

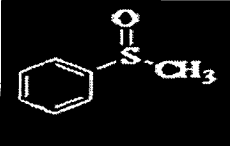
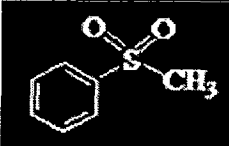
Time (min.)	Conversion (%)	Product selectivity (%)	
			
30	33.74	52.26	47.74
60	58.39	59.83	40.17
120	73.79	49.81	50.19
180	80.99	53.59	46.41
240	81.73	51.05	48.95

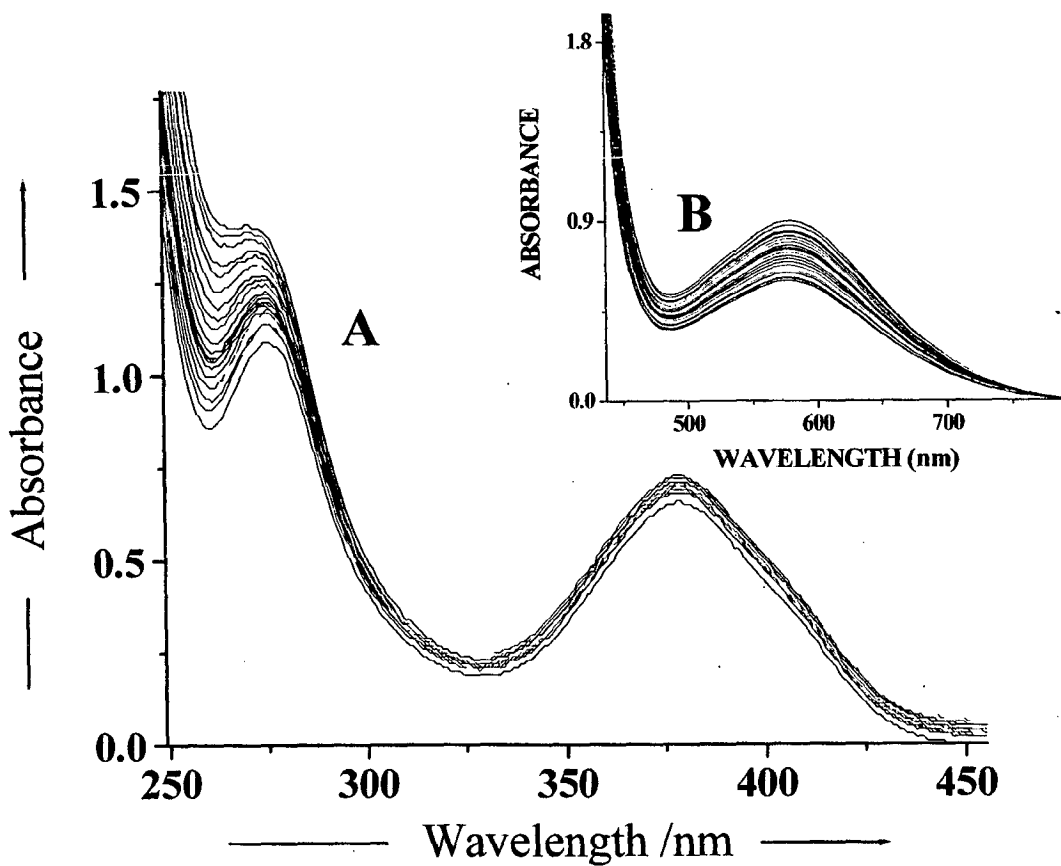
Table 3.12 shows the effect of time (for the period of four hours) on the oxidation conversion and product selectivity of methyl phenyl sulfide using [Cu(pydx-1,3-pn)]-Y as catalyst and H₂O₂ as oxidant.

3.3. Test for recycle ability and heterogeneity of the reactions

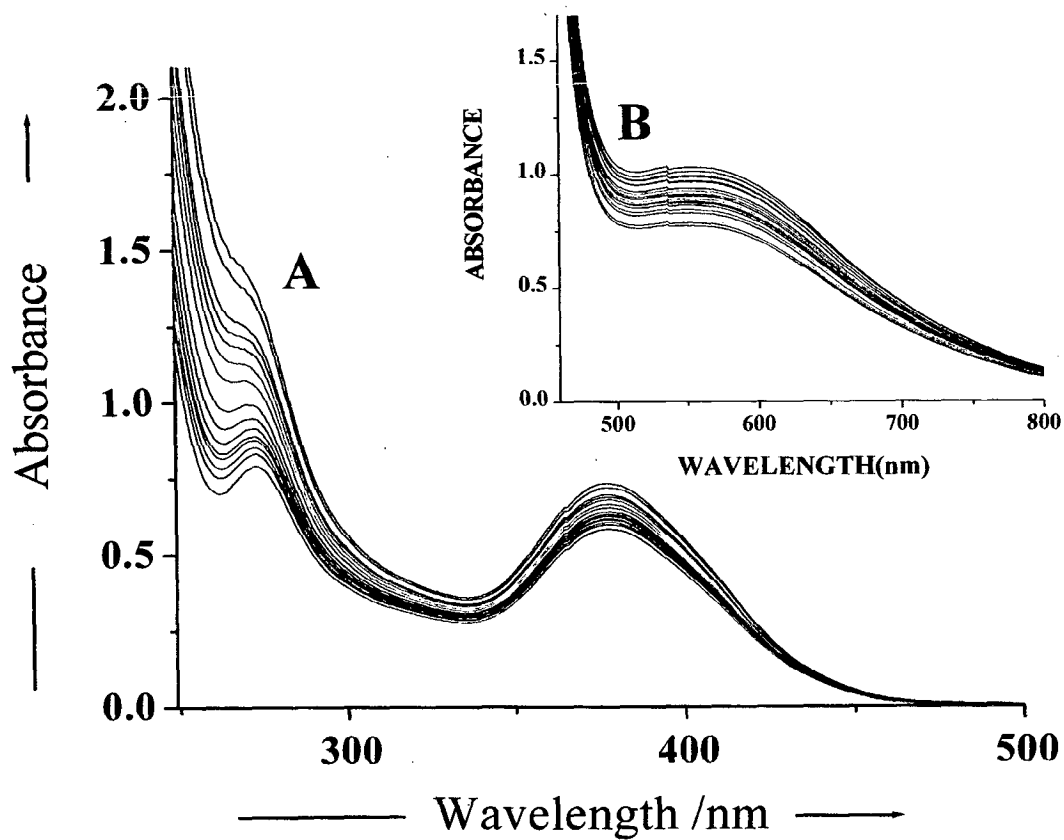
The recycle ability of both the encapsulated complexes has been tested in all three catalytic reactions. In a typical experiment e.g. for styrene, the reaction mixture after a contact time of 6 h was filtered and after activating the catalyst by washing with acetonitrile and drying at 120 °C, it was subjected to further catalytic reaction under similar conditions. No appreciable loss in catalytic activity suggests that complex is still present in the cavity of the zeolite-Y. The filtrate collected after separating the used catalyst was placed into the reaction flask and the reaction was continued after adding fresh oxidant for another 4 h. The gas chromatographic analysis showed no improvement in conversion and this confirms that the reaction did not proceed upon removal of the solid catalyst. The reaction was, therefore, heterogeneous in nature.

3.4. Possible reaction pathway of the catalysts

As H₂O₂ has been used as one of the oxidant in the catalytic oxidation, the neat complexes were treated with H₂O₂ and the progress of the reaction was monitored by electronic absorption spectroscopy in order to establish the reaction mechanism. Thus, the titration of ca. 10⁻⁴ M solution of **1** in DMSO with one-drop portions of 30 % H₂O₂ dissolved in methanol resulted in the spectral changes as shown in Figure 3.22. The intensity of the band at 277 nm increases marginally and 378 nm increases considerably while 235 nm band continuously gains ^{(not sh} in fig.) intensity and finally disappears. At the same time, the d – d band appearing at 590 nm broadens with increase in band maximum (see inset Figure 3.22). A very similar spectral pattern has also been observed for **2**; Figure 3.23. All these should suggested the interaction of copper(II) complexes with H₂O₂. Thus, it seems that catalytic reaction proceeds through intermediate peroxo species which finally transfer oxygen to the substrates.



Spectral changes due to
 Figure 3.22. Titration of methanolic solution of [Cu(pydx-en)] with aqueous 30 %
 H_2O_2 dissolved in methanol. A is at 10^{-4} M conc. and B is at 10^{-3} M
 conc.



spectral changes due to
 Figure 3.23. Titration of methanolic solution of $[\text{Cu}(\text{pydx-1,3-pn})]$ with aqueous 30% H_2O_2 dissolved in methanol. A is at 10^{-4}M conc. and B is at 10^{-3}M conc.

CONCLUSIONS

CHAPTER – 4

CONCLUSIONS

Zeolite-Y encapsulated copper(II) complexes with N,N'-ethylenebis(pyridoxyliminato) ($H_2pydx-en$) and N,N'-propylenebis(pyridoxyliminato) ($H_2pydx-1,3-pn$) have been prepared. These complexes have been abbreviated here in as $[Cu(pydx-en)]-Y$ and $[Cu(pydx-1,3-pn)]-Y$. Neat complexes, $[Cu(pydx-en)]$ and $[Cu(pydx-1,3-pn)]$ have also been prepared with these ligands and characterised.. The crystal and molecular structure of $[Cu(pydx-1,3-pn)].CH_3OH$, has been determined, confirming the ONNO binding mode of the ligands. The encapsulated complexes catalyse the oxidation, by H_2O_2 and *tert*-butylhydroperoxide, of styrene, cyclohexene and thioanisole efficiently. Under the optimised reaction conditions, the oxidation of styrene catalysed by $[Cu(pydx-en)]-Y$ and $[Cu(pydx-1,3-pn)]-Y$ gave 23.6 % and 28.0 % conversion, respectively using H_2O_2 as oxidant where styreneoxide, benzaldehyde, benzoic acid, and phenylacetaldehyde being the major products. Oxidation of cyclohexene catalysed by these complexes gave cyclohexenepoxide, 2-cyclohexene-1-ol, cyclohexane-1,2-diol and 2-cyclohexene-1-one as major products. A maximum of 90.1% conversion of cyclohexene with $[Cu(pydx-en)]-Y$ and 79.3% with $[Cu(pydx-1,3-pn)]-Y$ was obtained under optimized conditions. Similarly, a maximum of 68.4% conversion of methyl phenyl sulfide with $[Cu(pydx-en)]-Y$ and 81.0 % with $[Cu(pydx-1,3-pn)]-Y$ was observed where the selectivity of major product methyl phenyl sulfoxide was found to be ca. 60 %. All these reactions were carried out by using Gas Chromatography and their identities were confirmed by GC-MS. The catalytic activities of these zeolite encapsulated complexes have also been compared with the corresponding free complexes and it has been observed that in case of free complexes with methyl phenyl sulfide

compareable catalytic activities are obtained while in cases with styrene and cyclohexene encapsulated complexes shows better results. Tests for recycle ability and heterogeneity of the reactions have also been carried out and results suggest their recyclability. The recycle ability and easy separation of the encapsulated complexes from the reaction mixture make zeolite encapsulated metal complexes better catalyst over neat ones. Besides these, complexes are stable and do not leach during catalytic actions in solution. A possible reaction mechanism has been proposed by titrating methanolic solution of neat complexes, [Cu(pydx-en)] and [Cu(pydx-1,3-pn)] with H_2O_2 and identifying the possible intermediate.

Thus, synthesis and characterization of zeolite encapsulated metal complexes and their catalytic activities along with crystal and molecular structure of neat complex presented in this dissertation, contribute considerably to the existing knowledge and hope that these complexes may contribute to applications in many scientific disciplines, catalytic and all types of chemical process technologies.

REFERENCES

CHAPTER – 5

REFERENCES

1. S. Sivasanker, "Recent developments in catalysis" in *Catalysis: Principles and Applications*, Edited by: B. Viswanathan, S. Sivasanker and A.V. Ramaswamy, Narosa Publishing House, New Delhi, **2002**, p.272.
2. I. Chorkendorff and J.W. Niemantsverdriet, "Concept of Modern Catalysis and Kinetics", Wiley-VCH GmbH & Co. KGaA, Weinheim, Germany, 2003.
3. K Soai, M. Watanabe and A. Yamamoto, *J. Org. Chem.*, 55 (**1990**) 4832 – 4835.
4. P. Barbaro, C. Bianchini, V.D. Santoro, A. Meli, S. Moneti, R. Psaro, A. Scaffidi, L. Sordelli and F. Vizza, *J. Am. Chem. Soc.*, 128 (**2000**) 7065 – 7076.
5. H.G. Alt, P. Schertl and A. Köppl, *J. Organomet. Chem.*, 568 (**1998**) 263 – 269.
6. D.E. De Vos, M. Dams, B.F. Sels and P.A. Jacobs, *Chem Rev.*, 102 (**2000**) 3615 – 3640.
7. J. Topich, *Inorg. Chem.*, 21 (**1982**) 2079 – 2082.
8. A. Syamal and M.M. Singh, *Indian J. Chem.*, 32A (**1993**) 42 – 48.
9. A. Syamal and M.M. Singh, *J. Polym. Mater.*, 9 (**1992**) 105 – 111.
10. M.R. Maurya, U. Kumar and P. Manikandan, *Dalton. Trans.*, (**2006**) 3561 – 3575.
11. B.L. Meyers, S.R. Ely, N.A. Kutz, J.A. Kudak and E. Van den Bossche, *J. Catal.*, 91 (**1985**) 352 – 355.
12. R. Kumar and P. Ratnasamy, *Catal. Lett.*, 22 (**1993**) 227 – 237.
13. F. Bedioui, *Coord. Chem. Rev.*, 144 (**1995**) 39 – 68.

14. K.J. Balkus Jr. and A.G. Gabrielov, *J. Incl. Phenom. Mol. Recogn. Chem.*, **21** (1995) 159 – 184.
15. F. Velghe, R.A. Schoonheydt, J.B. Uytterhoeven, P. Peigneur and J.H. Lunsford, *J. Phy. Chem.*, **81** (1977) 1187 – 1194.
16. Y. Yamada, *Bull. Chem. Soc. Jpn.*, **45** (1972) 60 – 63.
17. E.F. Vasant and J.H. Lunsford, *J. Phy. Chem.*, **76** (1972) 2860 – 2865.
18. P. Gallezot, Y. Ben Taarit and B. Imelik, *J. Catal.*, **26** (1972) 295 – 302.
19. J.C. Vadrine, E.G. Derouane and Y. Ben Taarit, *J. Phy. Chem.*, **78** (1974) 531 – 535.
20. W. DeWilde, G. Peeters and J.H. Lunsford, *J. Phy. Chem.*, **84** (1980) 2306 – 2310.
21. W.H. Quayle and J.H. Lunsford, *Inorg. Chem.*, **21** (1982) 97 – 103.
22. W.H. Quayle, G. Peeters, G.L. De Roy, E.F. Vasant and J.H. Lunsford, *Inorg. Chem.*, **21** (1982) 2226 – 2231.
23. P.P. Knops-Gerrits, D. De Vos, F. Thibault-Starzyk and P.A. Jacobs, *Nature*, **369** (1994) 543 – 546.
24. C. Bowers and P.K. Dutta, *J. Catal.*, **122** (1990) 271 – 279.
25. M.R. Maurya, S. J. J. Titinchi and S. Chand, *Appl. Catal. A: Gen.*, **228** (2002) 177 – 187.
26. L.F. Rao, A. Fukuoka and M. Ichikawa, *J. Chem. Soc., Chem. Commun.*, (1988) 458 – 460.
27. L.F. Rao, A. Fukuoka, N. Kosugi, H. Kuroda and M. Ichikawa, *J. Phys. Chem.*, **94** (1990) 5317 – 5327.
28. N. Takahashi, A. Mijin, H. Suematsu, S. Shinohara and H. Matsuoka, *J. Catal.*, **117** (1989) 348 – 354.
29. B.E. Henson, M.E. Davis, D. Taylor and E. Rode, *Inorg. Chem.*, **23** (1984) 52 – 56.
30. A. Fukuoka, L.F. Rao, N. Kosugi, H. Kuroda and M. Ichikawa, *Appl. Catal.*, **50** (1989) 295 – 301.

31. G. Meyer, D. Woehrlé, M. Mobil and G. Schulz-Ekloff, *Zeolites*, 4 (1984) 30 – 34.
32. A.N. Zakharov and B.V. Romanosky, *J. Inclusion Phenom.*, 3 (1985) 389 – 393.
33. C.A. Tolman and N. Herron, *Catal. Today*, 3 (1988) 235 – 243.
34. R.F. Parton, D.R.C. Huybrechts, P. Buskens and P.A. Jacobs, *Stud. Surf. Sci. Catal.*, 65 (1991) 47 – 60.
35. K.J. Balkus Jr., A.A. Welch and B.E. Gnade, *J. Inclusion Phenom. Mol. Recogn. Chem.*, 10 (1991) 141 – 151.
36. A.G. Gabrielov, K.J. Balkus Jr., S.L. Bell, F. Bedioui and J. Devynck, *Microp. Mater.*, 2 (1994) 119 – 126.
37. K.J. Balkus Jr., A.G. Gabrielov, S.L. Bell, F. Bedioui, L. Roue and J. Devynck, *Inorg. Chem.*, 33 (1994) 67 – 72.
38. M. Nakamura, T. Tatsumi and H. Tominaga, *Bull. Chem. Soc. Jpn.*, 63 (1990) 3334 – 3336.
39. K.J. Balkus Jr., C.D. Hargis and S. Kowalak, *ACS Symposium Series*, 499 (1992) 347 – 354; CAN 117:153864.
40. M.R. Maurya, M. Kumar, S.J.J. Titinchi, H. S. Abbo and S. Chand, *Catal. Lett.*, 86 (2003) 97 – 105.
41. N. Ulagappan, Proceedings of the 31st Annual convention of chemists, Varanasi, India, (1994) F1.
42. K.J. Balkus Jr., A.K. Khanmamedova, K.M. Dixon and F. Bedioui, *Appl. Catal. A: Gen.*, 143 (1996) 159 – 173.
43. G.S. Mishra and A. Kumar, *Catal. Lett.*, 81 (2002) 113 – 117.
44. M.R. Maurya, S. J. J. Titinchi, S. Chand and I.M. Mishra, *J. Mol. Catal. A: Chem.*, 180 (2002) 201 – 209.
45. M.R. Maurya, S.J.J. Titinchi and S. Chand, *J. Mol. Catal. A: Chem.*, 193 (2003) 165 – 176.

46. M.R. Maurya, S.J.J. Titinchi and S. Chand, *J. Mol. Catal. A: Chem.*, 201 (2003) 119 – 130.
47. C.R. Jacob, S.P. Varkey and P. Ratnasamy, *Appl. Catal. A: Gen.*, 168 (1998) 353 – 364.
48. C.R. Jacob, S.P. Varkey and P. Ratnasamy, *Micropor. Mesopor. Mater.*, 22 (1998) 465 – 474.
49. S.P. Verkey, C. Ratnasamy and P. Ratnasamy, *J. Mol. Catal. A: Chem.*, 135 (1998) 295 – 306.
50. J. Poltowicz, K. Pamin, E. Tabor, J. Haber, A. Adamski and Z. Sojka, *Appl. Catal. A: Gen.*, 299 (2006) 235 – 242.
51. S.P. Verkey, C. Ratnasamy and P. Ratnasamy, *Appl. Catal. A: Gen.*, 182 (1999) 91 – 96.
52. S. Deshpande, D. Srinivas and P. Ratnasamy, *J. Catal.*, 188 (1999) 261 – 269.
53. D. Chatterjee and A. Mitra, *J. Mol. Catal. A: Chem.*, 144 (1999) 363 – 367.
54. T. Bein and S.B. Ogunwumi, Book of Abstracts, 212th ACS National Meeting, Orlando, FL, August, (1996) 25 – 29; AN 1996:416514.
55. M. Salavati-Niasari, F. Farzaneh, M. Ghandi and L. Turkian, *J. Mol. Catal. A: Chem.*, 157 (2000) 183 – 188.
56. M. Silva, C. Freire, B. de Castro and J.L. Figueiredo, *J. Mol. Catal. A: Chem.*, 258 (2006) 327 – 333.
57. T. Katsuki, *Coord. Chem. Rev.*, 140 (1995) 189 – 214.
58. M.J. Sabater, A. Corma, A. Domenech, V. Fornes and H. Garcia, *Chem. Commun.*, 14 (1997) 1285 – 1286.
59. T. Joseph, S.B. Halligudi, C. Satyanarayan, D.P. Sawant and S. Gopinathan, *J. Mol. Catal. A: Chem.*, 168 (2001) 87 – 97.
60. T. Joseph, D.P. Sawant, C.S. Gopinath and S.B. Halligudi, *J. Mol. Catal. A: Chem.*, 184 (2002) 289 – 299.

61. M.J. Alcón A. Corma, M. Iglesias and F. Sanchez, *J. Mol. Catal. A: Chem.*, 178 (2002) 253 – 266.
62. M.J. Alcón A. Corma, M. Iglesias and F. Sanchez, *J. Mol. Catal. A: Chem.*, 194 (2003) 137 – 152.
63. T.M. Salama, A.H. Ahmed and Z.M. El-Bahy, *Micropor. Mesopor. Mater.*, 89 (2006) 251 – 259.
64. M.R. Maurya, H. Saklani and S. Agarwal, *Catal. Commun.*, 5 (2004) 564 – 568.
65. M.R. Maurya, H. Saklani, A. Kumar and S. Chand, *Catal. Lett.*, 93 (2004) 121 – 127.
66. S.N. Rao, K.N. Munsri and N.N. Rao, *J. Mol. Catal. A: Chem.*, 145 (1999) 203 – 210.
67. M. Salavati- Niassary, F. Farzaneh and M. Ghandi, *J. Mol. Catal. A: Chem.*, 175 (2001) 105 – 110.
68. K.O. Xavier, J. Chacko, and K.K.M. Yusuff, *J. Mol. Catal. A: Chem.*, 178 (2002) 275 – 281.
69. K.O. Xavier, J. Chacko and K.K.M. Yusuff, *Appl. Catal. A: Gen.*, 258 (2004) 251 – 259.
70. K.K.M. Yusuff and J. Mathew, *Indian J. Chem.*, 36A (1997) 303 – 306.
71. M. R. Maurya, A. K. Chandrakar and S. Chand, *J. Mol. Catal. A: Chem.*, 263 (2007) 227 – 237.
72. M. R. Maurya, A. K. Chandrakar and S. Chand, *J. Mol. Catal. A: Chem.*, 270 (2007) 225 – 235.
73. M. R. Maurya, A. K. Chandrakar and S. Chand, *J. Mol. Catal. A: Chem.*, In press, available online.
74. I. Correia, J. Costa Pessoa, M.T. Duarte, R.T. Henriques, M.F.M. Piedade, L.F. Veiros, T. Jackusch, A. Dornyei, T. Kiss, M.M.C.A. Castro, C.F.G.C. Geraldes and F. Avecilla, *Chem. Eur. J.*, 10 (2004) 2301 – 2317.

75. I. Correia, A. Dornyei, T. Jakusch, F. Avecilla, T. Kiss and J. Costa Pessoa, *Eur. J. Inorg. Chem.*, (2006) 2819 – 2830.
76. J. Peisach and W.E. Blumberg, *Arch. Biochem. Bioph.*, 165 (1974) 691-708.
77. U. Sakaguchi, A.W. Addison, *J. Chem. Soc., Dalton Trans.*, (1979) 600-608.
78. S. Deshpande, D. Srinivas and P. Ratnasamy, *J. Catal.*, 188 (1999) 261-269.
79. V.T. Kasumov and F. Koksai, *Spectrochim. Acta Part A*, 61 (2005) 225-231.
80. K.M. Ananth, M. Kanthimathi and B.U. Nair, *Trans. Metal Chem.*, 26 (2001) 333-338.
81. V. Hulea, E. Dumitriu, *Appl. Catal. A. Gen.* 277 (2004) 99-106.

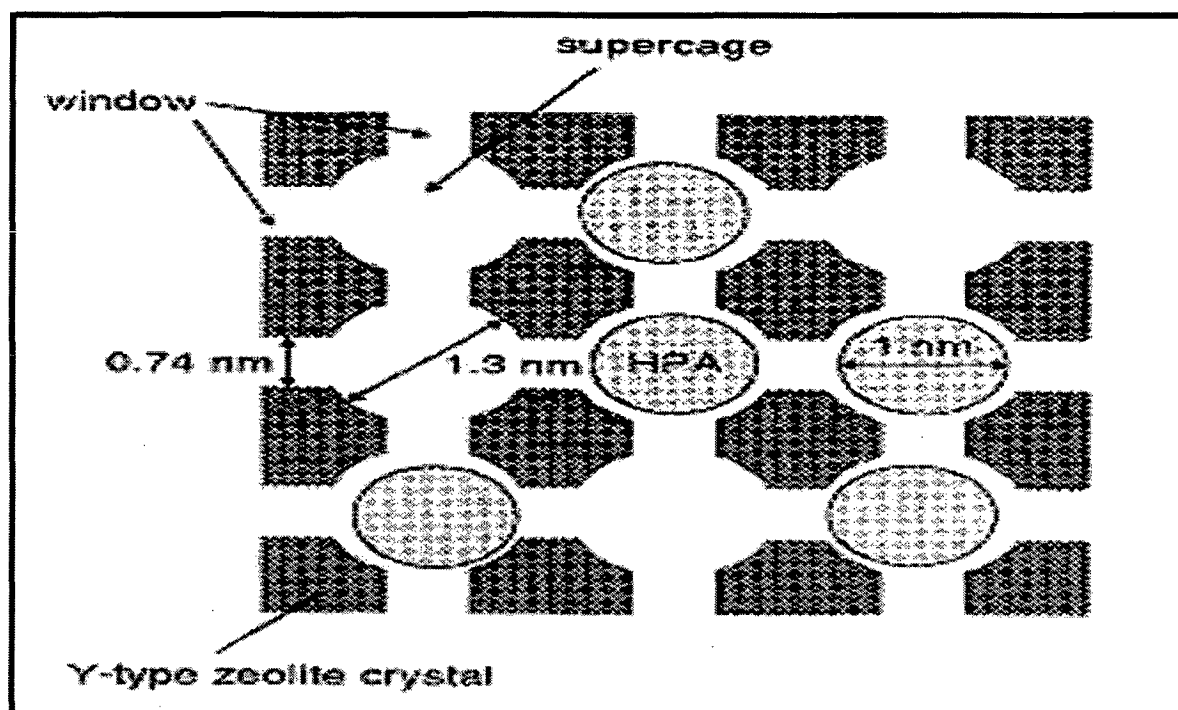
APPENDIX

ABBREVIATIONS & SYMBOLS USED

FTIR	Fourier Transform-Infrared
UV	Ultraviolet
EPR	Electron Paramagnetic Resonance
ESR	Electron Spin Resonance
SEM	Scanning electron microscopy
TGA	Thermo gravimetric Analysis
DTA	Differential Thermal Analysis
DTG	Derivative Thermo gravimetric Analysis
XRD	X-ray diffraction
GC-MS	Gas Chromatography- Mass Spectrometry
FID	Flame Ionization Detector
ICP	Inductively Coupled Plasma
ACN	Acetonitrile
TBHP	<i>Tert</i> -butylhydroperoxide
TAS	Thioanisole
DMF	Dimethylformaamide
DMSO	Dimethylsulfoxide
GC	Gas Chromatography

TOF	Turn Over Frequency
ZSM-5	Zeolite Sieve of Molecular Porosity 5
3D	3-Dimensional
KIP	Keto isophorone
KBr	Pottassium Bromide
pydx	Pyridoxal
en	Ethylenediammine
pn	Propylenediammine
nm	Nanometer
so	Styreneoxide
phaa	Phenylacetaldehyde
bza	Benzaldehyde
bzac	Benzoic acid
Z1	Zeolite 1
Z2	Zeolite 2

SCHEMATIC DIAGRAM OF ENCAPSULATED CATALYST



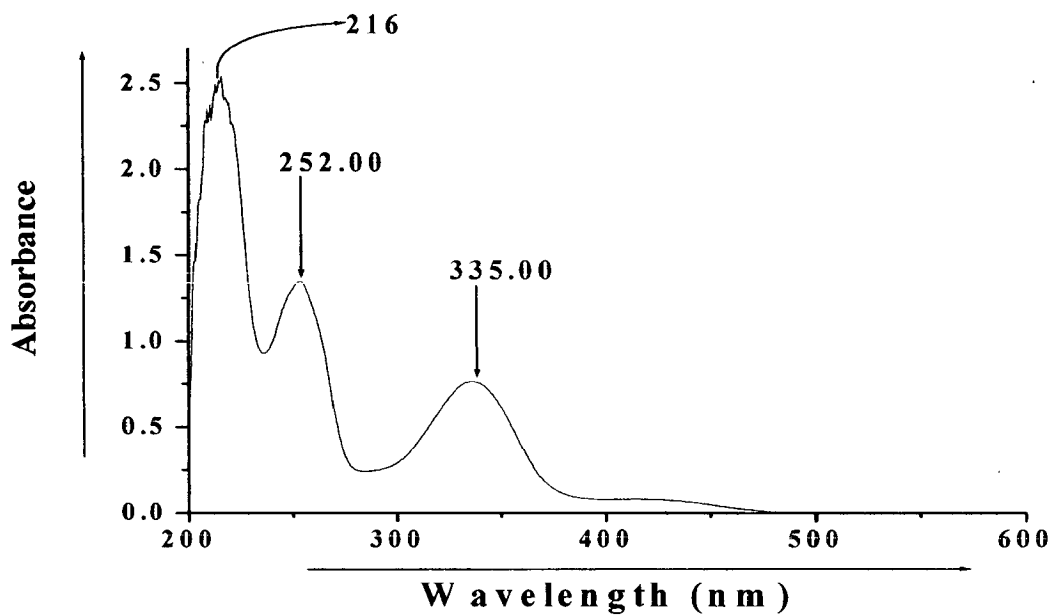
GENERAL METHODS FOR SYNTHESIS OF ZEOLITE ENCAPSULATED IN METAL COMPLEXES

- Ion Exchange Method
- Adsorption Method
- Template Synthesis Method
- Flexible Ligand Method
- Zeolite Synthesis Method

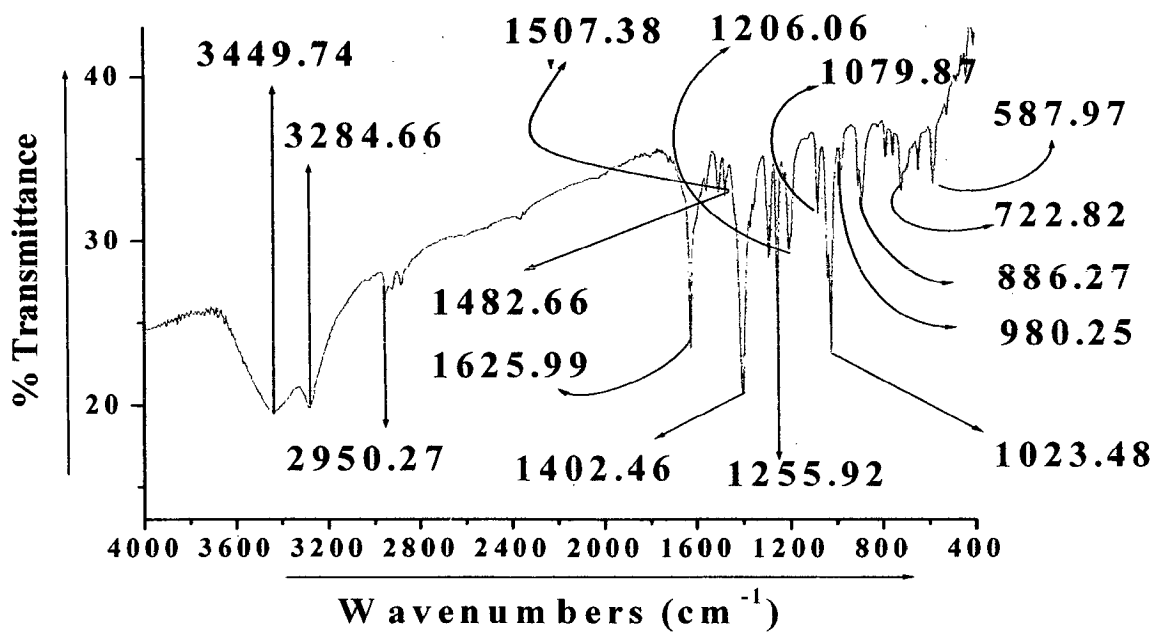
ADVANTAGES OF METAL COMPLEXES ENCAPSULATED IN ZEOLITES

- Activity
- Selectivity
- Thermostability
- Reusability (regeneration of deactivated catalyst)
- Ease of separation
- Handling and ecofriendly nature

UV-SPECTRUM OF LIGAND $H_2pydx-en$



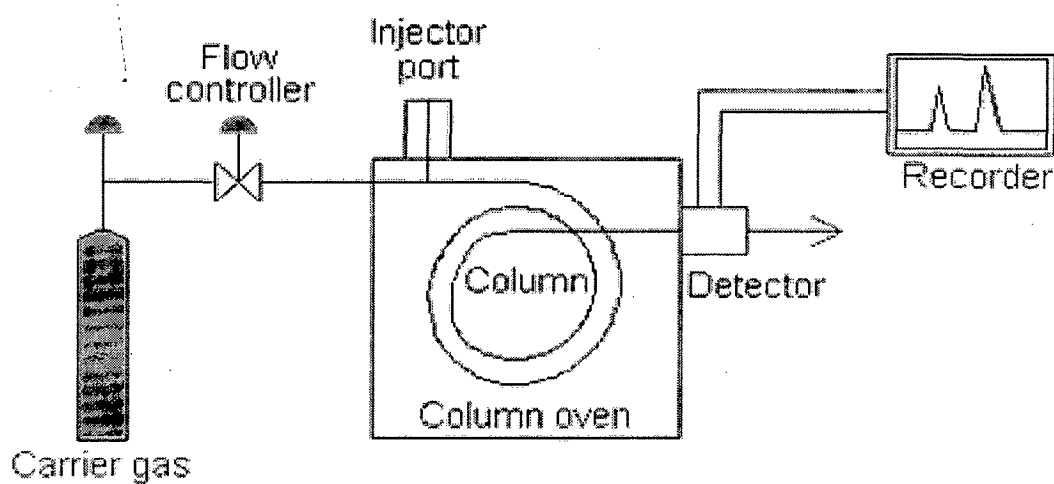
IR-SPECTRUM OF LIGAND $H_2pydx-en$



BASIC THEORY OF SOME TECHNIQUES USED

CHROMATOGRAPHY

Diagrammatic diagram of a gas chromatograph:



Instrumental components

- Carrier gas
- Sample injection port
- Columns
- Detectors

THEORY OF CHROMATOGRAPHY RETENTION -

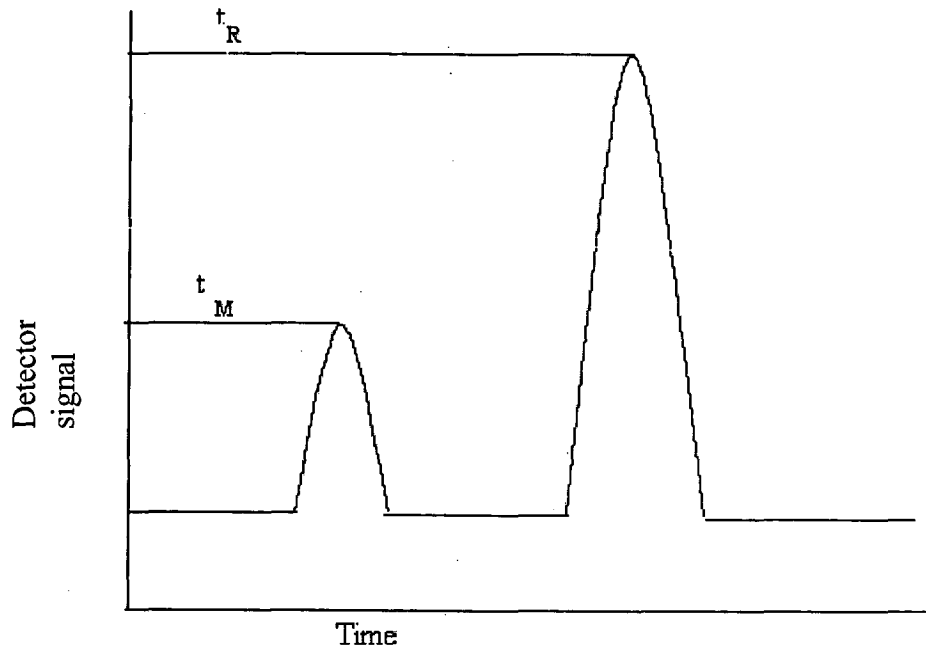
Distribution of analytes between phases

The distribution of analyte between two phases is governed by equilibrium;

A mobile \leftrightarrow A stationary

The equilibrium constant K is termed the partition coefficient.

The time between sample injection and an analyte peak reaching a detector at the end of the column is termed as the retention time (t_R).



The time taken for the mobile phase to pass through the column is called (t_M).

Partition Coefficient (K)

$K = C_s / C_m$; C_s and C_m are the concentration of solute in stationary and mobile phase respectively. When $K=1$, solute is equally distributed between the two phases.

Retention Factor (K') describes the migration of an analyte on the column and is defined for an analyte as

$$K' = \frac{t_R - t_M}{t_M} ; t_R = t_M (1 + k')$$

The optimum range for retention factor extends from 1 to 10

Selectivity factor (α) describes the separation of two species (A and B) on the column and can be determined with the help of following equation

$\alpha = K'_B / K'_A$ Where K'_B and K'_A are the retention factors for analyte A and B respectively.

Desirable Range for (α) = 1.05 to 2.0

Column efficiency

As a compound moves through a chromatographic column, the sample band gets broaden as function of time. This principle is expressed in terms of column efficiency which is given either quantitatively by the number of theoretical plate N (large N increases the efficiency of the column), or by stating the plate height; the height equivalent to the theoretical plate HETP (smaller the plate better the efficiency of the column). If the length of the column is L then the HETP is

$$\text{HETP} = L/N$$

The number of theoretical plates for a given column can be calculated as

$$N = 16(t_R/W)^2$$

$$N = 5.5 (t_R/W_{1/2})^2$$

Where W and $W_{1/2}$ are the peak width at base and at half- height respectively.

RESOLUTION

Although the selectivity factor, α describes the separation of band centers, it does not takes into account the peak width. Another measure of how well species has been separated is provided by measurement of the resolution.

The resolution of two species A and B is defined as

$$R = 2[(t_R)_B - (t_R)_A] / (W_A + W_B)$$

Base line resolution is achieved when $R=1.5$. It is useful to relate the resolution to the number of plates in the column. The selectivity factor and the retention factor of the two solutes is related by equation

$$R = (\sqrt{N/4}) [(\alpha - 1) / \alpha] [K' / (1 + K')]$$

To obtain high resolution, the three terms must be maximized.

FORMULAES USED--

- % Conversion = (Total area of products / Total area) × 100
- Selectivity = (Area of product / Total area of products) × 100
- % Yield = (Area of product / Total area) × 100
- Number of peaks correlates with the number of components present in the sample
- The area under each peak correlates with the relative amount of that component in the sample
- By comparing the retention time of the analyte with the available standard, the qualitative analysis can also be done.

- % Conversion, % Yield and % Selectivity data gives the analysis & separation performance by GC

UV- SPECTROSCOPY

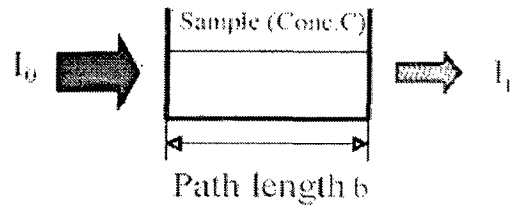
Lambert-Beer's Law

- ◆ Transmittance, t

$$I_1 / I_0 = t$$

- ◆ Absorbance, A

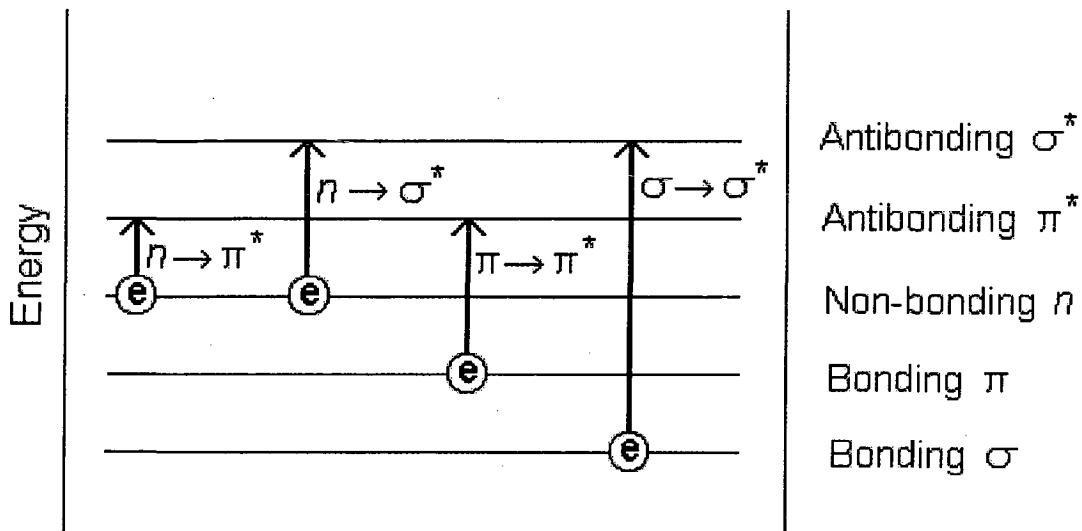
$$\log I_0 / I_1 = A$$



- ◆ Lambert – Beer's Law

$$A = abC, \quad A = \xi bC$$

- ✓ b : Sample Path length, C : Sample Concentration,
- ✓ a : Absorbance Constant
- ✓ ξ : Molecular Absorbance Constant



Energy values of different transitions are in the following order :

$$n \rightarrow \pi^* < \pi \rightarrow \pi^* < n \rightarrow \sigma^* < \sigma \rightarrow \sigma^*$$

In case of d- orbitals , when an external field is applied,d-orbitals split up.

Different possible origins for the electronic spectra of complexes are as:

- (I) Spectra principally associated with the ligand ($\pi \rightarrow \pi^*$)
- (II) Spectra associated with metal influenced by the presence of ligand.
- (III) Spectra involving metal and ligand
 - (a) Metal to Ligand ($M \rightarrow L$)
 - (b) Ligand to Metal ($L \rightarrow M$)

Charge Transfer Absorption

Many inorganic species show charge-transfer absorption and are called charge-transfer complexes. For a complex to demonstrate charge-transfer behaviour, one of its components must have electron donating properties and another component must be able to accept electrons. Absorption of radiation then involves the transfer of an electron from the donor to an orbital associated with the acceptor. Molar absorptivities from charge-transfer absorption are large (greater than $10,000 \text{ L mol}^{-1} \text{ cm}^{-1}$).

IR-SPECTROSCOPY

In general terms it is convenient to split an IR spectrum into two approximate regions:

$4000-1000 \text{ cm}^{-1}$ known as the functional group region, and $< 1000 \text{ cm}^{-1}$ known as the fingerprint region



$$\bar{\nu} = \frac{1}{2\pi} \sqrt{\frac{k}{\mu}}$$

$\bar{\nu}$ = frequency

$$\mu = \frac{m_1 \cdot m_2}{m_1 + m_2}$$

μ = reduced mass

K - force constant (which reflects the stiffness), & m_1 and m_2 - masses

ion carrying the unpaired electron, or the number of equivalent nuclei coupling to the electron.

Further interactions influencing the EPR spectrum are the zero-field splitting for systems with $S > 1/2$, the nuclear quadrupole interaction due to a quadrupole moment for nuclei with $I > 1/2$, and the nuclear Zeeman interaction.

light. When some of the light is absorbed by a metal, the beam's intensity is reduced. The detector records that reduction as an absorption. That absorption is shown on a readout by the data system. The figure above shows the schematic diagram of a flame AAS. As the diagram indicates, there are four primary parts to the system--the light source, the flame apparatus, the detector, and the data system. No chromatography is required for this instrument. We merely change lamps and adjust the detector wavelength. It finds the concentrations of metals in a sample running a series of calibration standards through the instrument. The instrument will record the absorption generated by a given concentration. By plotting the absorption versus the concentrations of the standards, a calibration curve can be plotted. The absorption for a sample solution and use the calibration curves to determine the concentration in that sample.

EPR

Principle of EPR

In spectroscopy, energy differences between atomic or molecular states are measured to gain insight into the identity, structure and dynamics of the sample under study. The energy differences studied by EPR are predominately due to interaction of unpaired electrons in the sample with a static magnetic field B_0 produced by an electromagnet or a supraconducting magnet (typical values of B_0 in EPR are between 0.1 T and 5 T). This effect is called the Zeeman effect. Because the electron has a magnetic moment μ , it acts like a compass when placed in a magnetic field. This magnetic moment is quantized, it can take only discrete values. The energy difference between the levels are proportional to B_0 . The free electron and a large number of samples studied by EPR have a spin $S=1/2$, which means they can take two different states. The energy between those states is given for a free electron by

$$\Delta E = h\nu = g_e\beta_e B_0 \quad (1)$$

where $\beta_e = 9.27402 \times 10^{-24} \text{ JT}^{-1}$ $g_e = 2.00232$. For real samples, g is a - often orientation-dependent - proportionality factor, which depends on the electronic configuration of the radical or ion being studied. It is one of the main information sources in EPR.

The interaction between the unpaired electron and nuclear spins is called hyperfine coupling and is orientation dependent as well. This is the second major source of information obtained with an EPR experiment. It provides information about the electron density at the nucleus, the distance and orientation of the nucleus to an

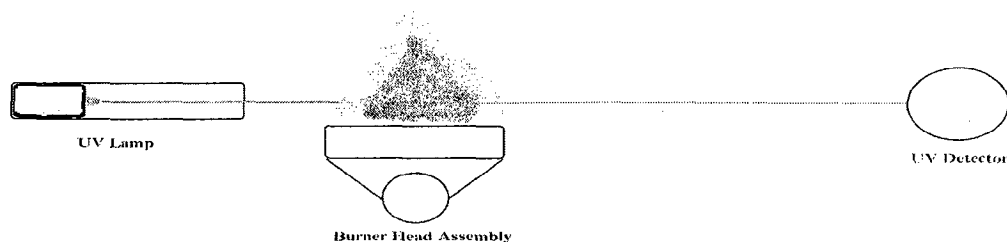
AAS

Atomic absorption spectroscopy (AAS) determines the presence of metals in liquid samples. Metals include Fe, Cu, Al, Pb, Ca, Zn, Cd and many more. It also measures the concentrations of metals in the samples. Typical concentrations range in the low mg/L range.

In their elemental form, metals will absorb ultraviolet light when they are excited by heat. Each metal has a characteristic wavelength that will be absorbed. The AAS instrument looks for a particular metal by focusing a beam of uv light at a specific wavelength through a flame and into a detector. The sample of interest is aspirated into the flame. If that metal is present in the sample, it will absorb some of the light, thus reducing its intensity. The instrument measures the change in intensity. A computer data system converts the change in intensity into an absorbance.

As concentration goes up, absorbance goes up. The researcher can construct a calibration curve by running standards of various concentrations on the AAS and observing the absorbances. In this lab, the computer data system will draw the curve for you! Then samples can be tested and measured against this curve.

In atomic absorption, there are two methods of adding thermal energy to a sample. A graphite furnace AAS uses a graphite tube with a strong electric current to heat the sample. In flame AAS, we aspirate a sample into a flame using a nebulizer. The flame is lined up in a beam of light of the appropriate wavelength. The flame (thermal energy) causes the atom to undergo a transition from the ground state to the first excited state. When the atoms make their transition, they absorb some of the light from the beam. The more concentrated the solution, the more light energy is absorbed!



The light beam is generated by a lamp that is specific for a target metal. The lamp must be perfectly aligned so the beam crosses the hottest part of the flame and travels into the detector. The detector then measures the intensity of the beam of

beam irradiates the specimen which in turn produces a signal in the form of either x-ray fluorescence, secondary or backscattered electrons.

The SEM at GMU has a secondary electron detector. The signal produced by the secondary electrons is detected and sent to a CRT image. The scan rate for the electron beam can be increased so that a virtual 3-D image of the specimen can be viewed. The image can also be captured by standard photography.

By changing the width (w) of the electron beam, the magnification (M) can be changed where

$$M = \frac{W}{w}$$

and W is the width of the CRT. Since W is constant, the magnification can be increased by decreasing w .

Sample preparation

The specimens examined by SEM must be able to withstand the strong electric currents produced by the electron beam. Samples that do not conduct electricity can be damaged by the charges that can build up. Non-conductive specimens must first be coated with a thin layer of conductive material. This coating is accomplished using a sputterer. A sputter coater produces a nanometer thickness of conductive material on the surface through a cold plasma process that retains the contours of the specimen. Since most biological samples are non-conductive, they must be sputter coated. However, many of these samples also need additional treatment prior to sputter coating to prevent the cells from collapsing under the intense electron beam. The types of treatments vary according to the specimens. This usually involves a process that fixes the components of the specimen. For example, gluteraldehyde can be used to crosslink the proteins to form rigid polymers. The tissues then need to be rinsed in a buffer followed by dehydrated. Dehydration can be as simple as adding ethanol or more complicated using freeze drying or critical point evaporation.

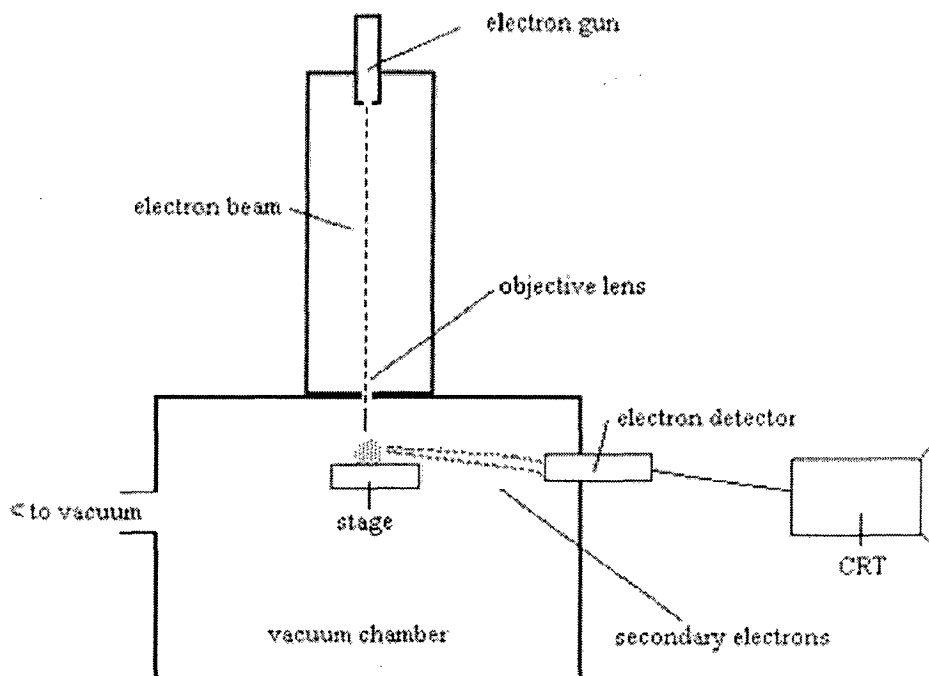
Once the specimen is fixed, it is then glued to a sample holder or "post." The post is placed into the sputter coater until a thin layer of gold is applied to the surface. The specimen is then placed in the SEM vacuum chamber and the electron gun is switched on.

Thermogravimetry

Thermogravimetry is a technique in which a change in the weight of a substance is recorded as a function of temperature or time. This is an available technique used for the assessment of the purity of materials and for % weight loss or total residue remained.

SEM

In light microscopy, a specimen is viewed through a series of lenses that magnify the visible-light image. However, the scanning electron microscope (SEM) does not actually view a true image of the specimen, but rather produces an electronic map of the specimen that is displayed on a cathode ray tube (CRT).

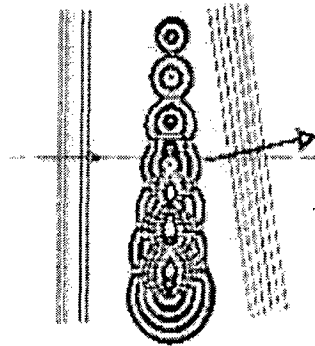


The figure above shows a schematic for a generic SEM. Electrons from a filament in an electron gun are beamed at the specimen in a vacuum chamber. The beam forms a line that continuously sweeps across the specimen at high speed. This

X-Ray Diffraction

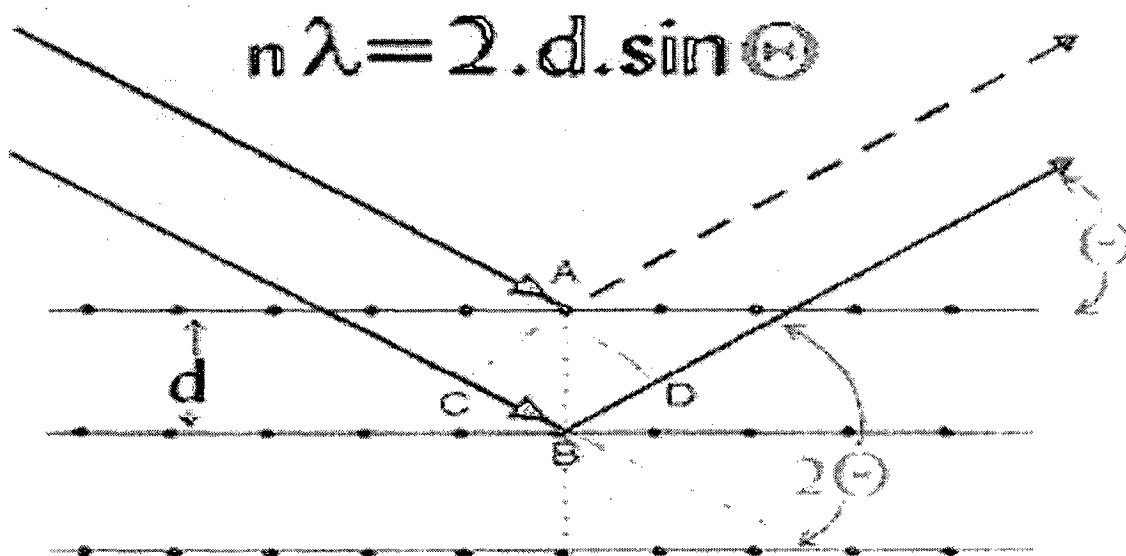
$$\sin\theta = n\lambda / 2d$$

When x-ray radiation passes through matter, the radiation interacts with the electrons in the atoms, resulting in scattering of the radiation.

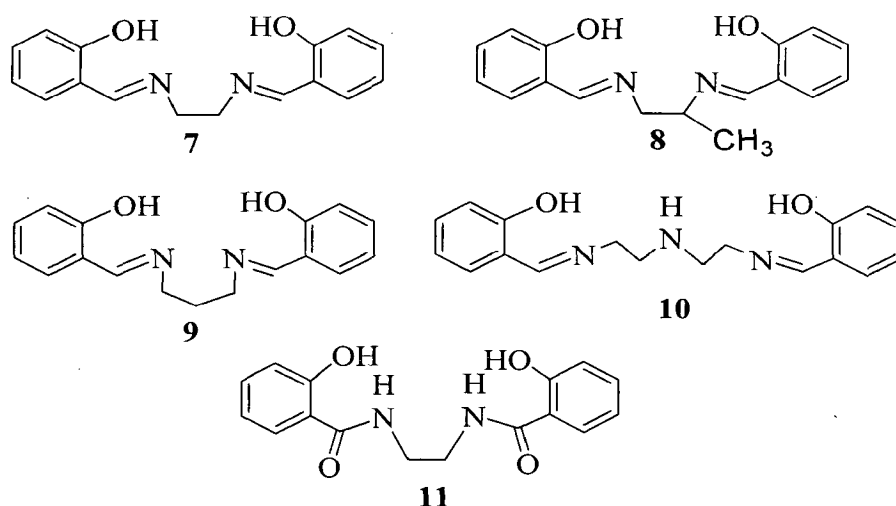


If the atoms are organized in planes (i.e. the matter is crystalline) and the distances between the atoms are of the same magnitude as the wavelength of the x-rays, constructive and destructive interference will occur.

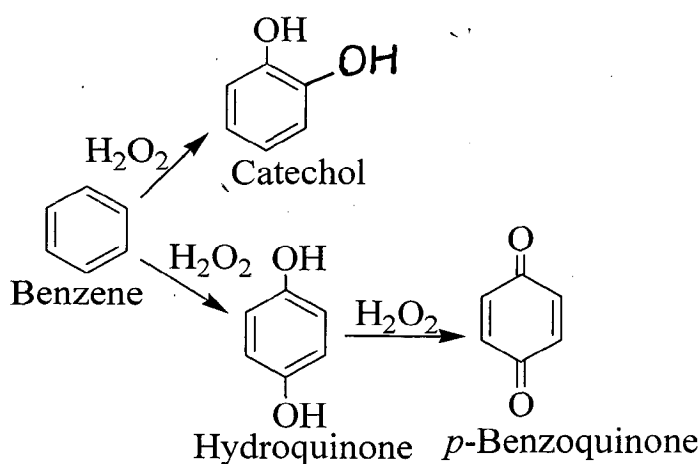
This results in diffraction where x-rays are emitted at characteristic angles based on the spaces between the atoms organized in crystalline structures called planes. Most crystals can have many sets of planes passed through their atoms. Each set of planes has a specific interplanar distance and will give rise to a characteristic angle of diffracted x-rays. The relationship between wavelength, atomic spacing (d) and angle was solved geometrically by Bragg as:



directing, the catalytic oxidation of phenol usually gives two products catechol and hydroquinone. In some cases a further oxidation also occurs to give *p*-benzoquinone as shown in Scheme 1.5. Under the optimized conditions [VO(sal-1,3-pn)]-Y has shown ca. 34 % conversion while other two complexes, [VO(salen)]-Y and [VO(saldien)] register only 33 % conversion. As high as 90 % selectivity of catechol has been observed by later two complexes [40]. The [VO(salen)]-Y has also been used as active catalyst in the oxidation of toluene by H₂O₂ to produce benzaldehyde, benzylalcohol, *o*-cresol and *p*-cresol [41]. Oxidation of cyclohexane has also been carried out by similar complexes [42, 43].



Scheme 1.4



Scheme 1.5. Various products of phenol oxidation.

Oxidation of phenol has also been reported using copper(II), nickel(II), iron(III), chromium(III), bismuth(III) and zinc(II) complexes of ligands **7**, **8**, **9**, **10** and **11** encapsulated in zeolite-Y. In all cases conditions have been optimized considering effect of amount of catalyst, effect of substrate, H₂O₂ concentration and volume of solvent. It was observed that substrates to oxidant ratio of 1:2 worked nicely to effect maximum oxidation. The 3D model structure of [Fe(hybe)(H₂O)₂]⁺ was created using CS Chem 3D ultra molecular modeling programme to show that zeolite-Y can accommodate the complex in its super cages without any strain; Figure 1.3 [44-46].

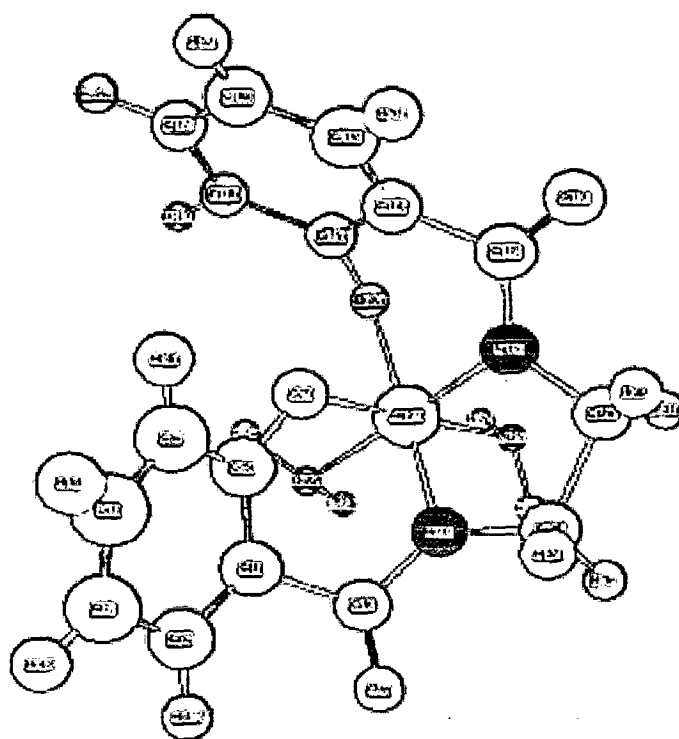


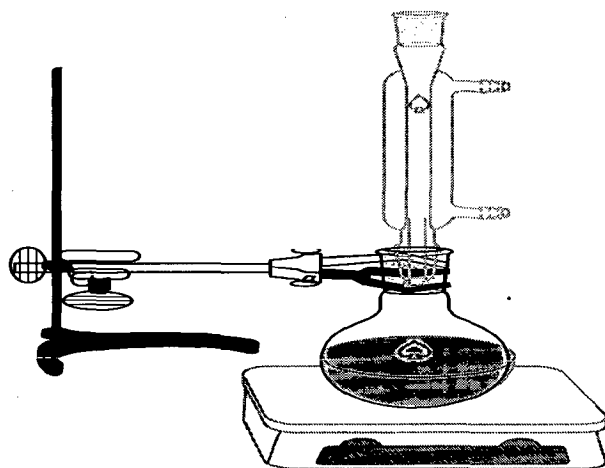
Figure 1.3. 3D model structure of [Fe(hybe)(H₂O)₂]⁺.

Zeolite encapsulated metal complexes prepared from other tetradentate Schiff base ligands also catalysed the oxidation of phenol using different oxidants. Thus, Cu(X-salen) [47], Mn(X-salen) [48] (X = H, Cl, Br or NO₂), have been used

Various parameters as mentioned below have been optimized to effect maximum oxidation of substrates.

- Concentration of Oxidant
- Amount of Catalyst
- Volume of Solvent
- Type of Oxidant
- Type of Catalyst
- Reaction Time

EXPERIMENTAL WORK



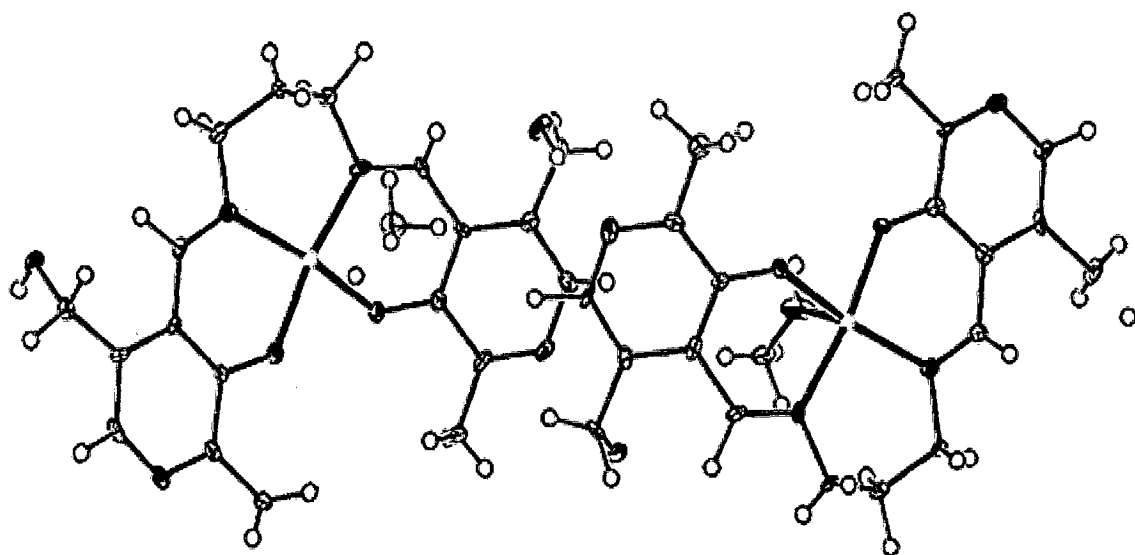


Figure 3.1. Crystal structure of $\{[\text{Cu}(\text{pydx-1,3-pn})] \cdot \text{CH}_3\text{OH}\}_2$. Both molecules of asymmetric unit are shown together.

Table 3.2. Various bond lengths in [Cu(pydx-1,3-pn)].CH₃OH

Bond Distance		Å	
Cu1-O2	1.887(4)	C38-C39	1.539(8)
Cu1-O1	1.948(4)	C24-H33	1.12(3)
Cu1-N2	1.984(5)	C32-H41	0.77(4)
Cu1-N3	1.998(5)	C1-C2	1.511(8)
Cu1-O5	2.352(5)	C1-H1	1.13(3)
Cu2-O7	1.906(4)	C1-H2	1.17(3)
Cu2-O6	1.961(4)	C27-C28	1.513(8)
Cu2-N6	1.991(5)	C22-C21	1.491(8)
Cu2-N7	2.001(5)	C22-C23	1.526(8)
Cu2-10	2.355(5)	C22-H29	0.81(4)
O6-C26	1.283(6)	C22-H30	1.07(4)
O1-C14	1.318(6)	C19-C18	1.480(8)
O7-C34	1.274(7)	C19-H20	0.75(4)
N6-C24	1.283(7)	C19-H21	0.94(4)
N6-C23	1.462(7)	C30-C29	1.378(7)
O2-C6	1.307(6)	C30-C31	1.535(7)
N2-C3	1.476(8)	C8-H9	1.13(3)
N7-C32	1.276(8)	C8-H8	0.92(4)
N7-C21	1.481(7)	C8-H10	0.72(5)
N3-C12	1.293(7)	C23-H32	0.76(4)
N3-C1	1.472(7)	C23-H31	0.81(3)
O4-C11	1.429(7)	C2-C3	1.535(8)
O4-H14	0.85(3)	C2-H4	0.70(5)
O3-C19	1.440(7)	C2-H3	1.04(5)
O3-H22	0.85(3)	C3-H6	0.74(4)
O8-C31	1.403(8)	C3-H5	1.09(3)
O8-H40	0.32(10)	C17-C18	1.368(8)
O9-C39	1.413(9)	C17-H19	0.81(4)
O9-H48	0.13(10)	C9-H11	1.04(3)
N8-C35	1.304(7)	C11-H13	0.97(4)
N8-C37	1.382(7)	C11-H12	1.00(3)
N4-C15	1.313(7)	C36-H42	1.05(4)
N4-C17	1.386(7)	C36-H44	0.75(4)
C13-C18	1.407(7)	C36-H43	1.08(4)
C13-C12	1.416(8)	C37-H45	1.00(4)
C13-C14	1.421(7)	C29-H37	1.13(4)
N1-C7	1.342(7)	C4-H7	1.07(4)
N1-C9	1.348(8)	C39-H47	0.99(4)
C26-C25	1.393(7)	C39-H46	0.99(5)
C26-C27	1.434(7)	C39-H48	1.50(10)
N5-C29	1.314(8)	O5-C20	1.398(8)

3.1.7. EPR studies

The EPR spectra of complexes [Cu(pydx-en)] and [Cu(pydx-1,3-pn)] were recorded in DMF at 77 K and Figure 3.8 presents the EPR spectra. In both cases, the Cu hyperfine structure is well defined. However, no superhyperfine “structure” resulting from the interaction of the unpaired d electron of Cu and the ^{14}N atoms ($I=1$) is observed. The calculated parameters are given Table 3.5.

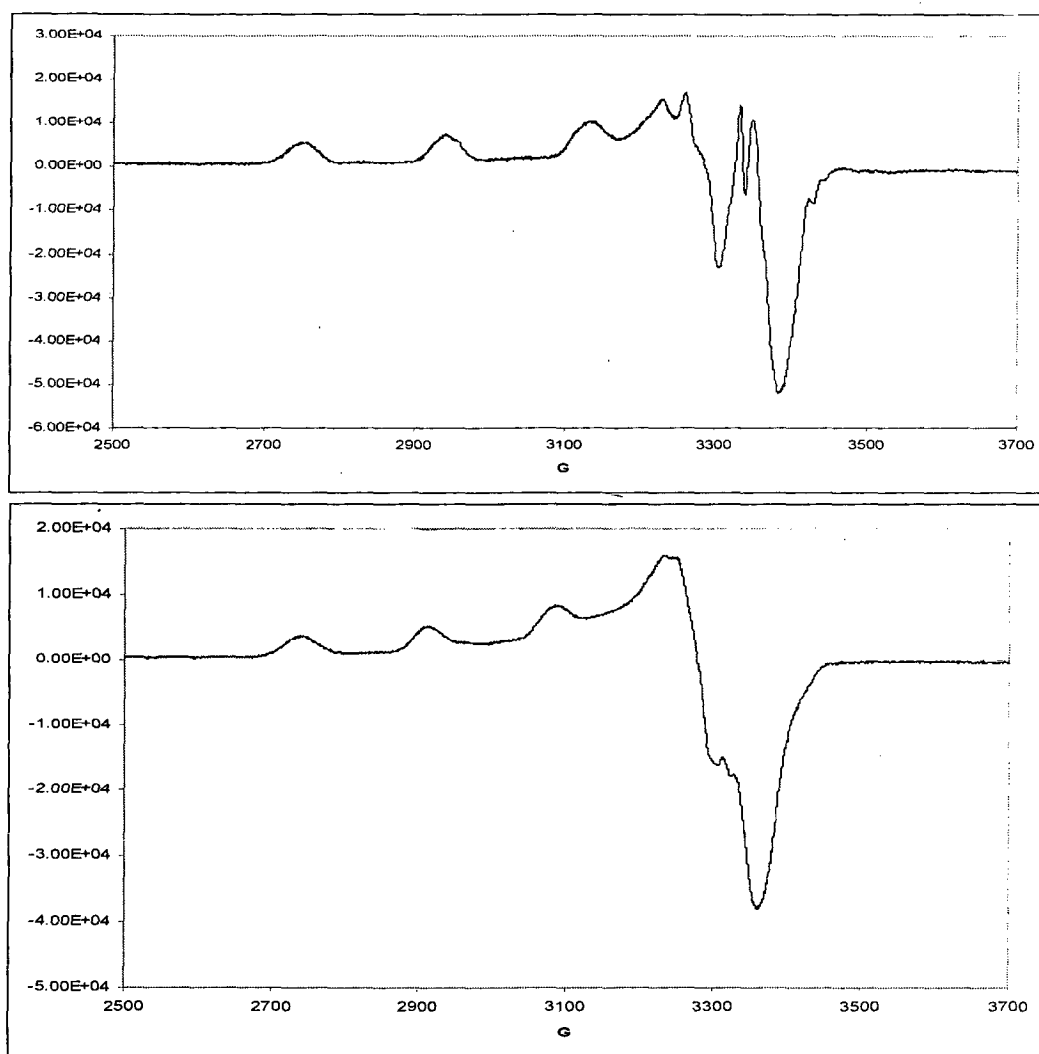


Figure 3.7. EPR spectra of [Cu(pydx-en)] (above) and [Cu(pydx-1,3-pn)] (below) in DMF at 77K . $\nu=9.453$ GHz.

Table 3.5. EPR parameters obtained for neat complexes in DMF at 77K.

Compound	g_{xx}	g_{yy}	$g_{zz(\parallel)}$	A_{xx} (10^{-4} cm^{-1})	A_{yy} (10^{-4} cm^{-1})	$A_{zz(\parallel)}$ (10^{-4} cm^{-1})
[Cu(pydx-en)]	2.07	2.03	2.22	17.39	28.43	196.94
[Cu(pydx-1,3-pn)]	2.04	2.06	2.24	21.85	16.88	178.53

According to the literature [76, 77], the correlation (Figure 3.8) between A_{\parallel} and g_{\parallel} for Cu(II) complexes may give some information on the coordinating groups in complexes with square planar geometry.

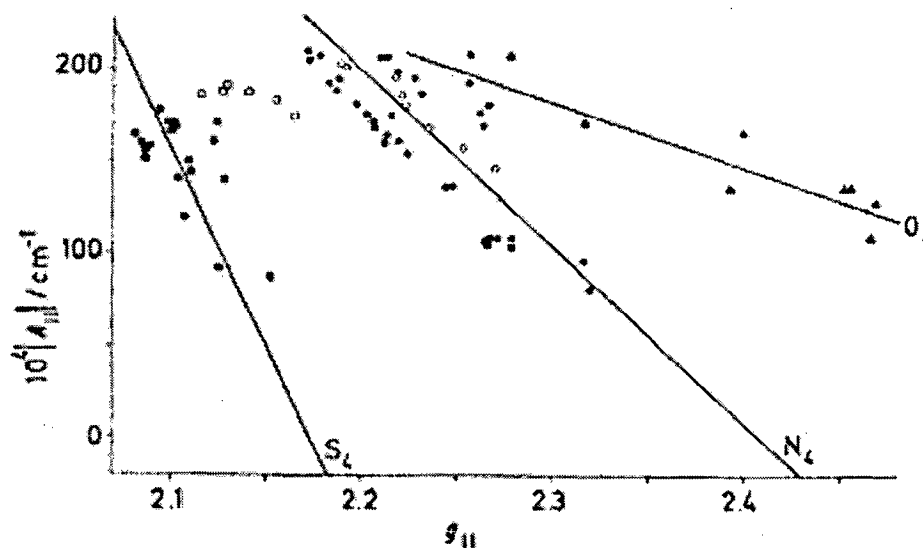


Figure 3.8. Correlation between A_{\parallel} and g_{\parallel} for Cu(II) complexes with several types of coordinating atoms with tetragonal or tetrahedral distortion: $S_4(\blacklozenge)$, $N_4(\bullet)$, $O_4(\blacktriangle)$, $N_2O_2(\odot)$ and $N_2S_2(\blacksquare)$.

The values obtained for [Cu(pydx-en)] and [Cu(pydx-1,3-pn)] fit well in group of N_2O_2 donating atoms of square planar geometry. The [Cu(pydx-1,3-pn)]